

Electronic Thesis and Dissertation Repository

8-16-2018 1:30 PM

Design, Synthesis, and Evaluation of Novel Protease-Activated Receptor 2 (PAR2)-Targeting Imaging Agents for Cancer

Jordan C. LeSarge, *The University of Western Ontario*

Supervisor: Luyt, Len G., *The University of Western Ontario*

A thesis submitted in partial fulfillment of the requirements for the Master of Science degree in Chemistry

© Jordan C. LeSarge 2018

Follow this and additional works at: <https://ir.lib.uwo.ca/etd>

 Part of the [Medicinal-Pharmaceutical Chemistry Commons](#)

Recommended Citation

LeSarge, Jordan C., "Design, Synthesis, and Evaluation of Novel Protease-Activated Receptor 2 (PAR2)-Targeting Imaging Agents for Cancer" (2018). *Electronic Thesis and Dissertation Repository*. 5533.
<https://ir.lib.uwo.ca/etd/5533>

This Dissertation/Thesis is brought to you for free and open access by Scholarship@Western. It has been accepted for inclusion in Electronic Thesis and Dissertation Repository by an authorized administrator of Scholarship@Western. For more information, please contact wlsadmin@uwo.ca.

Abstract

Aberrant function and over-expression of protease-activated receptor 2 (PAR2), a GPCR, is associated with various cancers and inflammatory diseases. PAR2-targeting ligands have been developed with therapeutic applications but the development of imaging probes is lacking. A series of PAR2-targeted fluorescent and ^{18}F -PET imaging agents were synthesized and assessed for PAR2-binding. A novel dye-conjugated peptide, Isox-Cha-Chg-ARK(Sulfo-Cy5)-NH₂ (EC_{50} =16nM, K_D =38nM), showed >10-fold increase in potency and binding affinity for PAR2 compared to the leading known fluorescent probe. A novel PET imaging ^{18}F -labeled peptide, Isox-Cha-Chg-AR-Dpr(^{18}F 4-FB)-NH₂, is the first PAR2-targeted *in vivo* imaging agent. It showed significant uptake in PAR2-expressing prostate cancer cells compared to controls ($P<0.001$) and the ^{19}F -standard was highly potent (EC_{50} =13nM) and PAR2-selective. The peptide was ^{18}F -labeled through standard prosthetic group labeling (RCY=37±3%, RCP>98%, A_m =20±2GBq/μmol, EOS=125±2min, n=4). These probes are useful chemical tools that could provide insight into PAR2 expression *in vitro* and *in vivo* with potential clinical applications in PAR2-related diseases.

Keywords

Molecular imaging, medicinal chemistry, protease-activated receptor 2 (PAR2), G protein-coupled receptor (GPCR), peptides, agonists, imaging agents, fluorescent agents, radiolabeled agents, positron emission tomography (PET), fluorine-18, cancer, inflammatory diseases.

Co-Authorship Statement

The majority of the work was performed by the author, except the following:

Chapter 2 and Chapter 3: Cell culture and transfections (except cell culture for flow cytometry experiment) were performed by Pierre Thibeault, a Ph.D. candidate in Dr. Rithwik Ramachandran lab (Assistant Professor in the Department of Physiology and Pharmacology, The University of Western Ontario). In addition, Pierre completed the entire confocal microscopy experiment (see Figure 2.4).

Chapter 3: Fluorine-18 was supplied by Dr. Michael Kovacs (Assistant Professor in the Departments of Medical Imaging and Medical Biophysics, The University of Western Ontario and Scientist at Lawson Cyclotron & PET Radiochemistry Facility, Lawson Health Research Institute).

Acknowledgments

Firstly, I would like to thank my supervisor, Dr. Len Luyt. He was a great role model and fantastic supervisor. He would always take the time to listen to my various questions, concerns, or updates, regardless of how non-concise I could be. Scientific research can definitely have its excitement and challenges, and Dr. Luyt was always there to help, assist, and support me throughout my project. In addition, Dr. Luyt always made a great effort to keep a strong, inclusive, and cohesive group; from his lab group socials to our Luyt group participation in the annual chemistry golf tournament (four consecutive year winner I might add), he has truly made this degree even more enjoyable!

Next, I would like to thank our incredible collaborators Pierre Thibeault and Dr. Rithwik Ramachandran. They continuously gave tremendous assistance in the projects; from insight in experiments and project goals, to performing/assisting in various experiments, to providing training for various biological experiments/instruments.

I would also like to give a huge thank you to the past and current Luyt lab members that assisted me during my time in this program. Thank you Will Turnbull, Emily Murrell, Mark Milne, Lihai Yu, JQ Hou, Marina Lazarakos, Axie Hauser-Kawaguchi, Tyler Lalonde, Emily Rodrigues, Megan Kelman, Claire Browne, Carlie Charron, Neha Sharma, and Zhanna Potetinova for all of your assistance, teaching, and support and for giving the lab such a welcoming and constructive atmosphere. In particular, thank you to Lihai Yu for your expertise and training in fluorine-18 chemistry as well as Will Turnbull, Emily Murrell, Marina Lazarakos, Axie Hauser-Kawaguchi, Tyler Lalonde, and Mark Milne for your training on various instruments and lab techniques such as the automated peptide synthesizer, HPLC, UHPLC, flash chromatography, and cell culture. Special thanks to Will Turnbull, Emily Murrell, and Mark Milne; you three went above and beyond in helping me in this project, from giving me insights on how to troubleshoot an experiment to helping me understand new concepts. No matter how many questions I would ask you Will, you would always take your time and answer me in the most helpful way possible.

Next, I would like to thank Mike Keeney (Coordinator Hematology/Flow Cytometry), Ben Hedley Ph.D., and Lori Lowes Ph.D. for their assistance in the flow cytometry experiments.

As well, I would like to thank Dr. Michael Kovacs and the Lawson Cyclotron & PET Radiochemistry Facility team for access in the radioactive facility and for the production of fluorine-18.

Further, I would like to thank Dr. Savita Dhanvantari (Assistant Professor in the Departments of Medical Biophysics and Medicine, The University of Western Ontario) for allowing me to use her laboratory space for fluorine-18 cell uptake studies.

In addition, I would like to thank Siobhan Smith for her assistance in transporting various materials between facilities as well as for her continuous support throughout my program. In addition, I would like to thank my friends and family for all of their everlasting help and support.

As well, I would like to thank the Natural Sciences and Engineering Research Council (NSERC) of Canada for funding this research.

Lastly, I would like to thank my examining committee, Dr. Elizabeth Gillies, Dr. Robert Hudson, and Dr. John Di Guglielmo for taking their time to read my thesis and participate in this examination.

Over these past two years, I have learned a great deal, made some fantastic memories, met some great friends, and further developed my passion for research. I strive to continue to perform research in my future endeavors.

Table of Contents

Abstract.....	ii
Co-Authorship Statement	iii
Acknowledgments.....	iv
List of Tables	x
List of Figures.....	xi
List of Schemes.....	xiii
List of Appendices	xiv
List of Abbreviations and Symbols.....	xv
Chapter 1.....	1
1 Introduction.....	1
1.1 Protease-activated Receptors.....	1
1.2 Protease-activated Receptor 2	2
1.3 Molecular Imaging.....	3
1.4 Fluorescence Imaging.....	5
1.5 Positron Emission Tomography Imaging	5
1.6 PAR2 Structure-Activity Relationship History.....	7
1.7 Labeling Strategy.....	9
1.8 Computational Distribution Coefficient	9
1.9 Bioluminescence Resonance Energy Transfer β -Arrestin 2 Recruitment Assay ..	10
1.10 Calcium Assay	11
1.11 Purpose of Thesis.....	12
1.12 References	14
Chapter 2.....	17
2 A Potent and High Affinity Fluorescent Probe for Protease-Activated Receptor 2.....	17

2.1	Introduction	17
2.2	Results and Discussion	20
2.2.1	General Peptide Synthesis Strategy	20
2.2.2	Design, Synthesis, and Evaluation of PAR2-Targeting Peptides	20
2.2.3	Synthesis and Evaluation of PAR2-Targeting Fluorescent Probes.....	23
2.3	Conclusions	27
2.4	Experimental Procedures	28
2.4.1	General Methods	28
2.4.2	Solid-Phase Peptide Synthesis	29
2.4.3	Solid-Phase Synthesis of 12	29
2.4.4	SPPS Reaction Monitoring.....	30
2.4.5	Solution-Phase Synthesis of 14 and 15	30
2.4.6	Cell Lines and Culture Conditions.....	30
2.4.7	BRET β -Arrestin 2 Recruitment Assay.....	31
2.4.8	Intracellular Calcium Release Assay.....	31
2.4.9	Flow Cytometry for Determination of K_D for 14 and 15 using Saturation Binding Experiments.....	32
2.4.10	Confocal Microscopy of 15 in PC3 Cells.....	33
2.5	References	35
	Chapter 3.....	38
3	A Novel PET Probe for <i>In Vivo</i> Imaging of Protease-Activated Receptor 2.....	38
3.1	Introduction	38
3.2	Results and Discussion	41
3.2.1	Peptide Synthesis	41
3.2.2	Synthesis and Evaluation of Class I PAR2-Targeted Peptides.....	42
3.2.3	Synthesis and Evaluation of First Generation Class II PAR2-Targeted Peptides.....	45

3.2.4	Synthesis and Evaluation of Second Generation Class II PAR2-Targeted Peptides.....	47
3.2.5	Synthesis and Evaluation of Third Generation Class II PAR2-Targeted Peptides.....	49
3.2.6	Radiosynthesis of [¹⁸ F] 29	52
3.2.7	Cell Uptake of [¹⁸ F] 29 in PC3 Cells	54
3.3	Conclusions and Future Work.....	55
3.3.1	Conclusions.....	55
3.3.2	Future Work.....	56
3.4	Experimental Procedures	57
3.4.1	General Methods.....	57
3.4.2	Solid-Phase Peptide Synthesis	58
3.4.3	Solid-Phase Orthogonal Alloc Deprotection	58
3.4.4	Solid-Phase Conjugation of 4-Fluorobenzoic Acid (19-20 , 22-24 , and 26-29)	59
3.4.5	Solution-Phase Conjugation of 4-Fluorobenzyl Chloride (21).....	59
3.4.6	Solution-Phase Conjugation of 4-Fluorobenzoic Acid (25).....	59
3.4.7	SPPS Reaction Monitoring.....	60
3.4.8	Cell Lines and Culture Conditions.....	60
3.4.9	BRET β-Arrestin 2 Recruitment Assay.....	60
3.4.10	Intracellular Calcium Release Assay.....	61
3.4.11	Synthesis of 4-(<i>tert</i> -butoxycarbonyl)-N,N,N-trimethylbenzenammonium triflate (32)	62
3.4.12	Synthesis of <i>N</i> -succinimidyl 4-fluorobenzoate (34)	62
3.4.13	General Methods for Radiochemistry	63
3.4.14	Synthesis of <i>N</i> -succinimidyl 4-[¹⁸ F]fluorobenzoate ([¹⁸ F] 34).....	63
3.4.15	Synthesis of Isox-Cha-Chg-AR-Dpr([¹⁸ F]4FB)-NH ₂ ([¹⁸ F] 29).....	64
3.4.16	Determination of [¹⁸ F] 29 Molar Activity	64

3.4.17 Cell uptake of [¹⁸ F]29.....	64
3.5 References	66
Chapter 4.....	69
4 Conclusions and Future Work.....	69
4.1 Conclusions	69
4.2 Future Work and Outlooks.....	72
4.3 References	74
Appendices.....	76
Curriculum Vitae.....	118

List of Tables

Table 2.1: PAR2-targeted peptides (1-2 and 6-12) with their EC ₅₀ and cLogD values.	21
Table 2.2: PAR2 selectivity of peptides 1-2 and 6-12	23
Table 2.3: Evaluation of Sulfo-Cy5 labeled peptides (14 and 15).	24
Table 2.4: HRMS data and purity of peptides 2 , 6-12 , and 14-15	29
Table 3.1: Class I PAR2-targeted peptides (2 and 17-20) and control peptides (1 and 13) with their EC ₅₀ values, PAR2 selectivity measures, and cLogD values.	44
Table 3.2: First generation Class II PAR2-targeted peptides (6 , 16 , and 21) with their EC ₅₀ values, PAR2 selectivity measures, and cLogD values.	46
Table 3.3: Second generation Class II PAR2-targeted peptides (7-11 and 22-25) with their EC ₅₀ values, PAR2 selectivity measures, and cLogD values.	48
Table 3.4: Third generation Class II PAR2-targeted peptides (26-29) with their EC ₅₀ values, PAR2 selectivity measures, and cLogD values.	50
Table 3.5: HRMS data and purity of peptides 2 , 6-7 , 16-29 , and 35	58

List of Figures

Figure 1.1: GPCR versus PAR agonist activation comparison. (A) Usual GPCR ligand activation, (B) PAR tethered ligand activation, (C) PAR free ligand activation.....	2
Figure 1.2: Comparison of spatial resolution and molecular sensitivity for various imaging modalities.....	4
Figure 1.3: Common imaging agent design.....	4
Figure 1.4: Positron decay, annihilation, and PET detection.....	7
Figure 1.5: Structure of (A) SLIGRL-NH ₂ , (B) 2f-LIGRLO-NH ₂ , and (C) Isox-Cha-Chg-X..	8
Figure 1.6: Structure of (A) [¹⁸ F]SFB and (B) Sulfo-Cy5 NHS ester.....	9
Figure 1.7: BRET β-arrestin 2 assay principle.....	11
Figure 1.8: Calcium assay principle for a PAR2-expressing cell.	12
Figure 2.1: Known PAR2-targeting peptide agonists.	18
Figure 2.2: PAR2 β-arrestin 2 recruitment dose-response curves for compound 1 , 14 , and 15 in HEK293T cells.....	25
Figure 2.3: Saturation binding experiments of (A) 14 and (B) 15 in HEK293T cells for determination of affinity measures (K _D).....	26
Figure 2.4: Confocal microscopy of 15 in PC3 cells and PAR2 KO PC3 cells.....	27
Figure 3.1: Known PAR2-targeting peptide agonists. (A) SLIGRL-NH ₂ , (B) Class I peptides, and (C) Class II peptides.	40
Figure 3.2: PAR2 β-arrestin 2 recruitment dose-response curves for 1 , 2 , 7 , and 29 in HEK293T cells.....	51

Figure 3.3: Overlay of RP-HPLC chromatogram and radio-trace of (A) SFB and [¹⁸ F]SFB, respectively, and (B) 29 and [¹⁸ F] 29 , respectively.....	54
Figure 3.4: Cell uptake of [¹⁸ F] 29 in PAR2 KO PC3 cells (white), PC3 cells blocked with 20 μM of 7 (grey), and PC3 cells (black).....	55
Figure 4.1: Several reported leading (A) agonists, (B) antagonists, and (C) imaging probes targeting PAR2.....	70
Figure 4.2: Structures of the lead PAR2-targeting (A) fluorescent probe, 15 , and (B) PET imaging agent, [¹⁸ F] 29 , developed in this thesis.....	72

List of Schemes

Scheme 2.1: General procedure for Fmoc-SPPS.....	20
Scheme 2.2: Alloc deprotection and subsequent acetylation.....	20
Scheme 2.3: Synthesis of PAR2-selective fluorescent probe, 15	24
Scheme 3.1: Conjugation of 4-FB to peptides.....	42
Scheme 3.2: Synthesis of [¹⁸ F] 29	52

List of Appendices

Appendix 1: Representative Examples of PAR2-Selectivity Measurements as Determined Through Calcium Response Assay in HEK293T and PAR2 KO HEK293T Cells	76
Appendix 2: Validation of Specific Binding for Flow Cytometry Experiments	77
Appendix 3: Characterization of Synthesized Peptides (2 , 6-12 , and 14-15).....	77
Appendix 4: PAR2 β -Arrestin 2 Recruitment Dose-Response Curves for Peptides 1 , 2 , 6-12 , and 14-15 in HEK293T Cells	84
Appendix 5: Representative Examples of PAR2-Selectivity Measurements as Determined Through Calcium Response Assay in PC3 and PAR2 KO PC3 Cells	90
Appendix 6: Representative Examples of PAR2-Selectivity Measurements as Determined Through Calcium Response Assay in HEK293T and PAR2 KO HEK293T Cells	91
Appendix 7: GE Tracer Lab FXN Automated Synthesis Display.	92
Appendix 8: Fluorine-18 Co-Injection Radio-traces and Chromatograms.	93
Appendix 9: Calibration Curve of 29 to Determine Molar Activity of [^{18}F] 29	94
Appendix 10: Characterization of Synthesized Peptides (2 , 6 , 7 , 16-29 , and 35)	94
Appendix 11: PAR2 β -Arrestin 2 Recruitment Dose-Response Curves for Peptides 1 , 2 , 6-7 , and 16-29 in HEK293T Cells	106
Appendix 12: NMR of <i>N</i> -succinimidyl 4-fluorobenzoate (34).....	116
Appendix 13: NMR of 4-(<i>tert</i> -butoxycarbonyl)- <i>N,N,N</i> -trimethylbenzenammonium triflate (32)	117

List of Abbreviations and Symbols

(Listed in alphabetical order.)

[¹⁸F]SFB: *N*-succinimidyl 4-[¹⁸F]fluorobenzoate

2f: 2-furoyl

4-FB: 4-Fluorobenzoyl

Isox: 5-isoxazoloyl

AEEA: [2-(2-amino)ethoxy]ethoxy]acetyl

Ahx: 6-aminohexanoyl

Alloc: allyloxycarbonyl

A_m: molar activity

arr2: β-arrestin 2

BRET: bioluminescence resonance energy transfer

BSA: bovine serum albumin

C-terminus: carboxy-terminus

Cha: L-cyclohexylalanine

Chg: L-cyclohexylglycine

cLogD: computation of the logarithm of the distribution coefficient

D: distribution coefficient

DCM: dichloromethane

DIPEA: *N,N*-diisopropylethylamine

DMF: *N,N*-dimethylformamide

DMSO: dimethyl sulfoxide

Dpr: L-2,3-diaminopropionic acid

DTPA: diethylenetriaminepentaacetic acid

e⁻: electron

EC₅₀: half-maximal effective concentration

EDC: 1-ethyl-3-(3-dimethylaminopropyl)carbodiimide

EDTA: ethylenediaminetetraacetic acid

EOS: end-of-synthesis

ESI: electrospray ionization

eYFP: enhanced yellow fluorescent protein

FBS: fetal bovine serum

Fluo-4 A: active fluo-4

Fluo-4 I: inactive fluo-4

Fmoc: fluorenylmethoxycarbonyl

GDP: guanosine diphosphate

GPCR: G protein-coupled receptor

GTP: guanosine triphosphate

HATU: *O*-(7-azabenzotriazol-1-yl)-*N,N,N,N'*-tetramethyluronium hexafluorophosphate

HBSS: Hank's balanced salt solution

HCTU: *O*-(1H-6-chlorobenzotriazole-1-yl)-1,1,3,3-tetramethyluronium hexafluorophosphate

HEK293T: highly transfectable human embryonic kidney cell line

HEPES: 4-(2-hydroxyethyl)-1-piperazineethanesulfonic acid

HRMS: high resolution mass spectrometry

K_D: dissociation binding constant

KLK4: kallikrein-related peptidase 4

KO: knock out

MeOTf: methyl trifluoromethanesulfonate

MR: magnetic resonance

MRI: magnetic resonance imaging

MS: mass spectrometry

N-terminus: amino-terminus

N: neutron

NHS: *N*-hydroxysuccinimide

NMR: nuclear magnetic resonance

P: proton

PAR: protease-activated receptor

PBS: phosphate buffered saline

PC3: prostate cancer cell line

pEC₅₀: $-\log[EC_{50}]$

PET: positron emission tomography

pH: $-\log[\text{H}^+]$

pK_D: $-\log[\text{K}_D]$

PTI: Photon Technologies Institute

r.t.: room temperature

RCP: radiochemical purity

RCY: decay corrected radiochemical yield

rluc: renilla luciferase

RP-HPLC: reverse-phase high-performance liquid chromatography

rpm: rotations per minute

SEM: standard error of the mean

SFB: *N*-succinimidyl 4-fluorobenzoate

SPECT: single-photon emission computed tomography

SPPS: solid-phase peptide synthesis

Sulfo-Cy5: Sulfo-Cyanine5

TFA: trifluoroacetic acid

THF: tetrahydrofuran

TIPS: triisopropylsilane

UV: ultra violet

β⁺: positron

γ : gamma ray

λ : wavelength

One or three letter abbreviations used for amino acids are in accordance with the IUPAC-IUB Joint Commission on Biochemical Nomenclature (JCBN). All unit abbreviations are in accordance with the IUPAC Gold Book.

Chapter 1

1 Introduction

1.1 Protease-activated Receptors

Protease-activated receptors (PARs) are a subfamily of G protein-coupled receptors (GPCRs). GPCRs are cell membrane receptors that are involved in a broad range of cellular processes, making them common therapeutic targets. They have a characteristic seven trans-membrane domain, extracellular ligand-binding site, and intracellular three-subunit G protein (α , β , and γ). GPCRs cause a cellular response through an intricate signal transduction pathway initiated when a ligand binds to, and activates, the receptor. Ligand binding initiates a conformational change in the receptor, causing its intracellular G protein to replace GDP with GTP.^{1,2} This replacement allows the α -subunit of the G protein to dissociate from the β - and γ -subunits.^{1,2} The dissociated G protein subunits can then elicit various effects on other intracellular signaling proteins or directly on functional proteins, such as the adenylate cyclase enzyme or ion channels.^{1,2} Further, the ligand-induced conformational change of the receptor can cause intracellular phosphorylation and subsequent recruitment of β -arrestin 1 and 2, which often results in receptor internalization, desensitization, and G protein independent signaling.^{1,2} PAR pathways are similar to those of the typical GPCR, except their unique method of ligand activation. Typical GPCRs are activated by a free endogenous ligand (Figure 1.1A), whereas PARs are activated through a covalently linked tethered ligand.^{1,2} In an inactive state, PARs have N-terminal amino acids that ‘mask’ the ligand. Specific proteases cleave off the N-terminal portion of the receptor revealing an ‘unmasked’ tethered ligand sequence that binds to the PAR binding region and activates the receptor (Figure 1.1B).^{1,2} It has been found that exogenous ligands resembling the tethered ligand sequence can activate a PAR in lieu of its endogenous tethered ligand (Figure 1.1C).^{1,2}

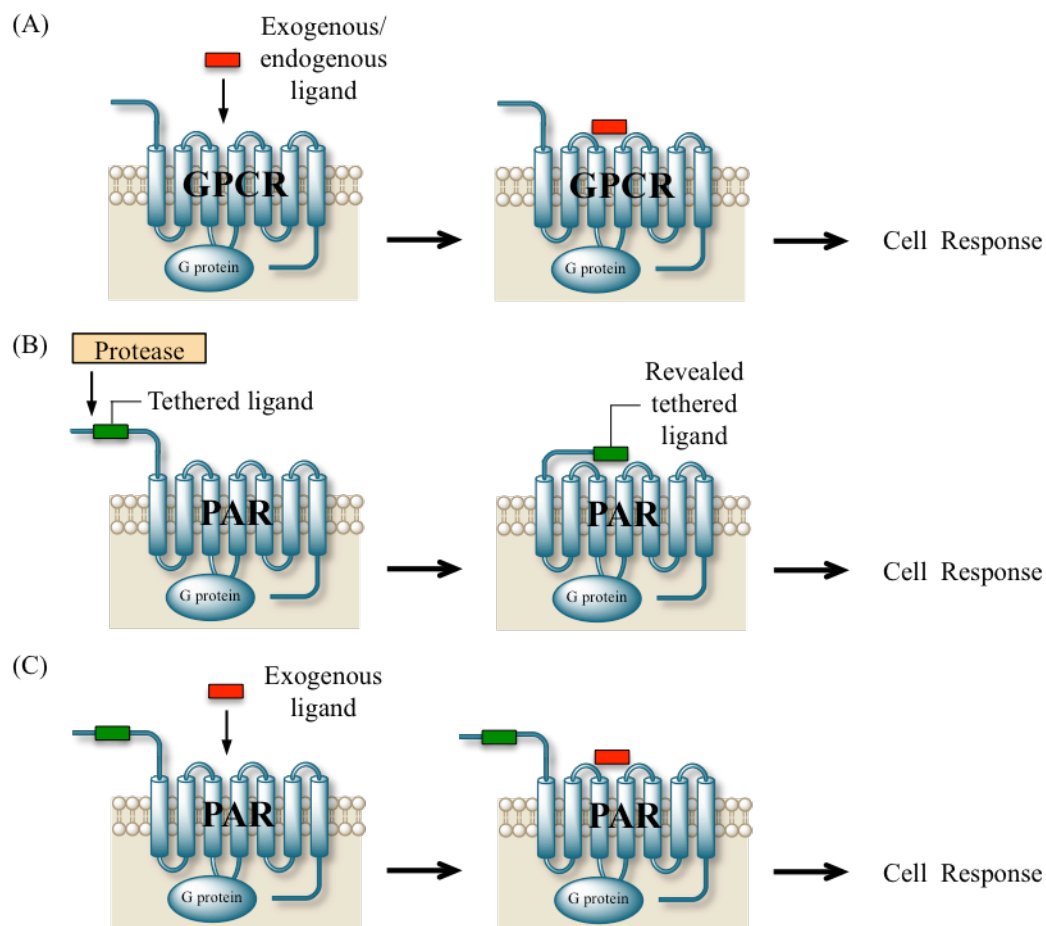


Figure 1.1: GPCR versus PAR agonist activation comparison. (A) Usual GPCR ligand activation, (B) PAR tethered ligand activation, (C) PAR free ligand activation.

1.2 Protease-activated Receptor 2

There are four known PARs, designated PAR1, PAR2, PAR3, and PAR4. All PARs have different but related functions, and have been linked to various diseases; the focus of this research is on PAR2. PAR2 is naturally expressed in various tissues, in which the pancreas, kidneys, liver, small intestine, and colon show the highest expression.³⁻⁵ The physiological role of PAR2 is generally involved in inflammation, cell migration, tissue metabolism, and gastrointestinal function. However, aberrant function or over-expression of PAR2 has been linked to various cancers and inflammatory diseases. More specifically, PAR2 is implicated in conditions including arthritis, colitis, asthma,

cardiovascular disease, prostate cancer, lung cancer, gastric cancer, colon cancer, melanoma, ovarian cancer, and breast cancer.⁶⁻²¹ In cancerous tissue, this undesirable activity of PAR2 has been shown to significantly contribute to cancer cell proliferation, angiogenesis, and metastasis.^{8,22,23} Of specific interest, there is up to a 16-fold increase in PAR2 expression in colon, lung, breast, prostate, ovarian, and gastric cancers and PAR2 expression levels have been positively correlated to cancer staging and progression.^{10,13,16,19,20,24,25} PAR2 is therefore an important biological target for therapeutics and imaging. Optimization of the PAR2-ligand interaction has been thoroughly explored, with some ligands showing therapeutic potential.² There is however a paucity of published research into the development of fluorescent ligands and no published research available on the development of *in vivo* imaging agents for PAR2.

1.3 Molecular Imaging

Molecular imaging is the visualization, characterization, and measurement of biological processes at the molecular and cellular levels in living systems.²⁶ It is a technique that is able to non-invasively study cellular processes, diagnose disease, monitor treatment response of patients, and stratify diseases of patients. Molecular imaging encompasses many imaging modalities such as positron emission tomography (PET), single photon emission computed tomography (SPECT), optical, and magnetic resonance (MR) imaging. Each of these common molecular imaging modalities have their various strengths and weaknesses when it comes to their spatial resolution, sensitivity, and depth of penetration (Figure 1.2).²⁷ Optical imaging has strong spatial resolution and sensitivity in comparison to the other common molecular imaging modalities, but is limited by its depth of penetration in living systems.²⁷ MR, PET, and SPECT imaging are not limited by their depth of penetration but have their own shortcomings.²⁷ MR imaging has poor sensitivity for its contrast agents whereas nuclear (PET and SPECT) imaging have poor resolution compared to the other common molecular imaging modalities.²⁷ Nuclear imaging does however have very strong sensitivity compared to the other common molecular imaging modalities.²⁷

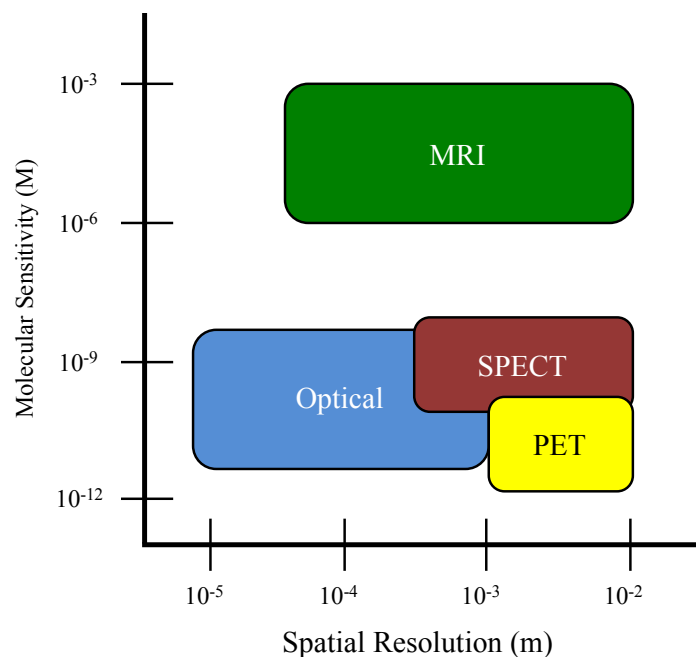


Figure 1.2: Comparison of spatial resolution and molecular sensitivity for various imaging modalities.

A crucial component to molecular imaging involves having a detectable agent referred to as a molecular imaging agent. Typical molecular imaging agents contain a targeting moiety that binds with high affinity and specificity to the biological target of interest, a linker, and an imaging moiety (Figure 1.3).

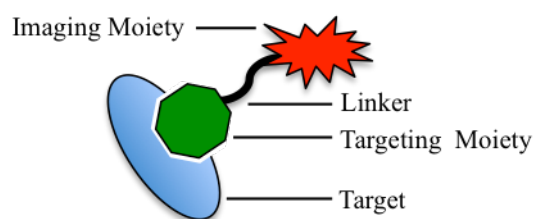


Figure 1.3: Common imaging agent design.

1.4 Fluorescence Imaging

Fluorescence is the emission of electromagnetic radiation from a substance that has absorbed some higher energy electromagnetic radiation, in which visual light emission is the most useful for molecular imaging.²⁸ This concept can be utilized for fluorescence molecular imaging through the use of fluorescent imaging agents. Similar to other imaging agents, these agents typically contain a targeting moiety and a fluorescent moiety (similar to Figure 1.3). The most significant limitation for imaging using fluorescent imaging agents is that detection through tissue is limited, with a maximum penetration of several centimeters.²⁹ They therefore have minimal uses for *in vivo* imaging of animals larger than rats.²⁹ Despite this, fluorescent imaging agents have a multitude of important applications, such as investigating biologically relevant interactions (i.e. receptor-ligand binding) in *in vitro* cell studies or small animal models, histology staining, and intraoperative imaging for image-guided surgeries (e.g. in tumour resection surgery, a fluorescent imaging agent targeting cancer could be used to aid in cancer-tissue visualization).^{29,30} Since PAR2 is linked to various diseases, such as cancer, PAR2-specific fluorescent imaging agents have potential applications in all of these categories.

1.5 Positron Emission Tomography Imaging

PET is a powerful, highly sensitive, quantitative, *in vivo* imaging technique that indirectly detects positron (β^+) radioactive decay. In PET molecular imaging, a β^+ emitting imaging agent acts as the source of the signal. These PET imaging agents can be directly labeled with a β^+ emitter, but for higher molecular weight entities they commonly have a targeting moiety linked to an imaging moiety (similar to Figure 1.3), where the imaging moiety often makes use of a prosthetic group. The prosthetic group is designed to allow for facile labeling with a radioactive isotope and conjugation to the targeting moiety; prosthetic group labeling is commonly used since direct labeling of peptide or protein targeting moieties is often not synthetically feasible. There are many examples of β^+ emitting isotopes used for PET, such as fluorine-18, copper-64, carbon-11, nitrogen-13,

gallium-68, and oxygen-15.²⁹ Each of these radionuclides have their own advantages and limitations; however, the most common radionuclide used today is fluorine-18. Fluorine-18 has facile cyclotron production, an ideal half-life for radiopharmaceuticals (109.8 min), diverse chemistry for introduction into various molecules, and the best spatial resolution compared to other PET isotopes.^{31,32} Fluorine-18 is produced from a cyclotron through proton irradiation of ^{18}O (a naturally occurring stable isotope of oxygen).^{29,32} Although PET requires fluorine-18 (or other β^+ emitters), signal detection does not directly measure β^+ decay. Initially, β^+ decay converts a proton into a neutron, a positron (an antiparticle counterpart of an electron), and a neutrino (Figure 1.4).^{32,33} The positron will travel until it has lost enough kinetic energy to annihilate with an electron, emitting two antiparallel 511 keV gamma photons.^{29,32} PET imaging uses a scintillator to detect these antiparallel gamma photons, in which areas of high radionuclide content result in high signal.³³ The high energy of these gamma photons ensures they will travel, and be detected, through tissue of any applicable distance, unlike other imaging methods such as fluorescence imaging.²⁹ Developing PET imaging agents targeting PAR2 can provide insight into areas of PAR2 expression *in vivo* and have potential clinical applications in the diagnosis and treatment of various cancers and inflammatory diseases.

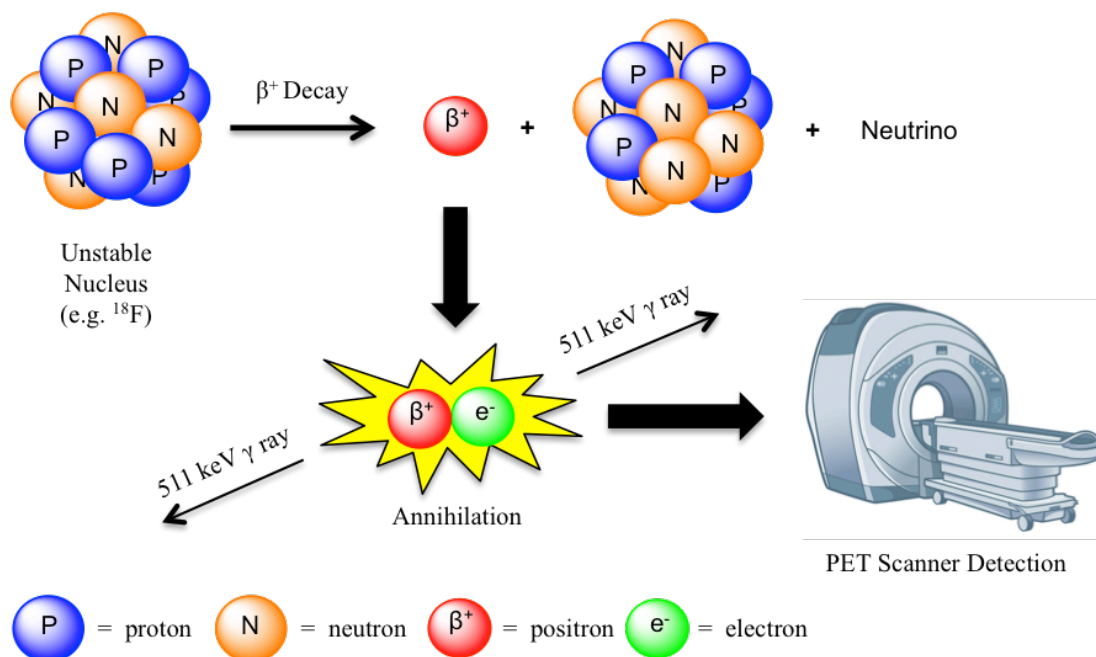


Figure 1.4: Positron decay, annihilation, and PET detection.

1.6 PAR2 Structure-Activity Relationship History

As described in section 1.1, PARs are activated through a specific protease that cleaves the N-terminus of the receptor to reveal a tethered ligand sequence that binds to and subsequently activates the receptor. Initial studies on ligands targeting PAR2 were based on the tethered ligand sequence of the native protein. The amino acid sequence of the tethered ligand was determined to be SLIGRL and SLIGKV in rodents and humans, respectively.³⁴ These sequences and their C-terminal amidated sequences were synthesized as six-mer peptides and were found to bind to and activate PAR2.^{34–37} Further, it was found that the amidated rodent sequence (SLIGRL-NH₂, Figure 1.5A) had the highest potency and binding affinity for human PAR2 compared to the other three sequences, partially due to the C-terminal amide resembling the secondary amide present in the tethered ligand sequence.^{35–38} Further structure-activity relationship studies involved substitution and addition of various natural and unnatural amino acids to SLIGRL-NH₂. Replacing serine in position one with various heterocyclic residues greatly

improved potency and affinity for PAR2, of which 2-furoyl (i.e. 2f-LIGRL-NH₂) was the best.³⁹ Addition of ornithine to the C-terminus of 2f-LIGRL-NH₂ (Figure 1.5B) was found to have no noticeable effect on potency or binding affinity, nor did the addition of a fluorescent dye to the side chain of ornithine.^{40,41} Recently, improvements in PAR2 affinity and potency of 2f-LIGRL-NH₂ have been made through the replacement of the 2-furoyl (2f) group with a 5-isoxazoyl (Isox) group as well as leucine and isoleucine with more hydrophobic analogues cyclohexylalanine (Cha) and cyclohexylglycine (Chg).^{39,42-44} Originally, the truncated sequence Isox-Cha-Chg-NH₂ (Figure 1.5C) showed a ten-fold increase in potency compared to 2f-LIGRLO-NH₂ through a calcium assay, but later was reported to have a reduced affinity for PAR2 through a competitive binding assay.^{42,43} This was likely due to the absence of the arginine positive charge; a charge that may contribute to a relatively strong ionic interaction with the receptor.⁴³ However, the sequence Isox-Cha-Chg-AR-NH₂ (Figure 1.5C) showed a greater than ten-fold increase in potency and affinity for PAR2 compared to 2f-LIGRL-NH₂ in those same assays.⁴³

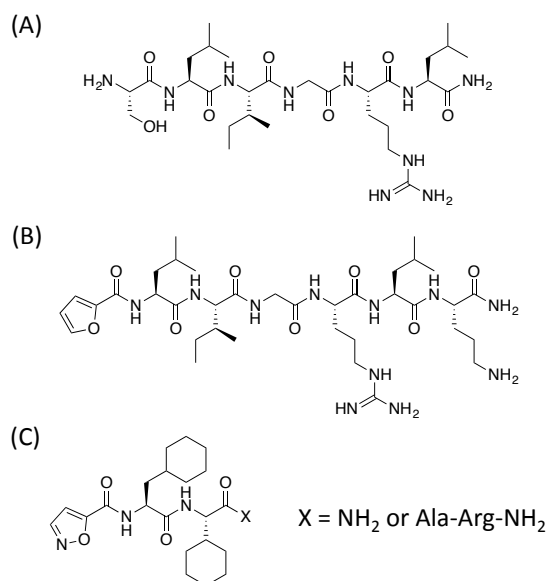


Figure 1.5: Structure of (A) SLIGRL-NH₂, (B) 2f-LIGRLO-NH₂, and (C) Isox-Cha-Chg-X.

1.7 Labeling Strategy

There are several ways to label targeting moieties with fluorine-18; however, due to the large number of potentially reactive functional groups, labeling of peptides generally proceeds using a prosthetic group. The prosthetic group, *N*-succinimidyl 4-¹⁸F]fluorobenzoate (¹⁸F]SFB, Figure 1.6A), was used for labeling of peptides in this thesis as it is one of the most common fluorine-18 peptide labeling prosthetic groups, which gives quick, efficient, and clean labeling with the ability to be automated.^{45,46} Commonly, as completed in this thesis, the 4-fluorobenzoyl (4-FB) with natural fluorine (fluorine-19) is conjugated to the targeting moiety to identify the lead candidate(s) through biological evaluation before the fluorine-18 version(s) are synthesized using ¹⁸F]SFB. The Sulfo-Cy5 NHS (Sulfo-Cyanine5 *N*-hydroxysuccinimide) ester fluorescent dye (Figure 1.6B) is a commercially available fluorescent dye that can undergo facile conjugation to primary amines, which was also used for labeling of peptides in this thesis.

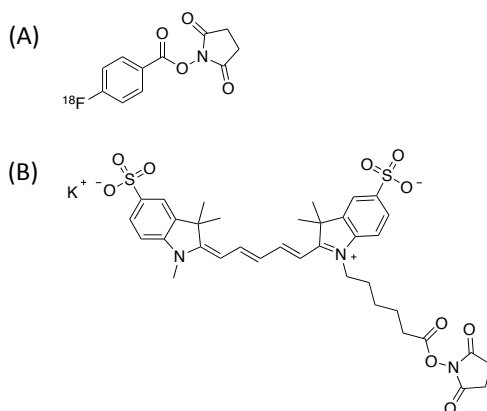


Figure 1.6: Structure of (A) [¹⁸F]SFB and (B) Sulfo-Cy5 NHS ester.

1.8 Computational Distribution Coefficient

The distribution coefficient (*D*) is a measure of the hydrophilicity/hydrophobicity of a compound. It is a ratio of the concentration of a compound that is dissolved in *n*-octanol compared to its concentration dissolved in water from a mixture of these two immiscible solvents at a given pH (Eqn. 1).⁴⁷

$$D = \frac{[\text{ionized \& unionized compound in octanol}]}{[\text{ionized \& unionized compound in water}]} \quad (1)$$

The distribution coefficient is usually expressed as a logarithm of D (logD), in which more hydrophobic compounds are generally more soluble in *n*-octanol thereby having a more positive value. More hydrophilic compounds are generally more soluble in water thereby having a more negative value. This value can be determined experimentally, or by the more feasible route, computationally to give a clogD value.⁴⁷

Development of imaging agents and therapeutic drugs can be improved by utilizing information from logD or clogD, as there is typically an ideal balance of hydrophobicity and hydrophilicity for *in vivo* applications.⁴⁷ Molecules with very negative logD or clogD values typically have rapid clearance and a difficult time passing biological barriers to get to the target *in vivo*. Molecules with very positive values typically have a high uptake in fatty tissue, blood solubility issues, and higher chances of producing toxic metabolites *in vivo*.⁴⁷

The clogD values for the compounds developed herein were calculated using Simulations Plus MedChem Designer ADMET Predictor.⁴⁸ This program contains several models with over 300 atomic and molecular descriptors as well as various algorithms to select the best model and prediction parameters to determine the computed distribution coefficient at a desired pH. Generally, the pH is set to 7.4 to resemble physiological conditions.

1.9 Bioluminescence Resonance Energy Transfer β -Arrestin 2 Recruitment Assay

Most GPCRs, including PAR2, initiate β -arrestin 2 (arr2) recruitment when a ligand binds to its orthosteric site. This signal is often involved in receptor internalization, desensitization, and G protein independent signaling.^{49,50} This recruitment can be used for a biological assay to determine receptor-ligand binding. In this assay, cells are transiently transfected with genes that encode for PAR2 tagged with enhanced yellow fluorescent protein (eYFP) and arr2 tagged with renilla luciferase (rluc). The cell then begins to

express both of these proteins, PAR2-eYFP on the cell membrane and arr2-rluc in the cytoplasm (Figure 1.7). Cells are then incubated with a PAR2-targeting ligand followed by h-coelenterazine. Renilla luciferase is an enzyme that catalyzes h-coelenterazine to emit at $\lambda_{\text{max}} = 480 \text{ nm}$ (i.e. bioluminescence). If arr2-rluc is in close proximity with PAR2-eYFP, resonance energy transfer occurs from the emitted wavelength to eYFP, which then subsequently re-emits at $\lambda_{\text{max}} = 527 \text{ nm}$. Both emissions are recorded and expressed as a ratio of eYFP over rluc-h-coelenterazine emission to control for transfection efficiency. The larger the ratio value, the more arr2 recruitment that occurred. This is completed at various concentrations of ligand of interest in order to determine a dose-response curve and subsequent EC_{50} value as a measure of potency.

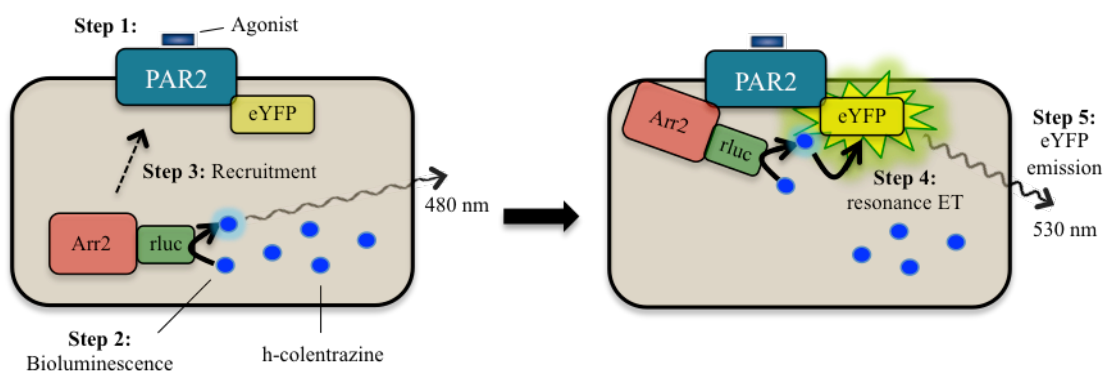


Figure 1.7: BRET β-arrestin 2 assay principle.

Step 1: binding of agonist to PAR2. Step 2: continuous h-coelenterazine-rluc bioluminescence. Step 3: arr2 recruitment. Step 4: resonance energy transfer. Step 5: emission of eYFP.

1.10 Calcium Assay

Similar to β-arrestin 2 recruitment, most GPCRs, including PAR2, initiate calcium release when activated by a ligand, which can also be used for a biological assay. Usually this calcium acts as a secondary messenger for the cell and delivers a cellular response. In this assay, a fluorescent dye, Fluo-4, is incubated with PAR2-expressing cells. Fluo-4 enters the cell, is activated by an enzyme, chelates calcium, and subsequently, emits fluorescence following the appropriate excitation (Figure 1.8). To reduce extracellular calcium reporting, Fluo-4 is designed to be activated only by intracellular enzymes. The

inactive Fluo-4 cannot chelate calcium and can passively diffuse across the cell membrane. The activated Fluo-4 can chelate calcium and cannot diffuse across the cell membrane, thereby ‘trapping’ it inside the cell and chelating only intracellular calcium. To control for variation within the experiment, each measurement is expressed as a percentage of maximum fluorescence through the use of ionomycin. Ionomycin is an ionophore that substantially increases the permeability of the cell membrane to calcium; since the extracellular fluid is supplemented with calcium, the limiting factor in the maximum response is the activated Fluo-4. This assay was used to determine PAR2 selective binding through the use of cells expressing and not expressing PAR2.

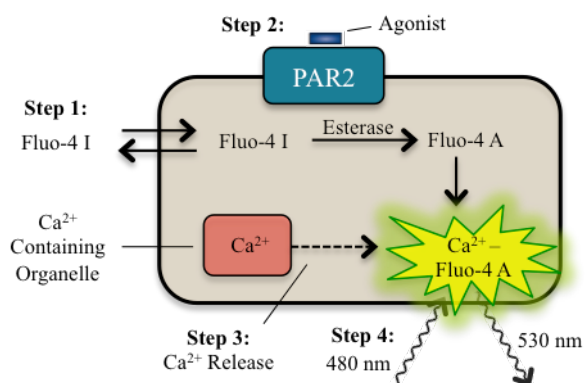


Figure 1.8: Calcium assay principle for a PAR2-expressing cell.

Step 1: passive uptake of Fluo-4 I (inactive) and esterase conversion to Fluo-4 A (active). Step 2: binding of agonist to PAR2. Step 3: calcium release due to agonist binding. Step 4: excitation and emission of Fluo-4 A chelated calcium.

1.11 Purpose of Thesis

The purpose of this thesis is to develop and evaluate an improved fluorescent and the first ever *in vivo* imaging agents targeting PAR2. The first goal was to synthesize and evaluate novel PAR2-targeting peptides with primary amines to allow for facile conjugation of imaging components based on known PAR2-selective peptides. The second goal was to develop an improved PAR2-selective fluorescent probe through the conjugation of a Sulfo-Cy5 NHS ester dye to the lead peptide. The third goal was to develop the first ever *in vivo* imaging agent targeting PAR2 through the radiolabeling of the lead peptide with

[¹⁸F]SFB for use in PET imaging. To determine the lead candidates for radiolabeling, peptide standards with [¹⁹F]4-fluorobenzoyl were synthesized and evaluated for PAR2-binding prior to radiolabeling. All peptides were synthesized through standard Fmoc-solid phase peptide synthesis (SPPS) and screened for their imaging ability by determining PAR2 potency using a BRET β-arrestin 2 recruitment assay, PAR2 selectivity using a calcium signaling assay, and hydrophobicity/hydrophilicity using clogD values. Lead imaging agents were then evaluated *in vitro* in prostate cancer cells and will continue to be evaluated *ex vivo* and *in vivo* in a preclinical model of prostate cancer.

1.12 References

- (1) Ramachandran, R.; Noorbakhsh, F.; DeFea, K.; Hollenberg, M. D. *Nat. Rev. Drug Discov.* **2012**, *11* (1), 69–86.
- (2) Yau, M.-K.; Lim, J.; Liu, L.; Fairlie, D. P. *Expert Opin. Ther. Pat.* **2016**, *26* (4), 471–483.
- (3) Nystedt, S.; Emilsson, K.; Larsson, a K.; Strömbeck, B.; Sundelin, J. *Eur. J. Biochem.* **1995**, *232* (1), 84–89.
- (4) Bohm, S. K.; Kong, W.; Bromme, D.; Smeekens, S. P.; Anderson, D. C.; Connolly, A.; Kahn, M.; Nelken, N. A.; Coughlin, S. R.; Payan, D. G.; Bunnett, N. W. *Biochem. J.* **1996**, *314* (12), 1009–1016.
- (5) Fagerberg, L.; Hallström, B. M.; Oksvold, P.; Kampf, C.; Djureinovic, D.; Odeberg, J.; Habuka, M.; Tahmasebpoor, S.; Danielsson, A.; Edlund, K.; Asplund, A.; Sjöstedt, E.; Lundberg, E.; Szigartyo, C. A.-K.; Skogs, M.; Takanen, J. O.; Berling, H.; Tegel, H.; Mulder, J.; Nilsson, P.; Schwenk, J. M.; Lindskog, C.; Danielsson, F.; Mardinoglu, A.; Sivertsson, Å.; von Feilitzen, K.; Forsberg, M.; Zwahlen, M.; Olsson, I.; Navani, S.; Huss, M.; Nielsen, J.; Ponten, F.; Uhlén, M. *Mol. Cell. Proteomics* **2014**, *13* (2), 397–406.
- (6) Cocks, T. M.; Fong, B.; Chow, J. M.; Anderson, G. P.; Frauman, A. G.; Goldie, R. G.; Henry, P. J.; Carr, M. J.; Hamilton, J. R.; Moffatt, J. D. *Nature* **1999**, *398* (6723), 156–160.
- (7) Damiano, B. P.; Cheung, W. M.; Santulli, R. J.; Fung-Leung, W. P.; Ngo, K.; Ye, R. D.; Darrow, a L.; Derian, C. K.; de Garavilla, L.; Andrade-Gordon, P. J. *Pharmacol. Exp. Ther.* **1999**, *288* (2), 671–678.
- (8) Su, S.; Li, Y.; Luo, Y.; Sheng, Y.; Su, Y.; Padia, R. N.; Pan, Z. K.; Dong, Z.; Huang, S. *Oncogene* **2009**, *28* (34), 3047–3057.
- (9) Antoniak, S.; Rojas, M.; Spring, D.; Bullard, T. A.; Verrier, E. D.; Blaxall, B. C.; MacKman, N.; Pawlinski, R. *Arterioscler. Thromb. Vasc. Biol.* **2010**, *30* (11), 2136–2142.
- (10) Chang, J. H.; Park, J. M.; Kim, S. W.; Jung, C. K.; Kang, W. K.; Oh, S. T. *Dis. Colon Rectum* **2010**, *53* (8), 1202–1208.
- (11) Kim, D. H.; Cho, Y. J.; Kim, J. H.; Kim, Y. B.; Lee, K. J. *J. Korean Med. Sci.* **2010**, *25* (9), 1330–1335.
- (12) Lohman, R.-J.; Cotterell, A. J.; Barry, G. D.; Liu, L.; Suen, J. Y.; Vesey, D. A.; Fairlie, D. P. *FASEB J.* **2012**, *26* (7), 2877–2887.
- (13) Aman, M.; Ohishi, Y.; Imamura, H.; Shinozaki, T.; Yasutake, N.; Kato, K.; Oda, Y. *Hum. Pathol.* **2017**, *64*, 156–163.
- (14) Cenac, N.; Coelho, A. M.; Nguyen, C.; Compton, S.; Andrade-Gordon, P.; MacNaughton, W. K.; Wallace, J. L.; Hollenberg, M. D.; Bunnett, N. W.; Garcia-Villar, R.; Bueno, L.; Vergnolle, N. *Am. J. Pathol.* **2002**, *161* (5), 1903–1915.

- (15) Ferrell, W. R.; Lockhart, J. C.; Kelso, E. B.; Dunning, L.; Plevin, R.; Meek, S. E.; Smith, A. J. H.; Hunter, G. D.; Mclean, J. S.; McGarry, F.; Ramage, R.; Jiang, L.; Kanke, T.; Kawagoe, J. *J. Clin. Invest.* **2003**, *111* (1), 35–41.
- (16) Jin, E.; Fujiwara, M.; Pan, X.; Ghazizadeh, M.; Arai, S.; Ohaki, Y.; Kajiwara, K.; Takemura, T.; Kawanami, O. *Cancer* **2003**, *97* (3), 703–713.
- (17) Massi, D.; Naldini, A.; Ardinghi, C.; Carraro, F.; Franchi, A.; Paglierani, M.; Tarantini, F.; Ketabchi, S.; Cirino, G.; Hollenberg, M. D.; Geppetti, P.; Santucci, M. *Hum. Pathol.* **2005**, *36* (6), 676–685.
- (18) Caruso, R.; Pallone, F.; Fina, D.; Gioia, V.; Peluso, I.; Caprioli, F.; Stolfi, C.; Perfetti, A.; Spagnoli, L. G.; Palmieri, G.; MacDonald, T. T.; Monteleone, G. *Am. J. Pathol.* **2006**, *169* (1), 268–278.
- (19) Fujimoto, D.; Hirono, Y.; Goi, T.; Katayama, K.; Hirose, K.; Yamaguchi, A. *J. Surg. Oncol.* **2006**, *93* (2), 139–144.
- (20) Black, P. C.; Mize, G. J.; Karlin, P.; Greenberg, D. L.; Hawley, S. J.; True, L. D.; Vessella, R. L.; Takayama, T. K. *Prostate* **2007**, *67*, 743–756.
- (21) Hyun, E.; Andrade-Gordon, P.; Steinhoff, M.; Vergnolle, N. *Gut* **2008**, *57* (9), 1222–1229.
- (22) Shi, X.; Gangadharan, B.; Brass, L. F.; Ruf, W.; Mueller, B. M. *Mol. Cancer Res.* **2004**, *2* (7), 395–402.
- (23) Uusitalo-Jarvinen, H.; Kurokawa, T.; Mueller, B. M.; Andrade-Gordon, P.; Friedlander, M.; Ruf, W. *Arterioscler. Thromb. Vasc. Biol.* **2007**, *27* (6), 1456–1462.
- (24) Kamath, L.; Meydani, A.; Foss, F. *Cancer Res.* **2001**, *61*, 5933–5940.
- (25) Jahan, I.; Fujimoto, J.; Alam, S. M.; Sato, E.; Sakaguchi, H.; Tamaya, T. *Ann. Oncol.* **2007**, *18* (9), 1506–1512.
- (26) What is Molecular Imaging. The American Board of Nuclear Medicine. <https://www.abnm.org/> (accessed July 18, 2018).
- (27) Meikle, S. R.; Kench, P.; Kassiou, M.; Banati, R. B. *Phys. Med. Biol.* **2005**, *50* (22).
- (28) Croney, J. C.; Jameson, D. M.; Learmonth, R. P. *Biochem. Mol. Biol. Educ.* **2001**, *29* (2), 60–65.
- (29) James, M. L.; Gambhir, S. S. *Physiol. Rev.* **2012**, *92* (2), 897–965.
- (30) Orosco, R. K.; Tsien, R. Y.; Nguyen, Q. T. *IEEE Rev. Biomed. Eng.* **2013**, *6*, 178–187.
- (31) Jacobson, O.; Kiesewetter, D. O.; Chen, X. *Bioconjug. Chem.* **2014**, *26*, 1–18.
- (32) Schubiger, P. A.; Lehmann, L.; Friebe, M. *PET Chemistry book*; 2007.
- (33) Reddy, S.; Robinson, M. *Semin Nucl Med* **2010**, *40* (3), 182–189.
- (34) Nystedt, S.; Emilsson, K.; Wahlestedt, C.; Sundelin, J. *Proc. Natl. Acad. Sci.* **1994**,

- 91 (20), 9208–9212.
- (35) Al-Ani, B.; Saifeddine, M.; Hollenberg, M. D. *Can. J. Physiol. Pharmacol.* **1995**, *73* (8), 1203–1207.
- (36) Hollenberg, M. D.; Saifeddine, M.; Al-Ani, B.; Kawabata, A. *Can. J. Physiol. Pharmacol.* **1997**, *75* (7), 832–841.
- (37) Kanke, T.; Ishiwata, H.; Kabeya, M.; Saka, M.; Doi, T.; Hattori, Y.; Kawabata, A.; Plevin, R. *Br. J. Pharmacol.* **2005**, *145* (2), 255–263.
- (38) Kanke, T.; Kabeya, M.; Kubo, S.; Kondo, S.; Yasuoka, K.; Tagashira, J.; Ishiwata, H.; Saka, M.; Furuyama, T.; Nishiyama, T.; Doi, T.; Hattori, Y.; Kawabata, A.; Cunningham, M.; Plevin, R. *Br. J. Pharmacol.* **2009**, *158* (1), 361–371.
- (39) Barry, G. D.; Suen, J. Y.; Low, H. B.; Pfeiffer, B.; Flanagan, B.; Halili, M.; Le, G. T.; Fairlie, D. P. *Bioorganic Med. Chem. Lett.* **2007**, *17* (20), 5552–5557.
- (40) Hollenberg, M. D.; Renaux, B.; Hyun, E.; Houle, S.; Vergnolle, N.; Saifeddine, M.; Ramachandran, R. *J Pharmacol Exp Ther* **2008**, *326* (2), 453–462.
- (41) Hoffman, J.; Flynn, A. N.; Tillu, D. V.; Zhang, Z.; Patek, R.; Price, T. J.; Vagner, J.; Boitano, S. *Bioconjug. Chem.* **2012**, *23* (10), 2098–2104.
- (42) Yau, M. K.; Suen, J. Y.; Xu, W.; Lim, J.; Liu, L.; Adams, M. N.; He, Y.; Hooper, J. D.; Reid, R. C.; Fairlie, D. P. *ACS Med. Chem. Lett.* **2016**, *7* (1), 105–110.
- (43) Jiang, Y.; Yau, M. K.; Kok, W. M.; Lim, J.; Wu, K. C.; Liu, L.; Hill, T. A.; Suen, J. Y.; Fairlie, D. P. *ACS Chem. Biol.* **2017**, *12* (5), 1217–1226.
- (44) Barry, G. D.; Suen, J. Y.; Le, G. T.; Cotterell, A.; Reid, R. C.; Fairlie, D. P. *J. Med. Chem.* **2010**, *53* (20), 7428–7440.
- (45) Lasne, M.-C.; Perrio, C.; Rouden, J.; Barré, L.; Roeda, D.; Dolle, F.; Crouzel, C. *Top. Curr. Chem.* **2002**, *222*, 203–258.
- (46) Olberg, D. E.; Hjelstuen, O. K. *Curr. Top. Med. Chem.* **2010**, *10* (16), 1669–1679.
- (47) Patrick, G. L. *An Introduction to Medicinal Chemistry*; 2013.
- (48) MedChem Designer ADMET Predictor, version 3.1.0.30, Simulations Plus, Inc., California, US.
- (49) Rajagopal, S.; Rajagopal, K.; Lefkowitz, R. J. *Nat. Rev. Drug Discov.* **2010**, *9* (5), 373–386.
- (50) Rankovic, Z.; Brust, T. F.; Bohn, L. M. *Bioorganic Med. Chem. Lett.* **2016**, *26* (2), 241–250.

Chapter 2

2 A Potent and High Affinity Fluorescent Probe for Protease-Activated Receptor 2

2.1 Introduction

Protease-activated receptors (PARs) are a class of G protein-coupled receptors (GPCRs) that are self-activated by a tethered ligand after a protease cleaves an N-terminal portion of the protein. There are four subtypes, denoted PAR1-PAR4. In PAR2, various proteases (e.g. trypsin, tryptase, Granzyme A, KLK4) are known to reveal the tethered ligand sequence SLIGKV (humans) and SLIGRL (rodents).¹⁻⁵

PAR2 is naturally expressed in various tissues (e.g. pancreas, liver, small intestine, colon) and is involved in inflammation and cell migration.⁶⁻⁸ However, abnormal function and inappropriate expression of PAR2 has been linked to various cancers and inflammatory diseases. More specifically, PAR2 is implicated in conditions such as arthritis, colitis, asthma, cardiovascular disease, prostate cancer, lung cancer, gastric cancer, melanoma, ovarian cancer, and breast cancer.⁹⁻²³ In cancerous tissue, this undesirable activity of PAR2 has been shown to significantly contribute to cell proliferation, angiogenesis, and metastasis.^{11,24,25}

Exogenous agonists have been developed, which bind and activate PAR2. Initial reports synthesized and evaluated peptides that resemble the tethered ligand sequences SLIGKV and SLIGRL as well as their amidated analogues, and showed that SLIGRL-NH₂ (**1**, Figure 2.1) had the highest potency/affinity for human PAR2, which has thus been widely used as a PAR2 agonist with micromolar potency.^{2,26,27} Extensive structure-activity relationship studies have involved substitutions of various natural and unnatural amino acids into these sequences, generating peptides with improved potency. In particular, substituting the serine residue in the first position with various heterocycles (e.g. 2-furoyl, 5-isoxazoloyl, 3-pyridoyl, 4-(2-methyloxazoloyl), and 2-aminothiazol-4-oyl) has substantially improved potency and affinity for PAR2.²⁸ Of these, 2-furoyl (2f) based peptides initially showed the best improvements and have been the most widely used.

Addition of ornithine to the C-terminus of the 2f-LIGRL-NH₂ hexapeptide (**2**, Figure 2.1) and conjugation of various bulky substituents to the side chain of that ornithine (e.g. Alexa Fluor 594, **3** and DTPA(Eu), **4**, Figure 2.1) have shown no appreciable effect on their potency, affinity, or selectivity for PAR2.^{29,30} More recently, Isox-Cha-Chg (5-isoxazoloyl-cyclohexylalanine-cyclohexylglycine) based peptides developed by Yau et al. (2016) and Jiang et al. (2017), most notably Isox-Cha-Chg-AR-NH₂ (**7**, Figure 2.1), have shown substantial improvements in potency and affinity for PAR2.^{31,32}

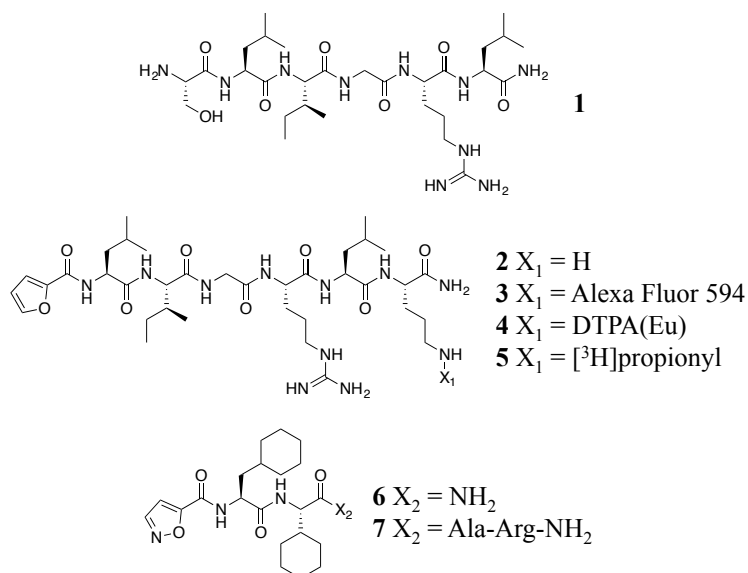


Figure 2.1: Known PAR2-targeting peptide agonists.^{26,29–33}

PAR2-targeting imaging probes developed to date have been limited, with only several fluorescent and tritiated probes having been reported.^{27,29,30,34,35} In particular, **3** has been the best fluorescent probe developed thus far with sub-micromolar affinity and with an Alexa Fluor 594 fluorescent dye (excitation maximum = 590 nm, emission maximum = 617 nm).²⁹ Development of higher affinity fluorescent probes improve uptake in cells and tissues expressing the receptor, which can result in benefits such as reduced off target binding, less compound required, and reduced adverse effects. Development of red-shifted fluorescent probes allow for improved *in vivo* imaging in small animals due to less absorption and scattering from biomolecules of the red-shifted light compared to blue-shifted light. Fluorescent probes targeting this receptor can act as useful chemical tools for various *in vitro* experiments (e.g. competitive binding assays, determination of

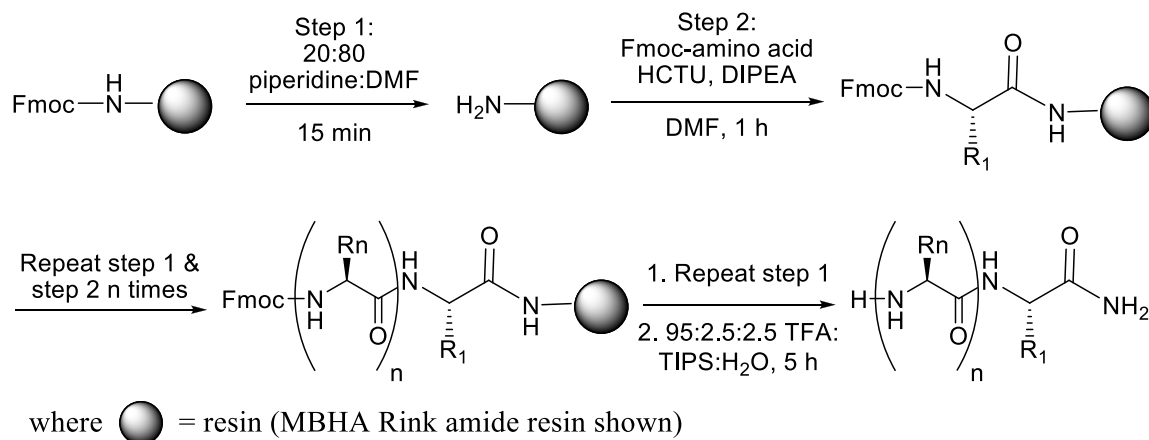
PAR2 expression levels, insight into PAR2 trafficking), for imaging PAR2 in small animals *in vivo*, and that have potential clinical relevance in PAR2-related diseases such as in pathological histology staining or intraoperative imaging for image guided surgery.

This work describes the development of Isox-Cha-Chg-AR-NH₂ related peptides that would allow for facile conjugation of imaging components in order to develop an improved PAR2-targeting fluorescent probe with low nanomolar affinity/potency for PAR2 and with a red-shifted fluorescent dye (Sulfo-Cy5, excitation maximum = 646 nm, emission maximum = 662 nm). In addition, this work describes the evaluation of the improved fluorescent probe *in vitro*. The insights gained from compounds like **3** and **4**, as well as reports demonstrating that the N-terminal portion of PAR2-targeting peptides are much more crucial for binding than the C-terminal portion, led us to make modifications to the C-terminus of **7** that contain a free primary amine for Sulfo-Cy5 dye conjugation.^{29,30,32}

2.2 Results and Discussion

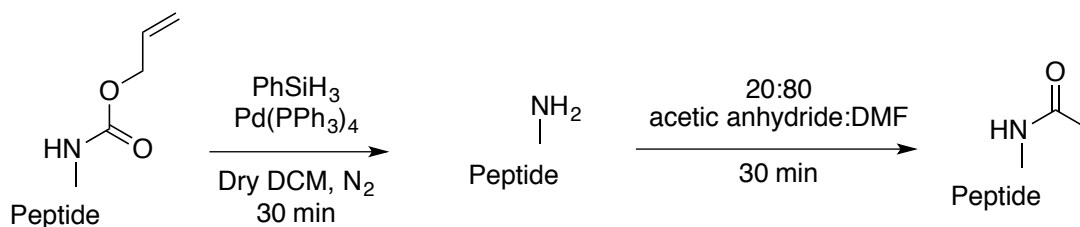
2.2.1 General Peptide Synthesis Strategy

All peptides (**2**, **6-12**, and **14-15**) were synthesized using standard Fmoc-solid phase peptide synthesis (SPPS) using a solid support MBHA Rink amide resin or 1,6-diaminohexane trityl resin (Scheme 2.1).



Scheme 2.1: General procedure for Fmoc-SPPS.

In addition to standard Fmoc-SPPS, **12** utilized an orthogonal protecting group, allyloxycarbonyl (Alloc), followed by subsequent acetylation for its synthesis (Scheme 2.2).



Scheme 2.2: Alloc deprotection and subsequent acetylation.

2.2.2 Design, Synthesis, and Evaluation of PAR2-Targeting Peptides

All Peptides were synthesized and evaluated for PAR2-binding through a β -arrestin 2 recruitment assay in HEK293T cells in an effort to develop a more potent, higher affinity

PAR2-selective fluorescent probe. In this assay and cell line reported here, compounds **1**, **2**, **6**, and **7** showed a similar potency trend to previous reports of binding affinity for PAR2 ($7 \gg 2 \gg 6 > 1$, from most to least potent, Table 2.1).^{27,29,32} Following these results, the best reported PAR2-targeting peptide (**7**) from Jiang et al. (2017) was modified with a primary amine on the C-terminus in various ways. These modifications were made since conjugation of imaging components directly to **7** was not synthetically feasible and because the addition of a linker region between the targeting moiety and the imaging moiety would help keep bulky substituents (e.g. Sulfo-Cy5) from interfering with the receptor-ligand interactions.

The first approach was the addition of an aminohexyl spacer extending from the peptide backbone of **7** to yield **8**. This was intended such that conjugation of the dye to the C-terminus would allow the dye to lie outside of the receptor binding pocket. This modification resulted in minimal to no reduction in potency but an increase in hydrophobicity from -0.85 to -0.70 (Table 2.1). This hydrophobicity change was disconcerting because the addition of the Sulfo-Cy5 dye to the peptides will cause an additional substantial increase in hydrophobicity, which is a concern for water solubility in its various current and future applications (e.g. *in vitro* experiments).

Table 2.1: PAR2-targeted peptides (**1-2** and **6-12**) with their EC₅₀ and cLogD values.

#	Compound	EC ₅₀ (nM)	pEC ₅₀ ± SEM	cLogD at pH 7.4
1	SLIGRL-NH ₂	7144	5.15 ± 0.03	-1.93
2	2f-LIGRLO-NH ₂	210	6.68 ± 0.04	-2.71
6	Isox-Cha-Chg-NH ₂	2555	5.59 ± 0.10	2.29
7	Isox-Cha-Chg-AR-NH ₂	14	7.86 ± 0.06	-0.85
8	Isox-Cha-Chg-AR-NH(CH ₂) ₆ NH ₂	16	7.79 ± 0.04	-0.70
9	Isox-Cha-Chg-ARLK-NH ₂	23	7.65 ± 0.07	-1.29
10	Isox-Cha-Chg-ARAK-NH ₂	15	7.82 ± 0.07	-1.77
11	Isox-Cha-Chg-ARK-NH ₂	10	8.00 ± 0.09	-1.72
12	Isox-Cha-Chg-ARK(COCH ₃)-NH ₂	16	7.78 ± 0.05	-0.84

EC₅₀ values determined through a dose-response curve from a β-arrestin 2 recruitment assay in HEK293T cells. cLogD values calculated through Simulations Plus MedChem Designer ADMET Predictor.

In an effort to reduce solubility concerns, **9** was synthesized. The addition of leucine-lysine (position 6 and 7) to the C-terminus of **7** was synthesized to resemble the

previously reported **2**, which added ornithine (position 7) to the C-terminus of 2f-LIGRL-NH₂. Although this modification lowered the hydrophobicity, it showed a decrease in potency (Table 2.1). From here, alanine-lysine was added to the C-terminus of **7** to further decrease hydrophobicity and to reduce steric bulk at position 6 while still allowing for the same peptide backbone length as **9** and **2**. This yielded **10**, which was found to have improved potency and hydrophobicity (Table 2.1). Compound **11** was synthesized through the direct addition of lysine to the C-terminus of **7**. It had a similar cLogD as **10** and fortunately showed a slight improvement in potency compared to **7** and **10** (Table 2.1). Therefore, **11** was taken forward as the lead candidate.

The lysine side chain of **11** was then acetylated to observe the effect of losing this positive charge. This yielded **12**, which was found to have only a slight reduction in potency compared to **11** (EC₅₀ = 16 nM vs. EC₅₀ = 10 nM, Table 2.1), suggesting this charge was not crucial for PAR2 binding, making **11** a good candidate to label with a fluorescent dye.

In addition to potency and hydrophobicity measures, receptor selectivity was also assessed through an intracellular calcium release assay to ensure the synthesized peptides target PAR2 specifically. All known and novel PAR2-targeting peptides (**1-2** and **6-12**) were found to bind selectively to the PAR2 receptor (Table 2.2, see Appendix 1 for PAR2-selectivity traces). This was evaluated by comparing calcium response in HEK293T cells expressing PAR2 compared to PAR2 knock out (KO) HEK293T cells. As a control, a PAR1-specific agonist (TFLLR-NH₂, **13**) was assessed for its calcium response in both of these cell lines as they both contain the PAR1 receptor (Table 2.2). These cells and this control were used (similar to previous reports) because it is known that some PAR2-targeting peptides can also bind to PAR1.^{31,32,36,37}

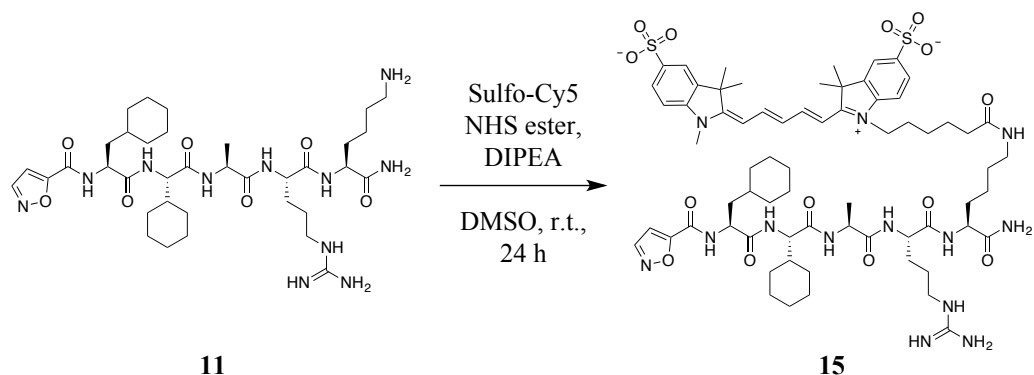
Table 2.2: PAR2 selectivity of peptides **1-2** and **6-12**.

#	Net % max Ca ²⁺ release in PAR2 expressing cells ± SEM	Net % max Ca ²⁺ release in PAR2 KO cells ± SEM
13	49.3 ± 4.4	67.5 ± 6.6
1	53.4 ± 7.9	-0.5 ± 0.5
2	53.0 ± 6.4	0.7 ± 1.2
6	17.2 ± 4.2	-1.4 ± 1.3
7	64.6 ± 4.9	-0.5 ± 0.5
8	68.6 ± 9.3	0.0 ± 0.4
9	69.9 ± 4.1	-0.4 ± 0.4
10	67.3 ± 3.9	-1.1 ± 0.5
11	72.0 ± 5.0	-0.9 ± 0.3
12	67.3 ± 2.6	-1.4 ± 0.5

Selectivity measures are shown as calcium response in PAR2 expressing (column two) versus PAR2 KO (column three) HEK293T cells.

2.2.3 Synthesis and Evaluation of PAR2-Targeting Fluorescent Probes

The lead candidate (**11**) was labeled through the lysine side chain with a Sulfo-Cy5 NHS ester fluorescent dye to yield compound **15** (Scheme 2.3). Compound **14** was synthesized to resemble the previously reported PAR2-targeting fluorescent probe with the highest potency/affinity (**3**).²⁹ Compound **14** contains an identical PAR2-targeting peptide sequence compared to **3**, but utilizes Sulfo-Cy5 dye conjugated through the ornithine side chain as opposed to an Alexa Fluor 594 dye. The Sulfo-Cy5 dye allows for a more direct comparison between the novel Sulfo-Cy5 dye conjugated peptide **15** reported here as well as it is a red-shifted and less costly dye. The potency of **14** (EC₅₀ = 296 nM, Table 2.3) was similar to its unlabeled counterpart, **2** (EC₅₀ = 210 nM, Table 2.1), which is consistent with previous reports of analogous probes modified from this peptide sequence.^{29,38} Compound **15** also showed similar potency (EC₅₀ = 16 nM, Table 2.3) compared to its unlabeled counterpart, **11** (EC₅₀ = 10 nM, Table 2.1). More importantly, **15** was found to have a greater than ten-fold increase in potency compared to **14** (EC₅₀ = 16 nM vs. EC₅₀ = 296 nM, Table 2.3, Figure 2.2).



Scheme 2.3: Synthesis of PAR2-selective fluorescent probe, **15**.

Table 2.3: Evaluation of Sulfo-Cy5 labeled peptides (**14** and **15**).

#	Compound	EC ₅₀ (nM)	pEC ₅₀ ± SEM	K _D (nM)	pK _D ± SEM	cLogD at pH 7.4
14	2f-LIGRLIO(Sulfo-Cy5)-NH ₂	296	6.53 ± 0.05	430	6.24 ± 0.13	3.57
15	Isox-Cha-Chg-ARK(Sulfo-Cy5)-NH ₂	16	7.81 ± 0.09	38	7.20 ± 0.22	3.94

EC₅₀ values determined through a dose-response curve from a β-arrestin 2 recruitment assay in HEK293T cells. K_D values determined through a flow cytometry saturation binding experiment. cLogD values calculated through Simulations Plus MedChem Designer ADMET Predictor.

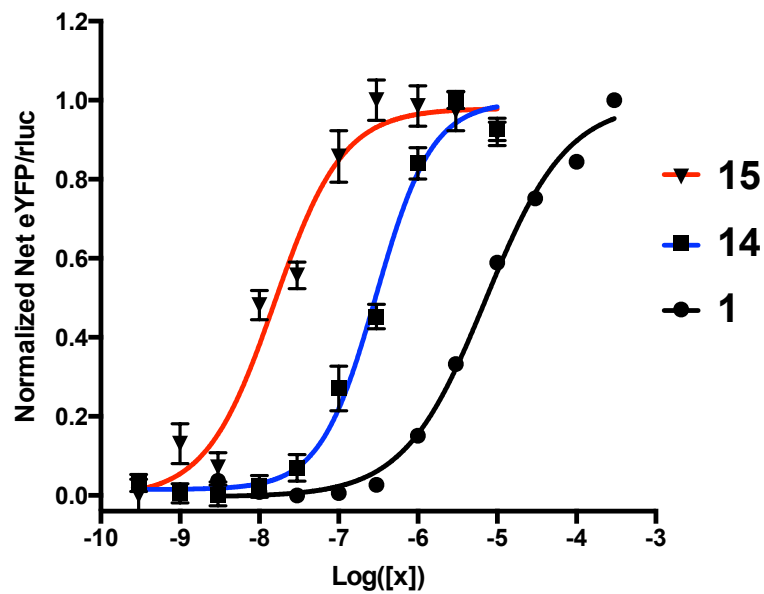


Figure 2.2: PAR2 β -arrestin 2 recruitment dose-response curves for compound **1**, **14**, and **15** in HEK293T cells.

Similar to the increase in potency, **15** had a similar increase in affinity compared to **14** (>10 fold) for PAR2 as determined through a saturation binding experiment using flow cytometry ($K_D = 38$ nM vs. $K_D = 430$ nM, Table 2.3, and binding curves shown in Figure 2.3). As a control, competition of **14** and **15** with an excess of a known PAR2-specific peptide (**7**) was completed, which showed a substantial decrease in fluorescence signal for both of the fluorescent peptides (see Appendix 2).

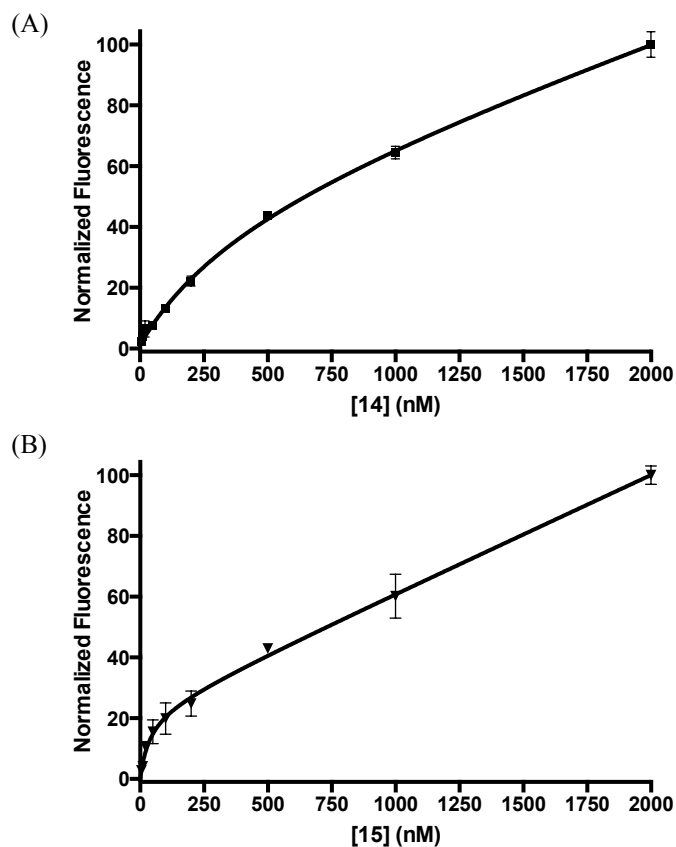


Figure 2.3: Saturation binding experiments of (A) **14** and (B) **15** in HEK293T cells for determination of affinity measures (K_D).

Compound **15** was further evaluated for its *in vitro* applications using confocal microscopy. It was found that this fluorescent probe binds selectively to the receptor and does not passively diffuse the cell membrane (Figure 2.4). This is demonstrated by the PAR2 expressing PC3 cells showing significant uptake of **15** (Figure 2.4A) compared to no uptake in the controls (PAR2 KO PC3 cells, Figure 2.4B, PAR2 expressing PC3 cells blocked with excess of an unlabeled known PAR2-selective peptide, **7**, Figure 2.4C, and PAR2 KO PC3 cells with excess of **7**, Figure 2.4D).

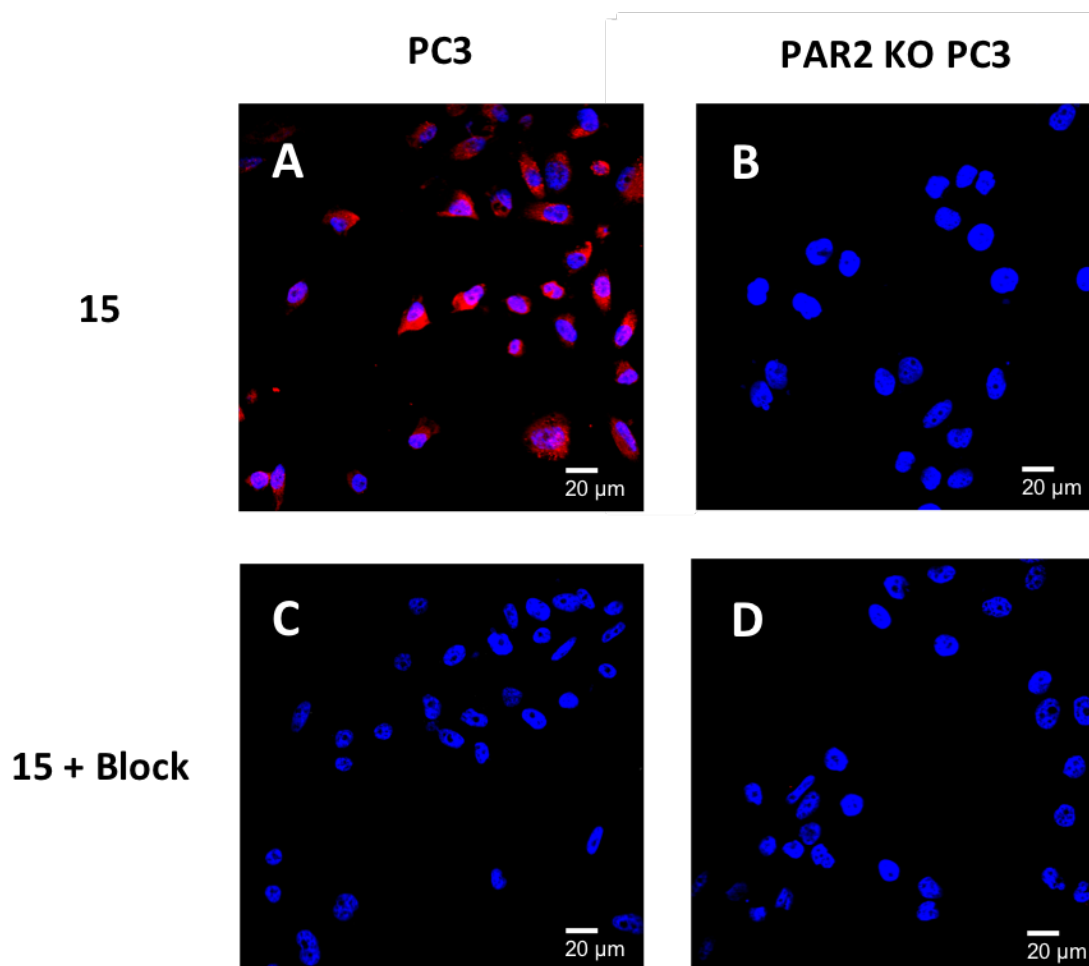


Figure 2.4: Confocal microscopy of **15** in PC3 cells and PAR2 KO PC3 cells.

Compound **15** (250 nM final concentration) incubated with (A) PC3 cells and (B) PAR2 KO PC3 cells. Compound **15** (250 nM final concentration) and PAR2-selective blocking peptide, **7** (2500 nM final concentration) co-incubated with (C) PC3 cells and (D) PAR2 KO PC3 cells. Uptake of **15** was effectively blocked upon co-incubation with **7**. Sulfo-Cy5 signal shown in red and DAPI signal shown in blue. Size reference = 20 μm.

2.3 Conclusions

The novel peptides described here show high potency and selectivity for PAR2. The various modifications led to slightly different structural and hydrophobic properties and each allow for facile conjugation of various imaging components (NHS ester dyes, common radioactive prosthetic groups, etc.) while showing minimal to no detrimental effect on PAR2 binding. To the best of our knowledge, compound **15** is the most potent,

highest affinity PAR2-targeting fluorescent probe reported to date with a red-shifted fluorophore and a greater than ten-fold improvement in potency and affinity when compared to the best previously reported probe.²⁹ Compound **15** was also validated in an *in vitro* confocal microscopy experiment, further demonstrating its candidacy as a useful chemical tool for various *in vitro* experiments as well as potential clinical relevance in PAR2-related diseases.

2.4 Experimental Procedures

2.4.1 General Methods

All reagents were purchased from Sigma-Aldrich, ChemImpex, or Thermo Fischer Scientific and used without further purification. Peptides were synthesized using standard Fmoc-solid phase peptide synthesis (SPPS), cleaved from resin using 95% TFA, 2.5% TIPS, and 2.5% H₂O for 5 h (except **8**: 20% TFA, 2.5% TIPS, 77.5% DCM for 1.5 h), precipitated in ice cold *tert*-butyl methyl ether, lyophilized, purified by preparative RP-HPLC, and further lyophilized to obtain a dry powder. Purity was assessed by analytical RP-HPLC and characterized by HRMS (Table 2.4). The analytical RP-HPLC was performed on a system consisting of an analytical Agilent Zorbax SB-C8 column (4.6 x 150 mm, 5 μ m), Waters 600 controller, Waters in-line degasser, and Waters Masslynx software (version 4.1). Two mobile phases were used; eluent A (0.1% TFA in acetonitrile) and eluent B (0.1% TFA in MilliQ water). The flow rate was set at 1.5 mLmin⁻¹ over 10 minutes with an additional 5-minute wash (95% solvent A in solvent B). A Waters 2998 Photodiode array detector (200-800 nm) and an ESI-MS (Waters Quattro Micro API mass spectrometer) were used to monitor the column eluate. The preparative RP-HPLC used the same system, eluents, and detection method as mentioned above for the analytical RP-HPLC, except that a preparative Agilent Zorbax SB-C8 column (21.2 x 150 mm, 5 μ m) at a flow rate of 20 mLmin⁻¹ was used. The high-resolution mass spectra for all peptides were determined in positive or negative mode using an electrospray ionization (ESI) ion source on a Bruker micrOToF II mass spectrometer. Simulations Plus MedChem Designer ADMET Predictor was used to

determine the cLogD values at a pH of 7.4.³⁹ All descriptive statistics are reported as mean \pm SEM where applicable.

Table 2.4: HRMS data and purity of peptides **2**, **6-12**, and **14-15**.

Cmpd #	Molecular Formula (M)	Evaluated HRMS m/z	Calc. m/z	Found m/z	Purity
2	C ₃₆ H ₆₃ N ₁₁ O ₈	[M+H] ⁺	778.4939	778.4945	> 95 %
6	C ₂₁ H ₃₂ N ₄ O ₄	[M+Na] ⁺	427.2321	427.2309	> 95 %
7	C ₃₀ H ₄₉ N ₉ O ₆	[M+H] ⁺	632.3884	632.3892	> 95 %
8	C ₃₆ H ₆₂ N ₁₀ O ₆	[M+H] ⁺	731.4932	731.4944	> 95 %
9	C ₄₂ H ₇₂ N ₁₂ O ₈	[M+H] ⁺	873.5674	873.5685	> 95 %
10	C ₃₉ H ₆₆ N ₁₂ O ₈	[M+H] ⁺	831.5205	831.5197	> 95 %
11	C ₃₆ H ₆₁ N ₁₁ O ₇	[M+H] ⁺	760.4834	760.4841	> 95 %
12	C ₃₈ H ₆₃ N ₁₁ O ₈	[M+H] ⁺	802.4939	802.4952	> 95 %
14	C ₆₈ H ₉₈ N ₁₃ O ₁₅ S ₂ ⁻	M ⁻	1400.6747	1400.6714	> 95 %
15	C ₆₈ H ₉₆ N ₁₃ O ₁₄ S ₂ ⁻	M ⁻	1382.6641	1382.6589	> 95 %

Purity assessed by analytical RP-HPLC UV detection.

2.4.2 Solid-Phase Peptide Synthesis

All compounds (except **8**) were synthesized on Rink amide MBHA resin (256 mg, 0.1 mmol, 0.39 mmol/g) using standard Fmoc-SPPS procedures and a Biotage® Syrowave™ automated peptide synthesizer (0.4 mmol of HCTU, 0.4 mmol of Fmoc-amino acids, 0.6 mmol of DIPEA, 1 h coupling). Manual coupling of 5-isoxazolyl (0.3 mmol) was performed using HATU (0.3 mmol) and DIPEA (0.6 mmol) for 24 h twice. Compound **8** was synthesized on 1,6-diaminohexane trityl resin (256 mg, 0.1 mmol, 0.39 mmol/g).

2.4.3 Solid-Phase Synthesis of **12**

The peptide sequence of **12** was synthesized on resin as described above but with Fmoc-Lys(Alloc)-OH used in position 6. Subsequently this sequence underwent an Alloc deprotection. The resin was swelled in DCM (15 min), washed thrice with dry DCM (3X 5 mL), and placed under an inert N₂ atmosphere. Phenylsilane (296 μ L, 2.4 mmol) in dry DCM (2 mL) was added to the resin. Tetrakis(triphenylphosphine) palladium(0) (23.1 mg, 20 μ mol) was dissolved in dry DCM (1 mL) and added to the resin. The peptide column was flushed with N₂ (2 min) before being shaken (5 min). The resin was washed thrice with dry DCM (3X 5 mL). The procedure was repeated and shaken (30 min). The

resin was washed four times with DCM (4X 5 mL) and DMF (4X 5 mL). Following the Alloc deprotection, a solution of 20% acetic anhydride in DMF (5 mL) was added and shaken (30 min). The final acetylated on resin peptide was cleaved and purified as usual.

2.4.4 SPPS Reaction Monitoring

Two methods were used to monitor SPPS reactions. The first and more frequent method is the Kaiser Test. In this method, several resin beads were placed in a test tube followed by the addition of 42.5 mM phenol in ethanol (50 μ L), 20 μ M potassium cyanide in pyridine (50 μ L), and 280.7 mM ninhydrin in ethanol (50 μ L). The mixture was then heated (100 $^{\circ}$ C, 5 min). A positive test indicates the presence of a free amine, which is observed by the resin beads turning blue. A negative test indicates no free amine is present, which is observed by resin beads remaining the same colour. The second method is a small-scale resin cleavage. In this method, several beads and cleavage cocktail (500 μ L) are shaken, worked up, and the desired peptide is confirmed through HPLC-MS.

2.4.5 Solution-Phase Synthesis of **14** and **15**

Purified **2** or **8** containing a free primary amine (6.16 mg or 6.05 mg, respectively, 6.1 μ mol) were dissolved in DMSO (0.5 mL). DIPEA (12.7 μ L, 73 μ mol) was then added to the reaction followed by the addition of Sulfo-Cy5 NHS ester (5.0 mg, 6.4 μ mol) in DMSO (0.5 mL). The mixture was shaken at room temperature in the dark (3 h). The solution was diluted with a water/acetonitrile mixture, frozen, and lyophilized. The product was purified by RP-HPLC, frozen, and lyophilized to yield **14** or **15**.

2.4.6 Cell Lines and Culture Conditions

All cell culture supplies were purchased from Thermo Fischer Scientific (Waltham, MA, US) unless otherwise stated. Human embryonic kidney (HEK-293T, ATCC, Manassas, VA, US), CRISPR/Cas9 PAR2 knockout HEK-293T (validated in Mihara et al., 2016), prostate cancer (PC3, ATCC, Manassas, VA, US), and CRISPR/Cas9 PAR2 knockout PC3 cells (see Appendix 5 for validation) were cultured in Dulbecco's Modified Eagle's Medium (HEK293T-derived cell lines) and Ham's F-12K Nutrient Mixture (PC3-derived cell lines) each supplemented with 10% fetal bovine serum (FBS), sodium pyruvate

(1mM), and 100 penicillin streptomycin (100 units/mL).⁴⁰ All culture performed under standard conditions (37 °C; 5% CO₂). Trypsin (25mM) or PBS-EDTA (1mM) was used to passage cell lines.

2.4.7 BRET β -Arrestin 2 Recruitment Assay

HEK293T cells were transfected with BRET pair PAR2-eYFP (2 μ g) and β -arrestin-2-rluc (0.2 μ g; generous gift from Michel Bouvier) using calcium phosphate and re-plated at 24 hours in tissue culture treated white 96-well plates (density approximately 8×10^2 - 1×10^3 cells/ μ L). Serial dilutions of agonist (ranging from 300 μ M to 300 pM depending on the agonist) were prepared in separate 96-well plates in Hank's Balanced Salt Solution (HBSS). Cell media was removed from 96-well plate containing seeded cells. Agonist was added from negative control (HBSS) through to highest concentration using a multichannel pipette to seeded plates and incubated (37 °C, 10 min). Renilla luciferase substrate (h-coelenterazine) was added to each well (5 μ M final) and incubated (37 °C, 10 min). BRET ratios are recorded on Berthold Mithras LB 940. Responses are expressed as net emission of eYFP/rluc (calculated by subtracting HBSS baseline eYFP/rluc ratio from agonist eYFP/rluc ratio) and normalized to a positive control (1 at 300 μ M). Experiments were completed in $n \geq 3$ and fitted with a non-linear regression analysis four-parameter dose-response curve using GraphPad Prism 6 to determine EC₅₀ values.

2.4.8 Intracellular Calcium Release Assay

HEK293T or PC3 cells endogenously expressing PAR2 or CRISPR/Cas9 HEK293T or PC3 PAR2 KO cells were lifted from confluent T75 flasks using PBS-EDTA (1 mM, 5 mL). PBS-EDTA was removed by centrifugation. Cells were re-suspended in 500 μ L of Fluo-4 NW (no wash) dye solution and assay buffer (1 x HBSS, 20 mM HEPES) and incubated at ambient temperature on a rocking platform (30 min). Fluo-4 NW cell suspensions were then increased to the volume required for the assay with HBSS (with Ca²⁺ and Mg²⁺). Cells were aliquoted into cuvettes (2 mL/cuvette final volume) containing a magnetic stir-bar to keep cells in suspension for the assay. Individual cuvettes were loaded into a Photon Technologies Institute (PTI) spectrophotometer. Time-based assay parameters were assigned through PTI software as follows: excitation

480 nm, emission 530 nm with 8 nm capture window, and 5000 seconds duration. Before the addition of agonist, individual cuvette emission was collected for approximately 10 seconds to obtain baseline emission. Agonist was pipetted into the cuvette (final concentration of 10 μ M for **2** and **6-12** and 100 μ M for **1** and **13**) and the fluorescence was measured. As a positive control, untreated cuvettes were treated with a calcium ionophore (ionomycin calcium salt in DMSO, 3 μ M final) to obtain maximum possible calcium response. As a negative control, untreated cuvettes were treated with HBSS only (no agonist). Response elicited by agonist treatment at individual concentrations ($n \geq 2$) was expressed as a net percentage of the average maximum response (calculated by subtracting no agonist treatment percentage from agonist treatment percentage).

2.4.9 Flow Cytometry for Determination of K_D for **14** and **15** using Saturation Binding Experiments

Assay was performed similar to previous reports.⁴¹ HEK293T cells were removed from 10 cm dish using 5 mL of 1 mM EDTA in PBS. EDTA solution was removed and cell pellet was re-suspended in media. Cells were placed into a 25 mL falcon tube, media removed, and rinsed with 2% FBS in PBS. The cells were then incubated with a 4% paraformaldehyde in PBS solution for 10 min at room temperature followed by being rinsed with 2% FBS in PBS. Cells were aliquoted into 300 000 cell portions, PBS was removed, and incubated with 500 μ L of 2% BSA in HBSS for 15 min at room temperature. Cells were then rinsed with 0.1% BSA in HBSS and incubated with 200 μ L of **14** or **15** at different concentrations (0, 5, 10, 20, 50, 100, 200, 500, 1000, and 2000 nM) in a 0.1% BSA in HBSS solution for 50 min at room temperature. The cell aliquots were washed twice with 1 mL of 2% FBS in PBS, re-suspended in 500 μ L of 2% FBS in PBS, and fluorescence was measured using a Navios flow cytometer [Beckman Coulter]. A 638 nm laser was used for excitation (set at a voltage of 449 V) and detected using a 660/20 band pass filter. Approximately 5000 cells were gated on forward and side scatter, and assessed for Cy5 fluorescence. Experiments were performed in $n \geq 4$. The K_D values for **14** and **15** were calculated using 'Binding – Saturation, One site – Total' (Eqn. 2) through GraphPad Prism 6.

$$Y = \frac{B_{\max} * X}{K_D + X} + NS * X + \text{Background} \quad (2)$$

where,

Y represents normalized fluorescence.

B_{\max} represents maximum specific binding in the same units as Y.

X represents the concentration of **14** or **15** in nM.

K_D represents the equilibrium binding constant in the same units as X. The concentration of **14** or **15** needed to achieve half-maximum binding at equilibrium.

NS represents the slope of non-specific binding in Y units divided by X units.

Background represents the amount of normalized fluorescence with no **14** or **15** added in the same units as Y.

2.4.10 Confocal Microscopy of **15** in PC3 Cells

PC3 cells were seeded to a density of 75 000 cells/well in a 12-well Nunc plate containing coverslips prepared with gelatin (15 minute incubation with a 2% gelatin solution followed by 15 minutes of drying). Cell media was removed 24 hours following seeding and replaced with serum free Ham's F-12K media to remove FBS (1 h, 37 °C). PC3 cells or PAR2 KO PC3 cells were incubated with 250 nM of dye labeled compound (**15**) with or without 10x concentrated unlabeled compound (**7**; blocking study) for 30 minutes at 37 °C. Following incubation, cells were rinsed thrice with PBS (3X 1 mL) to remove excess probe and then incubated in a paraformaldehyde solution (1 mL, w/v 4%, 20 min) to fix cells. Fixed cells were rinsed three additional times with PBS (3X 1 mL) to remove excess fixative. Coverslips were mounted to slides using ProLong Gold antifade reagent with DAPI (Invitrogen) and cured for 24 hours at 4 °C. Nail polish was used to seal slides following curing. Cells were imaged on an Olympus FV1000 confocal system at 40x magnification. DAPI was imaged with a diode 405 laser for excitation and emission collected at 430-470 nm. Cy5 was imaged with a HeNe₂ laser (635 nm) and emission recorded at 655-755 nm. Given the large spectral window differences between DAPI and Cy5, there were no concerns regarding spectral overlap. Kalman sequential

line scanning was employed to further increase confidence in emission profiles of the sample.

2.5 References

- (1) Molino, M.; Barnathan, E. S.; Clark, J.; Dreyer, M.; Hoxie, J. a; Schechter, N.; Woolkalis, M.; Brass, L. F.; Numerof, R.; Cumashi, A. *J. Biol. Chem.* **1997**, *272* (7), 4043–4049.
- (2) Nystedt, S.; Emilsson, K.; Wahlestedt, C.; Sundelin, J. *Proc. Natl. Acad. Sci.* **1994**, *91* (20), 9208–9212.
- (3) Hansen, K. K.; Sherman, P. M.; Cellars, L.; Andrade-Gordon, P.; Pan, Z.; Baruch, A.; Wallace, J. L.; Hollenberg, M. D.; Vergnolle, N. *Proc. Natl. Acad. Sci.* **2005**, *102* (23), 8363–8368.
- (4) Ramsay, A. J.; Dong, Y.; Hunt, M. L.; Linn, M.; Samaratunga, H.; Clements, J. A.; Hooper, J. D. *J. Biol. Chem.* **2008**, *283* (18), 12293–12304.
- (5) Adams, M. N.; Ramachandran, R.; Yau, M. K.; Suen, J. Y.; Fairlie, D. P.; Hollenberg, M. D.; Hooper, J. D. *Pharmacol. Ther.* **2011**, *130* (3), 248–282.
- (6) Nystedt, S.; Emilsson, K.; Larsson, a K.; Strömbeck, B.; Sundelin, J. *Eur. J. Biochem.* **1995**, *232* (1), 84–89.
- (7) Bohm, S. K.; Kong, W.; Bromme, D.; Smeekens, S. P.; Anderson, D. C.; Connolly, A.; Kahn, M.; Nelken, N. A.; Coughlin, S. R.; Payan, D. G.; Bunnett, N. W. *Biochem. J.* **1996**, *314* (12), 1009–1016.
- (8) Fagerberg, L.; Hallström, B. M.; Oksvold, P.; Kampf, C.; Djureinovic, D.; Odeberg, J.; Habuka, M.; Tahmasebpoor, S.; Danielsson, A.; Edlund, K.; Asplund, A.; Sjöstedt, E.; Lundberg, E.; Szigyaró, C. A.-K.; Skogs, M.; Takanen, J. O.; Berling, H.; Tegel, H.; Mulder, J.; Nilsson, P.; Schwenk, J. M.; Lindskog, C.; Danielsson, F.; Mardinoglu, A.; Sivertsson, Å.; von Feilitzen, K.; Forsberg, M.; Zwahlen, M.; Olsson, I.; Navani, S.; Huss, M.; Nielsen, J.; Ponten, F.; Uhlén, M. *Mol. Cell. Proteomics* **2014**, *13* (2), 397–406.
- (9) Cocks, T. M.; Fong, B.; Chow, J. M.; Anderson, G. P.; Frauman, A. G.; Goldie, R. G.; Henry, P. J.; Carr, M. J.; Hamilton, J. R.; Moffatt, J. D. *Nature* **1999**, *398* (6723), 156–160.
- (10) Damiano, B. P.; Cheung, W. M.; Santulli, R. J.; Fung-Leung, W. P.; Ngo, K.; Ye, R. D.; Darrow, a L.; Derian, C. K.; de Garavilla, L.; Andrade-Gordon, P. *J. Pharmacol. Exp. Ther.* **1999**, *288* (2), 671–678.
- (11) Su, S.; Li, Y.; Luo, Y.; Sheng, Y.; Su, Y.; Padia, R. N.; Pan, Z. K.; Dong, Z.; Huang, S. *Oncogene* **2009**, *28* (34), 3047–3057.
- (12) Antoniak, S.; Rojas, M.; Spring, D.; Bullard, T. A.; Verrier, E. D.; Blaxall, B. C.; MacKman, N.; Pawlinski, R. *Arterioscler. Thromb. Vasc. Biol.* **2010**, *30* (11), 2136–2142.
- (13) Kim, D. H.; Cho, Y. J.; Kim, J. H.; Kim, Y. B.; Lee, K. J. *J. Korean Med. Sci.* **2010**, *25* (9), 1330–1335.
- (14) Lohman, R.-J.; Cotterell, A. J.; Barry, G. D.; Liu, L.; Suen, J. Y.; Vesey, D. A.;

- Fairlie, D. P. *FASEB J.* **2012**, *26* (7), 2877–2887.
- (15) Aman, M.; Ohishi, Y.; Imamura, H.; Shinozaki, T.; Yasutake, N.; Kato, K.; Oda, Y. *Hum. Pathol.* **2017**, *64*, 156–163.
- (16) Cenac, N.; Coelho, A. M.; Nguyen, C.; Compton, S.; Andrade-Gordon, P.; MacNaughton, W. K.; Wallace, J. L.; Hollenberg, M. D.; Bunnett, N. W.; Garcia-Villar, R.; Bueno, L.; Vergnolle, N. *Am. J. Pathol.* **2002**, *161* (5), 1903–1915.
- (17) Ferrell, W. R.; Lockhart, J. C.; Kelso, E. B.; Dunning, L.; Plevin, R.; Meek, S. E.; Smith, A. J. H.; Hunter, G. D.; Mclean, J. S.; McGarry, F.; Ramage, R.; Jiang, L.; Kanke, T.; Kawagoe, J. *J. Clin. Invest.* **2003**, *111* (1), 35–41.
- (18) Jin, E.; Fujiwara, M.; Pan, X.; Ghazizadeh, M.; Arai, S.; Ohaki, Y.; Kajiwara, K.; Takemura, T.; Kawanami, O. *Cancer* **2003**, *97* (3), 703–713.
- (19) Massi, D.; Naldini, A.; Ardinghi, C.; Carraro, F.; Franchi, A.; Paglierani, M.; Tarantini, F.; Ketabchi, S.; Cirino, G.; Hollenberg, M. D.; Geppetti, P.; Santucci, M. *Hum. Pathol.* **2005**, *36* (6), 676–685.
- (20) Caruso, R.; Pallone, F.; Fina, D.; Gioia, V.; Peluso, I.; Caprioli, F.; Stolfi, C.; Perfetti, A.; Spagnoli, L. G.; Palmieri, G.; MacDonald, T. T.; Monteleone, G. *Am. J. Pathol.* **2006**, *169* (1), 268–278.
- (21) Fujimoto, D.; Hirono, Y.; Goi, T.; Katayama, K.; Hirose, K.; Yamaguchi, A. *J. Surg. Oncol.* **2006**, *93* (2), 139–144.
- (22) Black, P. C.; Mize, G. J.; Karlin, P.; Greenberg, D. L.; Hawley, S. J.; True, L. D.; Vessella, R. L.; Takayama, T. K. *Prostate* **2007**, *67*, 743–756.
- (23) Hyun, E.; Andrade-Gordon, P.; Steinhoff, M.; Vergnolle, N. *Gut* **2008**, *57* (9), 1222–1229.
- (24) Shi, X.; Gangadharan, B.; Brass, L. F.; Ruf, W.; Mueller, B. M. *Mol. Cancer Res.* **2004**, *2* (7), 395–402.
- (25) Uusitalo-Jarvinen, H.; Kurokawa, T.; Mueller, B. M.; Andrade-Gordon, P.; Friedlander, M.; Ruf, W. *Arterioscler. Thromb. Vasc. Biol.* **2007**, *27* (6), 1456–1462.
- (26) Al-Ani, B.; Saifeddine, M.; Hollenberg, M. D. *Can. J. Physiol. Pharmacol.* **1995**, *73* (8), 1203–1207.
- (27) Kanke, T.; Ishiwata, H.; Kabeya, M.; Saka, M.; Doi, T.; Hattori, Y.; Kawabata, A.; Plevin, R. *Br. J. Pharmacol.* **2005**, *145* (2), 255–263.
- (28) Barry, G. D.; Suen, J. Y.; Low, H. B.; Pfeiffer, B.; Flanagan, B.; Halili, M.; Le, G. T.; Fairlie, D. P. *Bioorganic Med. Chem. Lett.* **2007**, *17* (20), 5552–5557.
- (29) Hollenberg, M. D.; Renaux, B.; Hyun, E.; Houle, S.; Vergnolle, N.; Saifeddine, M.; Ramachandran, R. *J Pharmacol Exp Ther* **2008**, *326* (2), 453–462.
- (30) Hoffman, J.; Flynn, A. N.; Tillu, D. V.; Zhang, Z.; Patek, R.; Price, T. J.; Vagner, J.; Boitano, S. *Bioconjug. Chem.* **2012**, *23* (10), 2098–2104.
- (31) Yau, M. K.; Suen, J. Y.; Xu, W.; Lim, J.; Liu, L.; Adams, M. N.; He, Y.; Hooper,

- J. D.; Reid, R. C.; Fairlie, D. P. *ACS Med. Chem. Lett.* **2016**, 7 (1), 105–110.
- (32) Jiang, Y.; Yau, M. K.; Kok, W. M.; Lim, J.; Wu, K. C.; Liu, L.; Hill, T. A.; Suen, J. Y.; Fairlie, D. P. *ACS Chem. Biol.* **2017**, 12 (5), 1217–1226.
- (33) McGuire, J.; Saifeddine, M.; Triggle, C. *J. Pharmacol. Exp. Ther.* **2004**, 309 (3), 1124–1131.
- (34) Al-Ani, B.; Saifeddine, M.; Kawabata, a; Renaux, B.; Mokashi, S.; Hollenberg, M. D. *J. Pharmacol. Exp. Ther.* **1999**, 290 (2), 753–760.
- (35) Lau, C.; Lytle, C.; Straus, D. S.; DeFea, K. A. *AJP Cell Physiol.* **2011**, 300 (1), C113–C123.
- (36) Hollenberg, M. D.; Saifeddine, M.; Al-Ani, B.; Kawabata, A. *Can. J. Physiol. Pharmacol.* **1997**, 75 (7), 832–841.
- (37) Maryanoff, B. E.; Santulli, R. J.; McComsey, D. F.; Hoekstra, W. J.; Hoey, K.; Smith, C. E.; Addo, M.; Darrow, A. L.; Andrade-Gordon, P. *Arch. Biochem. Biophys.* **2001**, 386 (2), 195–204.
- (38) Boitano, S.; Flynn, A. N.; Schulz, S. M.; Hoffman, J.; Price, T. J.; Vagner, J. *J. Med. Chem.* **2011**, 54 (5), 1308–1313.
- (39) MedChem Designer ADMET Predictor, version 3.1.0.30, Simulations Plus, Inc., California, US.
- (40) Mihara, K.; Ramachandran, R.; Saifeddine, M.; Hansen, K. K.; Renaux, B.; Polley, D.; Gibson, S.; Vanderboor, C.; Hollenberg, M. D. *Mol. Pharmacol.* **2016**, 89 (5), 606–614.
- (41) Kuil, J.; Buckle, T.; Yuan, H.; Van Den Berg, N. S.; Oishi, S.; Fujii, N.; Josephson, L.; Van Leeuwen, F. W. B. *Bioconjug. Chem.* **2011**, 22 (5), 859–864.

Chapter 3

3 A Novel PET Probe for *In Vivo* Imaging of Protease-Activated Receptor 2

3.1 Introduction

Protease-activated receptors (PARs) are a class of G protein-coupled receptors (GPCRs), which uniquely are self-activated by a tethered ligand after a specific protease cleaves an N-terminal portion of the receptor. Before protease cleavage, the tethered ligand is 'masked' by multiple N-terminal amino acids, but afterwards, the 'unmasked' tethered ligand is able to bind to and activate the receptor. There are four PAR subtypes, denoted PAR1-PAR4. For PAR2, various proteases (e.g. trypsin, tryptase, Granzyme A, KLK4) are known to reveal the tethered ligand sequence SLIGKV (humans) and SLIGRL (rodents).¹⁻⁵

PAR2 is naturally expressed in multiple tissues (e.g. pancreas, liver, small intestine, colon) and is involved in inflammation and cell migration.⁶⁻⁸ However, aberrant function and over-expression of PAR2 has been linked to various cancers and inflammatory diseases. More specifically, PAR2 is implicated in conditions such as arthritis, colitis, asthma, cardiovascular disease, prostate cancer, lung cancer, gastric cancer, melanoma, ovarian cancer, and breast cancer.⁹⁻²³ In cancerous tissue, this undesirable activity of PAR2 has been shown to significantly contribute to cell proliferation, angiogenesis, and metastasis.^{11,24,25} Of specific interest, there is up to a 16-fold increase in PAR2 expression in various cancers and PAR2 expression levels have been positively correlated to cancer staging and progression.^{15,18,21,22,26,27}

Exogenous agonists that resemble the tethered ligand sequences have been developed, which bind to and activate PAR2. The tethered ligand sequences SLIGKV and SLIGRL as well as their C-terminally amidated analogues were synthesized in initial studies. These studies showed that SLIGRL-NH₂ (**1**, Figure 3.1) had the highest potency for human PAR2 and is widely used as a PAR2 agonist with micromolar potency.^{2,28,29} Extensive structure-activity relationship studies have involved substitutions of various

natural and unnatural amino acids into these sequences, which have generated peptides with improved potency. In particular, substituting the serine residue in the first position with various heterocycles (e.g. 2-furoyl, 5-isoxazoloyl, 3-pyridoyl, 4-(2-methyloxazoloyl), and 2-aminothiazol-4-oyl) has substantially improved potency and affinity for PAR2 to the sub-micromolar range.³⁰ Of these, 2-furoyl (2f) based peptides (e.g. **2**, Figure 3.1, referred to hereon in as Class I peptides) initially showed the best improvements and have been the most widely used. Addition of ornithine to the C-terminus of the 2f-LIGRL-NH₂ hexapeptide (**2**, Figure 3.1) and conjugation of various bulky substituents to the side chain of that ornithine (e.g. Alexa Fluor 594, **3** and DTPA(Eu), **4**, Figure 3.1) did not appreciably change the potency, affinity, or selectivity for PAR2.^{31,32} More recently, Isox-Cha-Chg (5-isoxazoloyl-cyclohexylalanine-cyclohexylglycine) based peptides developed by Jiang et al. (2017) and Yau et al. (2016), most notably Isox-Cha-Chg-AR-NH₂ (**7**, Figure 3.1), have shown substantial improvements in potency and affinity for PAR2.^{33,34} These Isox-Cha-Chg based peptides are referred to hereon in as Class II peptides. In addition, our recent work has shown that the addition of primary amines to various positions of **7** (**8-11**, Figure 3.1) and addition of a bulky substituent (**15**, Figure 3.1) resulted in peptides that maintained PAR2-selectivity and potency/affinity for PAR2 in the low nanomolar range (Chapter 2).

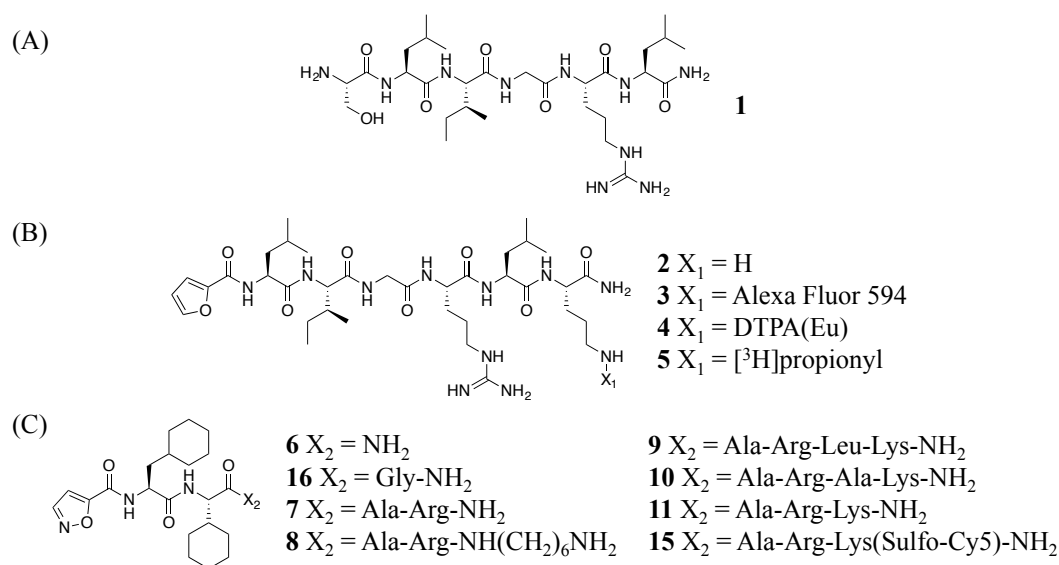


Figure 3.1: Known PAR2-targeting peptide agonists. (A) SLIGRL-NH₂, (B) Class I peptides, and (C) Class II peptides.^{28,31–35}

To our knowledge, PAR2-targeting imaging probes developed to date have been limited to *in vitro* or small animal *ex vivo* applications, which is because the probes are fluorescent or tritiated probes.^{29,31,32,36,37} A PAR2-targeting *in vivo* imaging agent could provide insight into PAR2 expression in real-time in living systems. In addition, it could have potential clinical relevance in the treatment and diagnosis of PAR2-related diseases such as various cancers and inflammatory diseases.

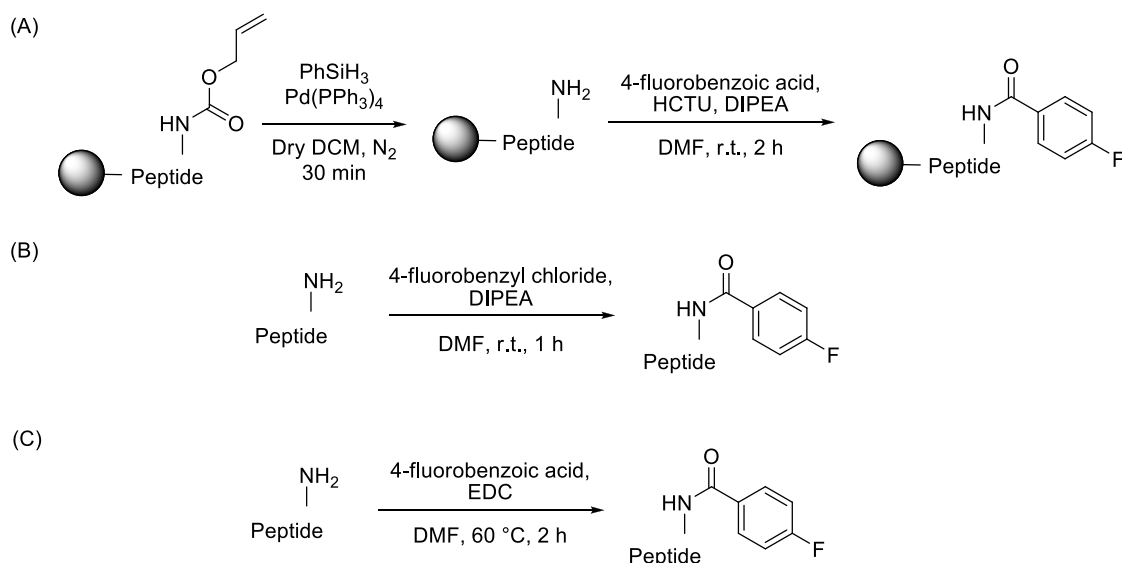
Positron emission tomography (PET) is a highly sensitive, quantitative imaging technique that could be used to achieve *in vivo* imaging of PAR2. Within PET imaging, various radionuclides and strategies can be used to label a targeting moiety with a radioactive isotope. Fluorine-18 was chosen for this application due to its facile cyclotron production, ideal half-life for radiopharmaceuticals (109.8 min), diverse chemistry for introduction into various molecules, and the highest spatial resolution compared to other PET isotopes.^{38,39} The *N*-succinimidyl 4-[¹⁸F]fluorobenzoate ([¹⁸F]SFB) prosthetic group was used for ¹⁸F-labeling as it is one of the most common prosthetic groups for ¹⁸F-labeling of peptides, because it gives quick, efficient, and clean labeling with the ability to be automated.^{40,41}

This work describes the design, synthesis, and evaluation of Class I and Class II PAR2-targeting peptides derived with a 4-fluorobenzoyl group through a free primary amine on the peptide. These 4-fluorobenzoyl conjugated peptides act as the ^{19}F -standard of a potential ^{18}F -labeled probe for use in *in vivo* imaging. Further, this work describes the radiosynthesis of the radiolabeled lead PAR2-targeting peptide and its evaluation *in vitro* in prostate cancer (PC3) cells.

3.2 Results and Discussion

3.2.1 Peptide Synthesis

Similar to Chapter 2, all peptides (**2**, **6-7**, **16-29**, and **35**) were synthesized using standard Fmoc-SPPS using a solid support MBHA Rink amide resin or 1,6-diaminohexane trityl resin (Scheme 2.1 – sec. 2.2.1). Compounds **18-19**, **22-24**, and **26-29** required additional orthogonal protecting group allyloxycarbonyl (Alloc) deprotection and subsequent conjugation of 4-fluorobenzoic acid (Scheme 3.1A). Compounds **21** and **25** were conjugated with the 4-fluorobenzoyl group off resin, as the primary amine being conjugated was protected by the solid support on resin (Scheme 3.1B and 3.1C, respectively).



Scheme 3.1: Conjugation of 4-FB to peptides.

(A) Solid-phase conjugation of 4-fluorobenzoic acid (**18-19**, **22-24**, and **26-29**), (B) solution-phase conjugation of 4-fluorobenzyl chloride (**21**), and (C) solution-phase conjugation of 4-fluorobenzoic acid (**25**).

3.2.2 Synthesis and Evaluation of Class I PAR2-Targeted Peptides

Similar to our previous work in Chapter 2, **2** shows a greater than ten-fold increase in potency for PAR2 (187 nM, Table 3.1) compared to **1** (7024 nM, Table 3.1) as determined by a β -arrestin 2 recruitment assay in HEK293T cells. This encouraged us to investigate Class I peptides for the development of PAR2-targeting PET imaging agents. Modifications to Class I peptide sequences were completed to improve PAR2 potency first before the conjugation of the 4-fluorobenzoyl group. Previous reports showed that the substitution of leucine with alanine at position six of 2f-LIGRL-NH₂ improved potency.³⁴ Thus, this substitution of **2** was completed to yield **17** where an expected increase in potency was observed (99 nM, Table 3.1). In addition, prior reports described that the addition of isoleucine to the C-terminus of related peptides (position seven) increased potency.^{30,34} Thus, **18** was synthesized with isoleucine at position seven and ornithine at position eight. Compound **18** was also found to have the expected increase in potency (56 nM, Table 3.1).

Next was the conjugation of the 4-fluorobenzoyl group to Class I peptides. The widely used PAR2-targeting peptide, **2**, and its more potent counterpart, **18**, were conjugated to

4-fluorobenzoic acid through the primary amine of the ornithine side chain to yield **19** and **20**, respectively. As shown in Table 3.1, **19** showed similar potency (151 nM) compared to **2** (187 nM), but with the addition of the isoleucine, **20** showed a substantial and unexpected decrease in potency (252 nM) compared to **18** (56 nM). As expected, the addition of the 4-fluorobenzoic moiety to these peptides resulted in a noticeable increase in hydrophobicity as demonstrated through the cLogD values (Table 3.1).

Further, PAR2 selectivity was evaluated by measuring intracellular calcium response caused by the receptor-peptide interaction in HEK293T cells endogenously expressing PAR2 compared to PAR2 knock out (KO) cells. As a control, a PAR1-specific agonist (TFLLR-NH₂, **13**) was assessed for its calcium response in both of these cell lines as they both contain the PAR1 receptor (Table 3.1, see Appendix 6 for representative examples of traces). These cells and this control were used (similar to previous reports) because it is known that some PAR2-targeting peptides can also bind to PAR1.^{33,34,42,43} Based on the calcium response in these cells, peptides **17-20** were found to be consistently selective to PAR2 (Table 3.1).

Table 3.1: Class I PAR2-targeted peptides (**2** and **17-20**) and control peptides (**1** and **13**) with their EC₅₀ values, PAR2 selectivity measures, and cLogD values.

#	Compound	EC ₅₀ (nM)	pEC ₅₀ ± SEM	Net % max Ca ²⁺ release in PAR2 expressing cells ± SEM	Net % max Ca ²⁺ release in PAR2 KO cells ± SEM	cLogD at pH 7.4
13	TFLLR-NH ₂	-	-	45.6 ± 2.9	63.5 ± 5.5	-0.67
1	SLIGRL-NH ₂	7024	5.15 ± 0.03	55.9 ± 4.4	-0.2 ± 0.4	-1.93
2	2f-LIGRLO-NH ₂	187	6.73 ± 0.05	58.2 ± 3.2	0.5 ± 0.2	-2.71
17	2f-LIGRAO-NH ₂	99	7.00 ± 0.05	54.2 ± 2.9	-0.9 ± 0.2	-3.22
18	2f-LIGRLIO-NH ₂	56	7.25 ± 0.07	62.9 ± 6.0	-0.5 ± 0.5	-2.29
19	2f-LIGRLO(4-FB)-NH ₂	151	6.82 ± 0.08	57.5 ± 3.5	0.1 ± 1.0	-0.94
20	2f-LIGRLIO(4-FB)-NH ₂	252	6.60 ± 0.08	18.5 ± 6.5	-2.2 ± 0.5	-0.51

EC₅₀ values determined through a dose-response curve from a β-arrestin 2 recruitment assay in HEK293T cells. Selectivity measures are shown as calcium response in PAR2 expressing (column five) versus PAR2 KO (column six) HEK293T cells. cLogD values calculated through Simulations Plus MedChem Designer ADMET Predictor.

3.2.3 Synthesis and Evaluation of First Generation Class II PAR2-Targeted Peptides

Since multiple reports have shown that Class II peptides can have improved potency and affinity for PAR2 compared to Class I peptides, they were also investigated for the development of PAR2-targeting PET imaging agents. The first generation Class II peptides were developed from the base peptide sequence of Isox-Cha-Chg. Reports of this peptide class including **6** and **16** showed a ten-fold increase in potency for PAR2 compared to **2** through a calcium assay, but later they were reported to have a reduced affinity for PAR2 through a competitive binding assay, likely due to the absence of strong hydrogen bond(s) or electrostatic interactions from the loss of the positively charged arginine residue when compared to **2**.^{33,34} The results from the β -arrestin 2 recruitment assay in the HEK293T cell line reported here show a decrease in potency for **6** and **16** compared to **2**; a similar trend to the affinity measures (Table 3.2). Nonetheless, the addition of an aminohexyl spacer conjugated to 4-fluorobenzoic acid extending from the peptide backbone of **6** was synthesized to yield **21**. Unfortunately, peptide **21** showed a large reduction in potency (>3000 nM), a loss of PAR2 selectivity, and a large, undesirable increase in hydrophobicity (Table 3.2).

Table 3.2: First generation Class II PAR2-targeted peptides (**6**, **16**, and **21**) with their EC₅₀ values, PAR2 selectivity measures, and cLogD values.

#	Compound	EC ₅₀ (nM)	pEC ₅₀ ± SEM	Net % max Ca ²⁺ release in PAR2 expressing cells ± SEM	Net % max Ca ²⁺ release in PAR2 KO cells ± SEM	cLogD at pH 7.4
6	Isox-Cha-Chg-NH ₂	1925	5.72 ± 0.07	14.6 ± 3.3	-0.1 ± 0.3	2.29
16	Isox-Cha-Chg-G-NH ₂	1179	5.93 ± 0.07	22.0 ± 5.5	-2.2 ± 0.1	1.54
21	Isox-Cha-Chg-NH(CH ₂) ₆ NH-4-FB	>3000	>5.53	7.0 ± 1.9	9.1 ± 4.0	5.00

EC₅₀ values determined through a dose-response curve from a β-arrestin 2 recruitment assay in HEK293T cells. Selectivity measures are shown as calcium response in PAR2 expressing (column five) versus PAR2 KO (column six) HEK293T cells. cLogD values calculated through Simulations Plus MedChem Designer ADMET Predictor.

3.2.4 Synthesis and Evaluation of Second Generation Class II PAR2-Targeted Peptides

Unsuccessful results from the first generation Class II peptides led to the development of a second generation of Class II imaging agents. These were based on known high potency/affinity PAR2-selective peptides with the base peptide sequence of Isox-Cha-Chg-Ala-Arg, such as **7** (Table 3.3, see Appendix 6 for representative examples of PAR2-selectivity traces) reported by Jiang et al. (2017) and **8-11** (Table 3.3) reported in our recent work with the development of PAR2-targeting fluorescent peptides (Chapter 2).³⁴ This generation of peptides contain the arginine positive charge at position five, which is likely the reason they have high affinity and potency in all reported assays compared to the first generation Class II peptides.

Peptides **8-11** from our previous work are highly potent and PAR2-selective peptides that contain a free primary amine. Thus, these peptides were used to conjugate a 4-fluorobenzoyl group to them to yield **22-25**. Peptides **22-24** showed similar potencies (10 to 23 nM, Table 3.3) compared to their unconjugated counterparts **8-11** (13 to 23 nM, Table 3.3), making **22** and **24** the most potent 4-fluorobenzoyl conjugated peptides and the leading candidates. However, **22-24** showed a lack of PAR2 selectivity, as indicated by their calcium response in HEK293T PAR2 KO cells (Table 3.3, see Appendix 6 for representative examples of PAR2-selectivity traces). Peptide **25** retained PAR2-selectivity, but, unfortunately, showed a substantial loss in potency (42 nM) compared to its unconjugated counterpart (**8**) and to **22** and **24** (Table 3.3).

In our previous work, Isox-Cha-Chg-ARK(COCH₃)-NH₂ (**12**) was found to be highly potent and have selective binding to PAR2 (Table 2.1, Chapter 2). This suggested that the presence of the 4-fluorobenzoyl group caused the lack of selectivity for PAR2 (likely due to hydrophobic or pi stacking interactions) as opposed to the loss of charge from the amide bond formed on the lysine side chain for peptides **22-24**. Therefore, this gave rise to the development of a third generation of Class II imaging agents which have the base peptide sequence of Isox-Cha-Chg-Ala-Arg-Xaa where the distance of the 4-fluorobenzoyl group to the peptide backbone of the position six amino acid was modified in an effort to improve PAR2 selectivity.

Table 3.3: Second generation Class II PAR2-targeted peptides (**7-11** and **22-25**) with their EC₅₀ values, PAR2 selectivity measures, and cLogD values.

#	Compound	EC ₅₀ (nM)	pEC ₅₀ ± SEM	Net % max Ca ²⁺ release in PAR2 expressing cells ± SEM	Net % max Ca ²⁺ release in PAR2 KO cells ± SEM	cLogD at pH 7.4
7	Isox-Cha-Chg-AR-NH ₂	12	7.92 ± 0.05 ^a	68.8 ± 3.9	-0.5 ± 0.3	-0.85
11	Isox-Cha-Chg-ARK-NH ₂	10 ^a	8.00 ± 0.09 ^a	72.0 ± 5.0 ^a	-0.9 ± 0.3 ^a	-1.72 ^a
22	Isox-Cha-Chg-ARK(4-FB)-NH ₂	13	7.89 ± 0.08	63.5 ± 4.6	8.8 ± 2.4	-0.06
9	Isox-Cha-Chg-ARLK-NH ₂	23 ^a	7.65 ± 0.07 ^a	69.9 ± 4.1 ^a	-0.4 ± 0.4 ^a	-1.29 ^a
23	Isox-Cha-Chg-ARLK(4-FB)-NH ₂	24	7.61 ± 0.15	70.5 ± 4.7	16.9 ± 4.1	0.26
10	Isox-Cha-Chg-ARAK-NH ₂	15 ^a	7.82 ± 0.07 ^a	67.3 ± 3.9 ^a	-1.1 ± 0.5 ^a	-1.77 ^a
24	Isox-Cha-Chg-ARAK(4-FB)-NH ₂	10	8.00 ± 0.06	66.4 ± 6.7	5.8 ± 1.3	-0.13
8	Isox-Cha-Chg-AR-NH(CH ₂) ₆ NH ₂	16 ^a	7.79 ± 0.04 ^a	68.6 ± 9.3 ^a	0.0 ± 0.4 ^a	-0.70 ^a
25	Isox-Cha-Chg-AR-NH(CH ₂) ₆ NH-4-FB	42	7.37 ± 0.05	58.3 ± 4.4	-1.0 ± 1.0	0.90

EC₅₀ values determined through a dose-response curve from a β-arrestin 2 recruitment assay in HEK293T cells. Selectivity measures are shown as calcium response in PAR2 expressing (column five) versus PAR2 KO (column six) HEK293T cells. cLogD values calculated through Simulations Plus MedChem Designer ADMET Predictor. ^aPeptide data originally found in Chapter 2, Table 2.1 and Table 2.2.

3.2.5 Synthesis and Evaluation of Third Generation Class II PAR2-Targeted Peptides

The first approach for the third generation Class II imaging agents was to extend the linker region that connected the peptide to the 4-fluorobenzoyl group. This was achieved by adding a spacer to the lysine side chain of **11**, followed by the conjugation of a 4-fluorobenzoyl group. Two spacers were used for this purpose, 6-aminohexanoyl (Ahx) and the longer, more hydrophilic spacer [2-(2-amino)ethoxy]ethoxy]acetyl (AEEA). This yielded **26** and **27**, respectively, which were selective for PAR2 (Table 3.4) but showed a slight reduction in potency (21 nM and 24 nM, respectively, Table 3.4) compared to **22** (13 nM, Table 3.3).

Table 3.4: Third generation Class II PAR2-targeted peptides (**26-29**) with their EC₅₀ values, PAR2 selectivity measures, and cLogD values.

#	Compound	EC ₅₀ (nM)	pEC ₅₀ ± SEM	Net % max Ca ²⁺ release in PAR2 expressing cells ± SEM	Net % max Ca ²⁺ release in PAR2 KO cells ± SEM	cLogD at pH 7.4
26	Isox-Cha-Chg-ARK(Ahx-4-FB)-NH ₂	21	7.68 ± 0.09	52.8 ± 5.5	-0.9 ± 0.2	0.43
27	Isox-Cha-Chg-ARK(AEEA-4-FB)-NH ₂	24	7.62 ± 0.06	58.8 ± 6.9	-1.6 ± 0.5	-0.07
28	Isox-Cha-Chg-ARO(4-FB)-NH ₂	8	8.13 ± 0.07	55.8 ± 3.8	7.4 ± 1.0	-0.26
29	Isox-Cha-Chg-AR-Dpr(4-FB)-NH ₂	13	7.89 ± 0.06	51.0 ± 7.8	-2.1 ± 0.4	-0.71

EC₅₀ values determined through a dose-response curve from a β-arrestin 2 recruitment assay in HEK293T cells. Selectivity measures are shown as calcium response in PAR2 expressing (column five) versus PAR2 KO (column six) HEK293T cells. cLogD values calculated through Simulations Plus MedChem Designer ADMET Predictor.

The other approach was to decrease the distance between the peptide backbone and the 4-fluorobenzoyl group by decreasing the side chain length of the position six lysine on **11**. Ornithine (O) was first used for this purpose, having one less carbon in its side chain compared to lysine, and although this peptide (**28**) showed good potency (8 nM, Table 3.4), it was unfortunately non-selective for PAR2 as indicated by its calcium response in HEK293T PAR2 KO cells (Table 3.4). Second, 2,3-diaminopropionic acid (Dpr), which has three carbons less than the side chain of lysine, was used to further shorten the chain, giving **29**. Compound **29** showed high potency (13 nM, Table 3.4) compared to **1** and **2** and similar potency compared to **7** (Figure 3.2) and was PAR2-selective (Table 3.4, see Appendix 6 for representative examples of PAR2-selectivity traces), making it the lead candidate for ^{18}F -labeling and subsequent *in vitro* and *in vivo* experiments.

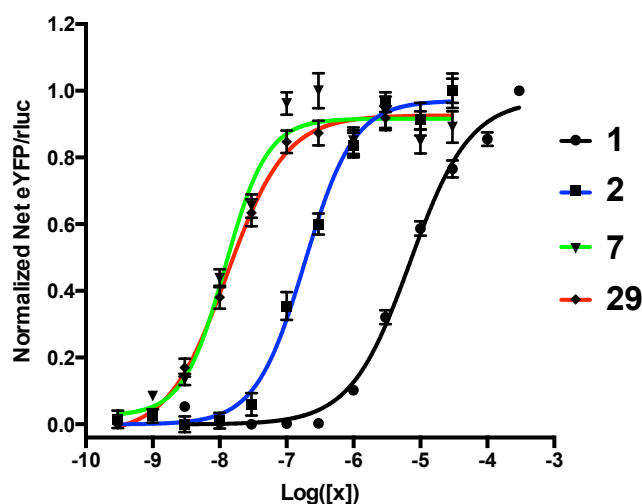
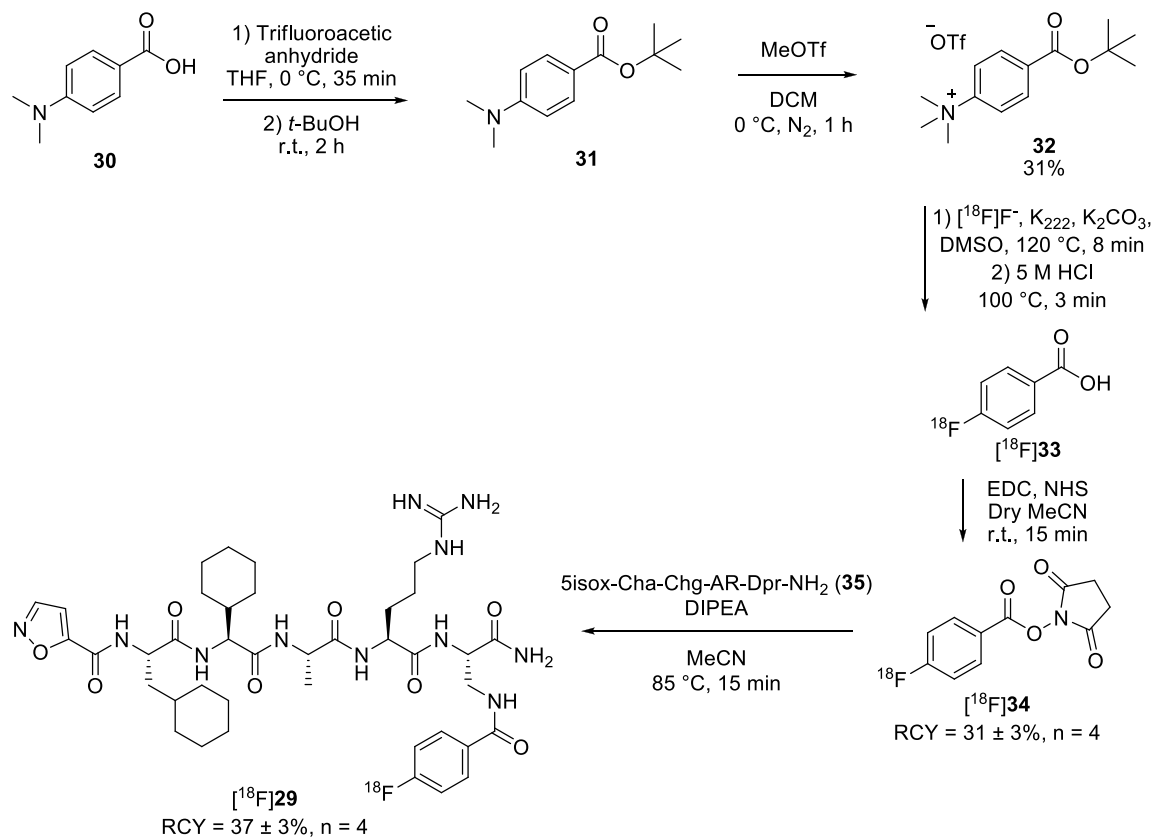


Figure 3.2: PAR2 β -arrestin 2 recruitment dose-response curves for **1**, **2**, **7**, and **29** in HEK293T cells.

Results from peptides **26**, **27**, and **29** further supported the insignificance of an amino functional group being present at position six of Class II peptides. Further, these results support that the specific location of an aromatic group to these Class II peptides is important, as the addition of the 4-fluorobenzoyl group can cause non-selective PAR2 binding as indicated through calcium response in HEK293T PAR2 KO cells, possibly caused by hydrophobic or pi stacking interactions between the ligand and a receptor.

3.2.6 Radiosynthesis of [¹⁸F]29

The overall synthesis of [¹⁸F]29 is outlined in Scheme 3.2. The radiosynthesis of [¹⁸F]29 made use of known radiochemistry.^{44,45} The first two steps in the synthesis involved preparation of the prosthetic group precursor, 32. Briefly, the carboxylic acid of 30 was protected with a *tert*-butyl group, followed by methylation of the tertiary amine using MeOTf to obtain the radiolabeling precursor 32.



Scheme 3.2: Synthesis of [¹⁸F]29.

Radiolabeling of 32 with [¹⁸F]F⁻ was accomplished through an automated synthetic protocol previously developed in our lab to yield the ¹⁸F-prosthetic group, 34 (see Appendix 7 for the automated synthesis display). Compound 32 was reacted with azeotropically dried [¹⁸F]F⁻ to obtain *tert*-butyl [¹⁸F]4-fluorobenzoate through a nucleophilic aromatic substitution reaction, followed by subsequent deprotection of the *tert*-butyl ester with 5M HCl to yield [¹⁸F]33. This product was purified by solid-phase extraction, reacted with EDC hydrochloride and NHS to provide the activated ester

([¹⁸F]**34**), and purified on RP-HPLC (RCY = 31 ± 3%, RCP > 98%, n = 4, Figure 3.3A, see Appendix 8A for **34** and [¹⁸F]**34** RP-HPLC co-injection).

The final step in the radiosynthesis was the conjugation of the ¹⁸F-prosthetic group to the peptide to yield [¹⁸F]**29**. Compound [¹⁸F]**34** was conjugated to **35** through nucleophilic acyl substitution followed by RP-HPLC purification to obtain [¹⁸F]**29**. Peptide **35** did not require protecting groups and subsequent deprotection step(s), unlike other peptide labeling reports, because the [¹⁸F]SFB prosthetic group is preferentially selective for primary amines under these conditions and because **35** was designed to contain one primary amine. A water and acetonitrile (v/v 1:3) mixture was initially used for this conjugation as **35** had poor solubility in pure acetonitrile; however, hydrolysis of [¹⁸F]**34** was observed and poor yields of [¹⁸F]**29** were obtained (RCY = 18 ± 4%, n = 2). Acetonitrile was used to prevent hydrolysis despite poor solubility of the starting material. Reaction temperatures of 85 °C improved solubility, resulting in improved radiochemical yields (RCY = 37 ± 3%, RCP > 98%, A_m = 20 ± 2 GBq/μmol, EOS = 125 ± 2 min, n = 4, Figure 3.3B, see Appendix 8B for **29** and [¹⁸F]**29** RP-HPLC co-injection).

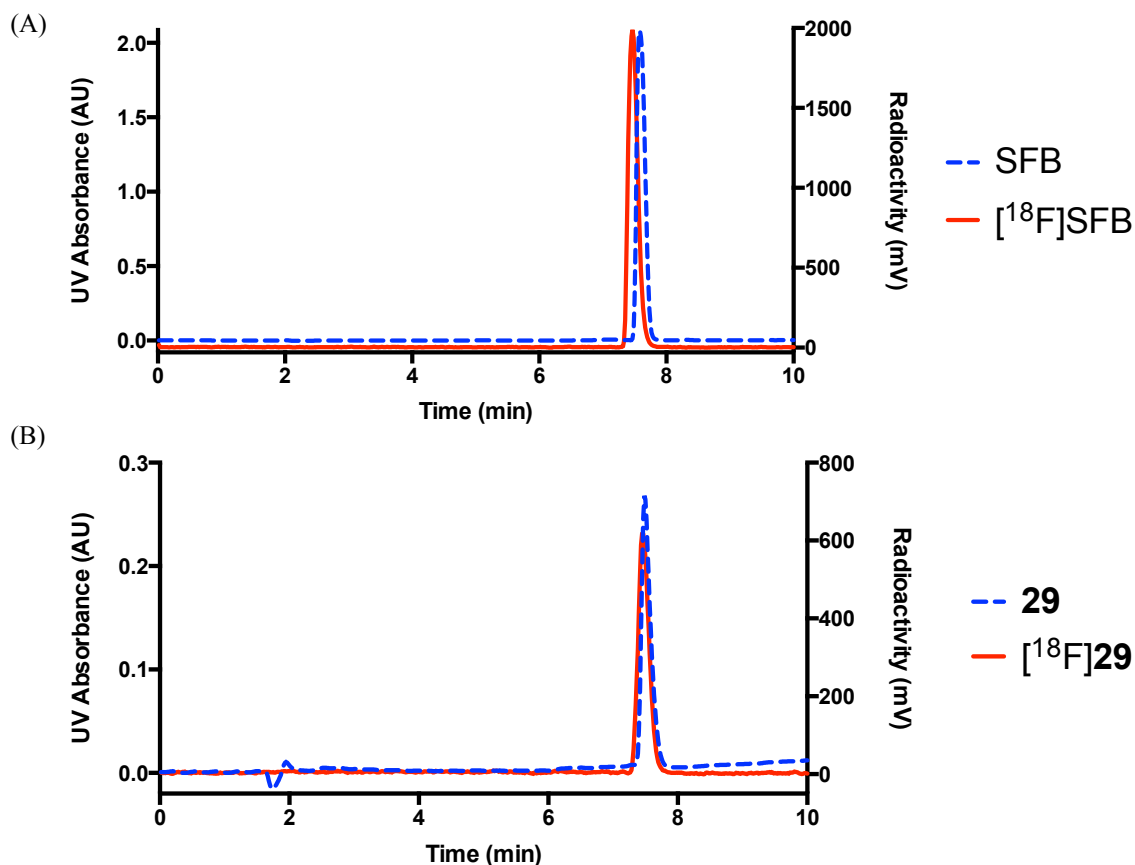


Figure 3.3: Overlay of RP-HPLC chromatogram and radio-trace of (A) SFB and $[^{18}\text{F}]$ SFB, respectively, and (B) **29** and $[^{18}\text{F}]$ **29**, respectively.

3.2.7 Cell Uptake of $[^{18}\text{F}]$ **29** in PC3 Cells

Upon successful synthesis of $[^{18}\text{F}]$ **29**, cell uptake studies were completed in a prostate cancer cell line (PC3) that endogenously over-expresses PAR2 as well as in a PAR2 KO PC3 cell line. As shown in Figure 3.4, $[^{18}\text{F}]$ **29** showed a significant uptake in the PAR2 expressing cell line at 20 and 60 minutes ($7.9 \pm 0.7\%$, $7.4 \pm 0.7\%$, respectively) compared to the PAR2 KO cell line ($2.3 \pm 0.1\%$, $2.3 \pm 0.1\%$, respectively) and the PAR2 expressing cell line blocked with **7** ($1.6 \pm 0.2\%$, $2.1 \pm 0.1\%$, respectively). This suggests that there is receptor selective binding as well as that $[^{18}\text{F}]$ **29** is not passively diffusing the cell membrane. This is consistent with our results of a similar, but even more hydrophobic fluorescent probe (**15**), which showed PAR2-selective uptake and no passive diffusion across the cell membrane (Figure 2.4, Chapter 2).

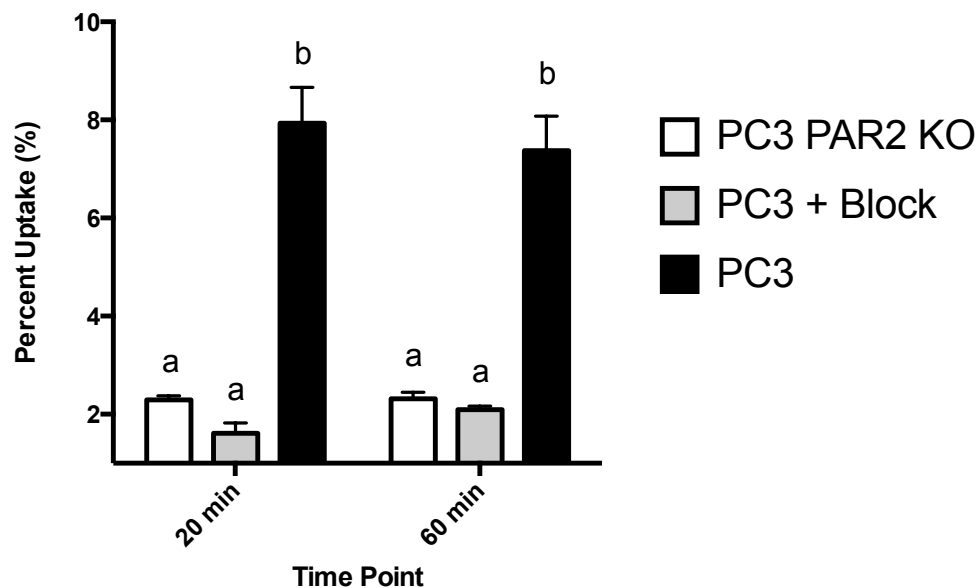


Figure 3.4: Cell uptake of [^{18}F]29 in PAR2 KO PC3 cells (white), PC3 cells blocked with 20 μM of 7 (grey), and PC3 cells (black).

A two way ANOVA (cell condition, time) for percent uptake followed by a post-hoc Tukey multiple comparisons test was used to assess significance (significance set at 0.05). Overall cell condition effect was significant ($P < 0.001$) but the overall time effect was not significant ($P = 0.956$). Different letters represent significance ($P \leq 0.05$).

3.3 Conclusions and Future Work

3.3.1 Conclusions

Many novel peptides described here show high potency and selectivity for PAR2, while also having potential to be PET imaging agents for PAR2. The first approach to obtain these peptides was through the synthesis and evaluation of various Class I peptides (2f-LIGRLO-NH₂ based sequences) for PAR2-binding. These results lead to peptide **18** being the most potent ($EC_{50} = 56$ nM, Table 3.1); however, conjugation of it with a 4-fluorobenzoyl group showed an unexpected decrease in potency, making **19** the leading PAR2-targeting Class I imaging agent ($EC_{50} = 151$ nM, Table 3.1). The next approach was the synthesis and evaluation of Class II peptides (based on Isox-Cha-Chg based sequences). The first generation of Class II peptides showed poor potency for PAR2 (Table 3.2), likely because of the absence of arginine at position five. The second

generation of Class II peptides (containing arginine in position five) showed substantial improvements in potency ($EC_{50} = 10$ to 42 nM, Table 3.3), but the lead candidates **22-24** showed non-selective PAR2 binding as measured through a calcium assay in HEK293T PAR2 KO cells (Table 3.3). The third generation of Class II peptides modified the distance of the 4-fluorobenzoyl group to the peptide backbone of the position six amino acid since the specific position of this 4-fluorobenzoyl group was the expected cause of non-selective PAR2 binding. This generation of Class II peptides had several candidates (**26**, **27**, and **29**) that showed high potency ($EC_{50} = 13$ to 24 nM, Table 3.4) and selectivity for PAR2 (Table 3.4).

The investigation of these various PAR2-targeting probes gave rise to five peptides (**19**, **25-27**, and **29**) that have various structural and hydrophobic properties with strong potential as PET imaging agents for PAR2, of which, **29** was the lead candidate ($EC_{50} = 13$ nM, Table 3.4). The ^{18}F -labeled version of **29** was then successfully synthesized with radiochemical yields of $37 \pm 3\%$, radiochemical purity of $>98\%$, molar activity of 20 ± 2 GBq/ μmol , and end of synthesis time of 125 ± 2 min ($n = 4$). Compound [^{18}F]**29** showed a significantly higher uptake in a PAR2-expressing prostate cancer cell line compared to the controls ($P < 0.001$, Figure 3.4) and is the first ever developed PAR2-targeted *in vivo* imaging agent.

Compound [^{18}F]**29** can serve as a chemical tool that could provide insight into areas of PAR2 expression *in vivo* and has potential clinical applications as a non-invasive imaging approach for patient diagnosis, stratification, and treatment monitoring of various PAR2-related cancers and inflammatory diseases.

3.3.2 Future Work

Compound [^{18}F]**29** is currently being evaluated through *ex vivo* biodistribution studies in mice and *in vivo* imaging in a xenograft mouse model of prostate cancer.

3.4 Experimental Procedures

3.4.1 General Methods

All reagents were purchased from Sigma-Aldrich, ChemImpex, or Thermo Fischer Scientific and used without further purification. Peptides were synthesized using standard Fmoc-solid phase peptide synthesis (SPPS), cleaved from resin using 95% TFA, 2.5% TIPS, and 2.5% H₂O for 5 h (except **21** and **25**: 20% TFA, 2.5% TIPS, 77.5% DCM for 1.5 h), precipitated in ice cold *tert*-butyl methyl ether, lyophilized, purified by preparative RP-HPLC, and further lyophilized to obtain a dry powder. Purity was assessed by analytical RP-HPLC and characterized by HRMS (Table 3.5). The analytical RP-HPLC was performed on a system consisting of an analytical Agilent Zorbax SB-C8 column (4.6 x 150 mm, 5 μ m), Waters 600 controller, Waters in-line degasser, and Waters Masslynx software (version 4.1). Two mobile phases were used; eluent A (0.1% TFA in acetonitrile) and eluent B (0.1% TFA in MilliQ water). The flow rate was set at 1.5 mLmin⁻¹ over 10 minutes with an additional 5-minute wash (95% solvent A in solvent B). A Waters 2998 Photodiode array detector (200-800 nm) and an ESI-MS (Waters Quattro Micro API mass spectrometer) were used to monitor the column eluate. The preparative RP-HPLC used the same system, eluents, and detection method as mentioned above for the analytical RP-HPLC, except that a preparative Agilent Zorbax SB-C8 column (21.2 x 150 mm, 5 μ m) at a flow rate of 20 mLmin⁻¹ was used. The high-resolution mass spectra for all peptides were determined in positive mode using an electrospray ionization (ESI) ion source on a Bruker micrOTOF II mass spectrometer. For small molecules, high-resolution mass spectra were determined in positive mode using an electron ionization (EI) ion source on a Thermo Scientific Double Focusing Sector mass spectrometer. Simulations Plus MedChem Designer ADMET Predictor was used to determine the cLogD values at a pH of 7.4.⁴⁶ NMR spectra for appropriate compounds were recorded on a Bruker Avance III HD 400 spectrometer at 400 and 100 MHz for ¹H and ¹³C experiments, respectively. All descriptive statistics are reported as mean \pm SEM where applicable.

Table 3.5: HRMS data and purity of peptides **2**, **6-7**, **16-29**, and **35**.

Cmpd #	Molecular Formula (M)	Evaluated HRMS m/z	Calc. m/z	Found m/z	Purity
2	C ₃₆ H ₆₃ N ₁₁ O ₈	[M+H] ⁺	778.4939	778.4945	> 95 %
6	C ₂₁ H ₃₂ N ₄ O ₄	[M+Na] ⁺	427.2321	427.2309	> 95 %
7	C ₃₀ H ₄₉ N ₉ O ₆	[M+H] ⁺	632.3884	632.3892	> 95 %
16	C ₂₃ H ₃₅ N ₅ O ₅	[M+Na] ⁺	484.2536	484.2526	> 95 %
17	C ₃₃ H ₅₇ N ₁₁ O ₈	[M+H] ⁺	736.4470	736.4475	> 95 %
18	C ₄₂ H ₇₄ N ₁₂ O ₉	[M+H] ⁺	891.5780	891.5801	> 95 %
19	C ₄₃ H ₆₆ FN ₁₁ O ₉	[M+H] ⁺	900.5107	900.5129	> 95 %
20	C ₄₉ H ₇₇ FN ₁₂ O ₁₀	[M+H] ⁺	1013.5948	1013.5955	> 95 %
21	C ₃₄ H ₄₈ FN ₅ O ₅	[M+Na] ⁺	648.3537	648.3550	> 95 %
22	C ₄₃ H ₆₄ FN ₁₁ O ₈	[M+H] ⁺	882.5002	882.5011	> 95 %
23	C ₄₉ H ₇₅ FN ₁₂ O ₉	[M+H] ⁺	995.5842	995.5852	> 95 %
24	C ₄₆ H ₆₉ FN ₁₂ O ₉	[M+H] ⁺	953.5373	953.5398	> 95 %
25	C ₄₃ H ₆₅ FN ₁₀ O ₇	[M+H] ⁺	853.5100	853.5110	> 95 %
26	C ₄₉ H ₇₅ FN ₁₂ O ₉	[M+H] ⁺	995.5842	995.5855	> 95 %
27	C ₄₉ H ₇₅ FN ₁₂ O ₁₁	[M+H] ⁺	1027.5741	1027.5745	> 95 %
28	C ₄₂ H ₆₂ FN ₁₁ O ₈	[M+H] ⁺	868.4845	868.4864	> 95 %
29	C ₄₀ H ₅₈ FN ₁₁ O ₈	[M+H] ⁺	840.4532	840.4525	> 95 %
35	C ₃₃ H ₅₅ N ₁₁ O ₇	[M+H] ⁺	718.4364	718.4372	> 95 %

Purity assessed by analytical RP-HPLC UV detection.

3.4.2 Solid-Phase Peptide Synthesis

All compounds (except **21** and **25**) were synthesized on Rink amide MBHA resin (256 mg, 0.1 mmol, 0.39 mmol/g) using standard Fmoc-SPPS procedures and a Biotage® Syrowave™ automated peptide synthesizer (0.4 mmol of HCTU, 0.4 mmol of Fmoc-amino acids, 0.6 mmol of DIPEA, 1 h coupling). Manual coupling of 5-isoxazolyl (0.3 mmol) was performed using HATU (0.3 mmol) and DIPEA (0.6 mmol) for 24 h twice. Compound **21** and **25** were synthesized on 1,6-diaminohexane trityl resin (256 mg, 0.1 mmol, 0.39 mmol/g).

3.4.3 Solid-Phase Orthogonal Alloc Deprotection

On resin peptide sequences were synthesized as described above but with Fmoc-Lys(Alloc)-OH, Fmoc-Orn(Alloc)-OH, or Fmoc-Dpr(Alloc)-OH. After the sequence was synthesized on resin, the Alloc protecting group was selectively removed. Briefly, the

resin was swelled in DCM (15 min) and washed three times with dry DCM (3X 5 mL). The resin was placed under an inert N₂ atmosphere and phenylsilane (296 μL, 2.4 mmol) in dry DCM (2 mL) was added to the resin. Tetrakis(triphenylphosphine) palladium(0) (23.1 mg, 20 μmol) was dissolved in dry DCM (1 mL) and added to the resin. The peptide column was flushed with N₂ (2 min) before being shaken (5 min). The resin was washed three times with dry DCM (3X 5 mL). The procedure was repeated and shaken (30 min). The resin was washed four times with DCM (4X 5 mL) and DMF (4X 5 mL).

3.4.4 Solid-Phase Conjugation of 4-Fluorobenzoic Acid (**19-20**, **22-24**, and **26-29**)

4-Fluorobenzoic acid (28.0 mg, 0.2 mmol), HCTU (82.7 mg, 0.2 mmol), and DIPEA (70 μL, 0.4 mmol) were combined in DMF and shaken (5 min) to activate the acid. This mixture was then added to the peptide on resin (0.1 mmol) and shaken (2 h). The final on resin peptides (**19-20**, **22-24**, and **26-29**) were cleaved and purified as usual.

3.4.5 Solution-Phase Conjugation of 4-Fluorobenzyl Chloride (**21**)

Isox-Cha-Chg-NH(CH₂)₆NH₂ was cleaved off resin and purified by RP-HPLC. The purified product containing a free primary amine (4.0 mg, 6.5 μmol) was dissolved in DMF (1 mL) followed by the addition of DIPEA (7.9 μL, 45.5 μmol). 4-Fluorobenzyl chloride (4.67 μL, 39 μmol) was added to the mixture and shaken (1 h). Following the addition of water, the product was lyophilized and purified by RP-HPLC.

3.4.6 Solution-Phase Conjugation of 4-Fluorobenzoic Acid (**25**)

Isox-Cha-Chg-AR-NH(CH₂)₆NH₂ (**8**) was cleaved off resin and purified by RP-HPLC. Peptide **8** containing a free primary amine (10.8 mg, 11.3 μmol) was dissolved in DMF (1 mL). Separately, 4-fluorobenzoic acid (7.9 mg, 56.3 μmol) and EDC hydrochloride (10.8 mg, 56.3 μmol) were dissolved in DMF (1 mL) and shaken (15 min). The EDC mixture was added to the peptide solution, stirred, and heated (60 °C, 2 h). Following the addition of water, the product was lyophilized and purified by RP-HPLC.

3.4.7 SPPS Reaction Monitoring

Two methods were used to monitor SPPS reactions. The first and more frequent method is the Kaiser Test. In this method, several resin beads were placed in a test tube followed by the addition of 42.5 mM phenol in ethanol (50 μ L), 20 μ M potassium cyanide in pyridine (50 μ L), and 280.7 mM ninhydrin in ethanol (50 μ L). The mixture was then heated (100 $^{\circ}$ C, 5 min). A positive test indicates the presence of a free amine, which is observed by the resin beads turning blue. A negative test indicates no free amine is present, which is observed by resin beads remaining the same colour. The second method is a small-scale resin cleavage. In this method, several beads and cleavage cocktail (500 μ L) are shaken, worked up, and the desired peptide is confirmed through HPLC-MS.

3.4.8 Cell Lines and Culture Conditions

All cell culture supplies were purchased from Thermo Fischer Scientific (Waltham, MA, US) unless otherwise stated. Human embryonic kidney (HEK-293T, ATCC, Manassas, VA, US), CRISPR/Cas9 PAR2 knockout HEK-293T (validated in Mihara et al., 2016), prostate cancer (PC3, ATCC, Manassas, VA, US), and CRISPR/Cas9 PAR2 knockout PC3 cells (see Appendix 5 for validation) were cultured in Dulbecco's Modified Eagle's Medium (HEK293T-derived cell lines) and Ham's F-12K Nutrient Mixture (PC3-derived cell lines) each supplemented with 10% fetal bovine serum (FBS), sodium pyruvate (1mM), and 100 penicillin streptomycin (100 units/mL).⁴⁷ All culture performed under standard conditions (37 $^{\circ}$ C; 5% CO₂). Trypsin (25mM) or PBS-EDTA (1mM) was used to passage cell lines.

3.4.9 BRET β -Arrestin 2 Recruitment Assay

HEK293T cells were transfected with BRET pair PAR2-eYFP (2 μ g) and β -arrestin-2-rluc (0.2 μ g; generous gift from Michel Bouvier) using calcium phosphate and re-plated at 24 hours in tissue culture treated white 96-well plates (density approximately 8×10^2 - 1×10^3 cells/ μ L). Serial dilutions of agonist (ranging from 300 μ M to 300 pM depending on the agonist) were prepared in separate 96-well plates in Hank's Balanced Salt Solution (HBSS). Cell media was removed from 96-well plate containing seeded cells. Agonist was added from negative control (HBSS) through to highest concentration using a

multichannel pipette to seeded plates and incubated (37 °C, 10 min). Renilla luciferase substrate (h-coelenterazine) was added to each well (5 μM final) and incubated (37 °C, 10 min). BRET ratios are recorded on Berthold Mithras LB 940. Responses are expressed as net emission of eYFP/rLuc (calculated by subtracting HBSS baseline eYFP/rLuc ratio from agonist eYFP/rLuc ratio) and normalized to a positive control (**1** at 300 μM). Experiments were completed in $n \geq 3$ and fitted with a non-linear regression analysis four-parameter dose-response curve using GraphPad Prism 6 to determine EC₅₀ values.

3.4.10 Intracellular Calcium Release Assay

HEK293T cells endogenously expressing PAR2 or CRISPR/Cas9 HEK293T PAR2 KO cells were lifted from confluent T75 flasks using PBS-EDTA (1 mM, 5 mL). PBS-EDTA was removed by centrifugation. Cells were re-suspended in 500 μL of Fluo-4 NW (no wash) dye solution and assay buffer (1 x HBSS, 20 mM HEPES) and incubated at ambient temperature on a rocking platform (30 min). Fluo-4 NW cell suspensions were then increased to the volume required for the assay with HBSS (with Ca²⁺ and Mg²⁺). Cells were aliquoted into cuvettes (2 mL/cuvette final volume) containing a magnetic stir-bar to keep cells in suspension for the assay. Individual cuvettes were loaded into a Photon Technologies Institute (PTI) spectrophotometer. Time-based assay parameters were assigned through PTI software as follows: excitation 480 nm, emission 530 nm with 8 nm capture window, and 5000 seconds duration. Before the addition of agonist, individual cuvette emission was collected for approximately 10 seconds to obtain baseline emission. Agonist was pipetted into the cuvette (final concentration of 10 μM for **2**, **6**, **7**, and **16-29** and 100 μM for **1** and **13**) and the fluorescence was measured. As a positive control, untreated cuvettes were treated with a calcium ionophore (ionomycin calcium salt in DMSO, 3 μM final) to obtain maximum possible calcium response. As a negative control, untreated cuvettes were treated with HBSS (no agonist). Response elicited by agonist treatment at individual concentrations ($n \geq 2$) was expressed as a net percentage of the average maximum response (calculated by subtracting no agonist treatment percentage from agonist treatment percentage).

3.4.11 Synthesis of 4-(*tert*-butoxycarbonyl)-N,N,N-trimethylbenzenammonium triflate (**32**)

Synthesis was completed as previously described.⁴⁸ Briefly, 4-dimethylaminobenzoic acid (1.00 g, 6.05 mmol) was dissolved in THF (50 mL) and cooled (0 °C), followed by the dropwise addition of trifluoroacetic anhydride (1.85 mL, 13.3 mmol) and stirring (35 min). *tert*-Butanol (11.4 mL, 119 mmol) was then added and stirred at room temperature (120 min). A saturated solution of sodium bicarbonate (200 mL) was added to the reaction mixture and extracted with DCM (3X 100 mL, 3X 50mL). The organic layers were then combined, dried over MgSO₄, and gravity filtered. The solvent was removed *in vacuo*, dissolved in DCM, and eluted through a silica pad with DCM (60 mL). Solvent was removed *in vacuo*, dissolved in dry DCM (30 mL), and cooled to 0 °C under N₂. Methyl trifluoromethanesulfonate (0.86 mL, 7.61 mmol) was added to the mixture and stirred (60 min, 0 °C). Ice-cold diethyl ether (200 mL) was added to precipitate the product. The solid was then collected by vacuum filtration to yield white crystals (721 mg, 31%). ¹H-NMR (400 MHz, CD₃COCD₃); δ 8.22 (m, 4H), 3.93 (s, 9H), 1.60 (s, 9H) ppm; ¹³C-NMR (100 MHz, CD₃COCD₃); δ 205.19, 164.41, 134.70, 131.96, 121.72, 82.66, 57.81, 28.16 ppm; HRMS (EI-MS): [M-H]⁺ 235.1567 (calc.) 235.1198 (found).

3.4.12 Synthesis of *N*-succinimidyl 4-fluorobenzoate (**34**)

4-Fluorobenzoic acid (140.1 mg, 1.0 mmol) was dissolved in DCM (10 mL). EDC hydrochloride (210.9 mg, 1.1 mmol) and NHS (126.6 mg, 1.1 mmol) were added and the solution was stirred (24 h). The organic solution was washed and extracted with water thrice (3X 10 mL), saturated sodium bicarbonate (10 mL), and saturated sodium chloride (10 mL). The organic layer was then dried with MgSO₄, gravity filtered, and solvent removed *in vacuo* to obtain a white solid (121 mg, 52%). ¹H-NMR (400 MHz, CDCl₃); δ 8.17 (m, 2H), 7.20 (m, 2H), 2.91 (s, 4H) ppm; ¹³C-NMR (100 MHz, CDCl₃); δ 169.29 (s), 166.02 (d, ¹J_{CF} = 256.2 Hz), 161.06 (s), 133.54 (d, ³J_{CF} = 9.7 Hz), 121.54 (d, ⁴J_{CF} = 3.1 Hz), 116.46 (d, ²J_{CF} = 22.1 Hz), 25.81 (s) ppm; HRMS (EI-MS): [M⁺] 237.0437 (calc.) 237.0436 (found).

3.4.13 General Methods for Radiochemistry

[¹⁸F]Fluoride was produced by a GE PETtrace 880 cyclotron (Lawson Cyclotron & PET Radiochemistry Facility, Lawson Health Research Institute, London, Ontario, Canada) through the ¹⁸O(p,n)¹⁸F reaction involving proton bombardment of [¹⁸O]H₂O. GE Tracer Lab FXN was used for the automated synthesis and purification of [¹⁸F]SFB. Compounds were analyzed on a system consisting of an analytical RP-HPLC Waters Atlantis T3 column (6 x 150 mm, 5 μm), Waters 1525 binary pump system, Waters in-line degasser, and Breeze software (version 3.30, 2002 Waters Corporation). Two mobile phases were used; eluent A (0.1% TFA in acetonitrile) and eluent B (0.1% TFA in MilliQ water). The flow rate was set at 1.5 mLmin⁻¹ over 10 min with an additional 5-minute wash (95% solvent A in solvent B). A Waters 2487 Dual λ absorbance detector set at 220 nm and 254 nm and a radioactive flow count detector were used to monitor the column eluate. Compounds were purified using semi-preparative RP-HPLC with the same system, eluents, and detection method as mentioned above for the analytical RP-HPLC, except that a semi-preparative Agilent Zorbax SB-C8 column (9.4 x 150 mm, 5 μm) at a flow rate of 4 mLmin⁻¹ over 15 minutes with an additional 5-minute wash was used. A Biotage V-10 evaporator (Uppsala Sweden) was used to remove solvent.

3.4.14 Synthesis of *N*-succinimidyl 4-[¹⁸F]fluorobenzoate ([¹⁸F]34)

Synthesis was prepared on the GE Tracer Lab FXN using an automated synthesis procedure (see Appendix 7 for the automated synthesis display). Aqueous [¹⁸F]F⁻ was trapped on a Waters Sep-Pak Accell plus carbonated QMA light cartridge. The trapped [¹⁸F]F⁻ was eluted into a reaction vial with a solution of acetonitrile/water (v/v 9:1, 1 mL) containing potassium carbonate (1.0 mg, 7.2 μmol) and Kryptofix 2.2.2 (7 mg, 18.6 μmol). This solvent was removed azeotropically under *vacuo* with helium flow (75 °C). Anhydrous acetonitrile (2X 1 mL) was used to dry the [¹⁸F]F⁻ twice under *vacuo* with helium flow (75 °C). 4-(*tert*-Butoxycarbonyl)-*N,N,N*-trimethylbenzenammonium triflate (5 mg, 13.0 μmol) in anhydrous DMSO (0.5 mL) was then added under helium flow. The reaction vial was sealed and stirred (120 °C, 8 min). The reaction was cooled (40 °C), followed by the addition of aqueous HCl (1 mL, 5 N) and further stirring (100 °C, 3 min). The reaction was cooled again (40 °C) followed by the addition of H₂O (2.5 mL) to dilute

the reaction mixture. The product was trapped on a Waters Sep-Pak C18 light cartridge and eluted into a reaction vial containing NHS (*N*-hydroxysuccinimide, 20.0 mg, 0.17 mmol) and EDC (1-ethyl-3-(3-dimethylaminopropyl)carbodiimide) hydrochloride (200.0 mg, 1.04 mmol) with acetonitrile (1.5 mL). The reaction mixture was stirred at room temperature (15 min). H₂O (3.0 mL) was added to the reaction mixture followed by purification on semi-preparative RP-HPLC (36% MeCN in H₂O, $t_R = 7-9$ min) to yield [¹⁸F]**34** (RCY = 31 ± 3% and RCP >98%, n = 4).

3.4.15 Synthesis of Isox-Cha-Chg-AR-Dpr([¹⁸F]4FB)-NH₂ ([¹⁸F]**29**)

Compound **35** (1.0 mg, 1 μmol) was dissolved in acetonitrile (300 μL) followed by the addition of DIPEA (5 μL, 29 μmol). This mixture was added to a vial containing [¹⁸F]**34** and heated at 85 °C (15 min). The solution was cooled to room temperature, followed by the addition of water (0.7 mL) and purification on RP-HPLC (30-55% solvent A in solvent B, $t_R = 9-10$ min) to yield [¹⁸F]**29** (RCY = 37 ± 3%, RCP >98%, and $A_m = 20 ± 2$ GBq/μmol, n = 4).

3.4.16 Determination of [¹⁸F]**29** Molar Activity

A calibration curve was made from five concentrations (1, 5, 10, 50, and 100 μM) of **29** to determine the molar activity of [¹⁸F]**29**. For each of the five concentrations, at least two analytical HPLC runs were completed in order to obtain the area under the peak (at 230 nm absorbance) associated with **29** within 5% of each other. This was plotted as concentration versus area under the peak and non-linear regression was performed to determine an equation of the line (Appendix 9). The molar activity was calculated based on determining the amount of radioactivity from the [¹⁸F]**29** sample, the volume the [¹⁸F]**29** sample was dissolved in, the area under the peak of the [¹⁸F]**29** sample analytical HPLC trace at 230 nm, and the linear equation from the calibration curve.

3.4.17 Cell uptake of [¹⁸F]**29**

Cells were seeded into 6-well tissue culture plates at a density of 5.0 x 10⁵ cells for PC3 cells and 1.0 x 10⁶ cells for PC3 PAR2 KO cells per 35-mm well. Appropriate seeding densities were determined prior to experiment. Cells were allowed to seed for 48 hours

before cell uptake was performed. On the day of experiment after [¹⁸F]29 was synthesized, serum media was removed and washed with HBSS (1 mL/well). A 2% BSA in HBSS solution (3 mL) was added to each well and incubated (37 °C, 30 min) to help block non-specific binding. The BSA solution was removed and 1mL of 50 to 100 kBq of [¹⁸F]29 in HBSS (with or without 20 μM of block peptide, 7) was added to each well and incubated (20 or 60 min). At the end of the incubation, plates were wash with HBSS (3X 1mL/well) thrice to remove any unbound probe. This wash solution was collected and activity was measured on a gamma counter. PBS (1mL) was added to each well and cells were removed from the wells using a cell scrapper. Wells were then rinsed with PBS two additional times (2X 1 mL) to ensure all cells were collected. Collected cells were measured on a gamma counter to determine cell uptake activity. Experiments were completed in n ≥ 6. Data was decay corrected and expressed as a percentage of cell uptake over total activity (where total activity = wash + uptake). A two way ANOVA (cell condition, time) for percent uptake followed by a post-hoc Tukey multiple comparisons test was used to assess significance through GraphPad Prism 6 (significance set at 0.05).

3.5 References

- (1) Molino, M.; Barnathan, E. S.; Clark, J.; Dreyer, M.; Hoxie, J. a; Schechter, N.; Woolkalis, M.; Brass, L. F.; Numerof, R.; Cumashi, A. *J. Biol. Chem.* **1997**, *272* (7), 4043–4049.
- (2) Nystedt, S.; Emilsson, K.; Wahlestedt, C.; Sundelin, J. *Proc. Natl. Acad. Sci.* **1994**, *91* (20), 9208–9212.
- (3) Hansen, K. K.; Sherman, P. M.; Cellars, L.; Andrade-Gordon, P.; Pan, Z.; Baruch, A.; Wallace, J. L.; Hollenberg, M. D.; Vergnolle, N. *Proc. Natl. Acad. Sci.* **2005**, *102* (23), 8363–8368.
- (4) Ramsay, A. J.; Dong, Y.; Hunt, M. L.; Linn, M.; Samaratunga, H.; Clements, J. A.; Hooper, J. D. *J. Biol. Chem.* **2008**, *283* (18), 12293–12304.
- (5) Adams, M. N.; Ramachandran, R.; Yau, M. K.; Suen, J. Y.; Fairlie, D. P.; Hollenberg, M. D.; Hooper, J. D. *Pharmacol. Ther.* **2011**, *130* (3), 248–282.
- (6) Nystedt, S.; Emilsson, K.; Larsson, a K.; Strömbeck, B.; Sundelin, J. *Eur. J. Biochem.* **1995**, *232* (1), 84–89.
- (7) Bohm, S. K.; Kong, W.; Bromme, D.; Smeekens, S. P.; Anderson, D. C.; Connolly, A.; Kahn, M.; Nelken, N. A.; Coughlin, S. R.; Payan, D. G.; Bunnett, N. W. *Biochem. J.* **1996**, *314* (12), 1009–1016.
- (8) Fagerberg, L.; Hallström, B. M.; Oksvold, P.; Kampf, C.; Djureinovic, D.; Odeberg, J.; Habuka, M.; Tahmasebpoor, S.; Danielsson, A.; Edlund, K.; Asplund, A.; Sjöstedt, E.; Lundberg, E.; Szigyaró, C. A.-K.; Skogs, M.; Takanen, J. O.; Berling, H.; Tegel, H.; Mulder, J.; Nilsson, P.; Schwenk, J. M.; Lindskog, C.; Danielsson, F.; Mardinoglu, A.; Sivertsson, Å.; von Feilitzen, K.; Forsberg, M.; Zwahlen, M.; Olsson, I.; Navani, S.; Huss, M.; Nielsen, J.; Ponten, F.; Uhlén, M. *Mol. Cell. Proteomics* **2014**, *13* (2), 397–406.
- (9) Cocks, T. M.; Fong, B.; Chow, J. M.; Anderson, G. P.; Frauman, A. G.; Goldie, R. G.; Henry, P. J.; Carr, M. J.; Hamilton, J. R.; Moffatt, J. D. *Nature* **1999**, *398* (6723), 156–160.
- (10) Damiano, B. P.; Cheung, W. M.; Santulli, R. J.; Fung-Leung, W. P.; Ngo, K.; Ye, R. D.; Darrow, a L.; Derian, C. K.; de Garavilla, L.; Andrade-Gordon, P. *J. Pharmacol. Exp. Ther.* **1999**, *288* (2), 671–678.
- (11) Su, S.; Li, Y.; Luo, Y.; Sheng, Y.; Su, Y.; Padia, R. N.; Pan, Z. K.; Dong, Z.; Huang, S. *Oncogene* **2009**, *28* (34), 3047–3057.
- (12) Antoniak, S.; Rojas, M.; Spring, D.; Bullard, T. A.; Verrier, E. D.; Blaxall, B. C.; MacKman, N.; Pawlinski, R. *Arterioscler. Thromb. Vasc. Biol.* **2010**, *30* (11), 2136–2142.
- (13) Kim, D. H.; Cho, Y. J.; Kim, J. H.; Kim, Y. B.; Lee, K. J. *J. Korean Med. Sci.* **2010**, *25* (9), 1330–1335.
- (14) Lohman, R.-J.; Cotterell, A. J.; Barry, G. D.; Liu, L.; Suen, J. Y.; Vesey, D. A.;

- Fairlie, D. P. *FASEB J.* **2012**, *26* (7), 2877–2887.
- (15) Aman, M.; Ohishi, Y.; Imamura, H.; Shinozaki, T.; Yasutake, N.; Kato, K.; Oda, Y. *Hum. Pathol.* **2017**, *64*, 156–163.
- (16) Cenac, N.; Coelho, A. M.; Nguyen, C.; Compton, S.; Andrade-Gordon, P.; MacNaughton, W. K.; Wallace, J. L.; Hollenberg, M. D.; Bunnett, N. W.; Garcia-Villar, R.; Bueno, L.; Vergnolle, N. *Am. J. Pathol.* **2002**, *161* (5), 1903–1915.
- (17) Ferrell, W. R.; Lockhart, J. C.; Kelso, E. B.; Dunning, L.; Plevin, R.; Meek, S. E.; Smith, A. J. H.; Hunter, G. D.; Mclean, J. S.; McGarry, F.; Ramage, R.; Jiang, L.; Kanke, T.; Kawagoe, J. *J. Clin. Invest.* **2003**, *111* (1), 35–41.
- (18) Jin, E.; Fujiwara, M.; Pan, X.; Ghazizadeh, M.; Arai, S.; Ohaki, Y.; Kajiwara, K.; Takemura, T.; Kawanami, O. *Cancer* **2003**, *97* (3), 703–713.
- (19) Massi, D.; Naldini, A.; Ardinghi, C.; Carraro, F.; Franchi, A.; Paglierani, M.; Tarantini, F.; Ketabchi, S.; Cirino, G.; Hollenberg, M. D.; Geppetti, P.; Santucci, M. *Hum. Pathol.* **2005**, *36* (6), 676–685.
- (20) Caruso, R.; Pallone, F.; Fina, D.; Gioia, V.; Peluso, I.; Caprioli, F.; Stolfi, C.; Perfetti, A.; Spagnoli, L. G.; Palmieri, G.; MacDonald, T. T.; Monteleone, G. *Am. J. Pathol.* **2006**, *169* (1), 268–278.
- (21) Fujimoto, D.; Hirono, Y.; Goi, T.; Katayama, K.; Hirose, K.; Yamaguchi, A. *J. Surg. Oncol.* **2006**, *93* (2), 139–144.
- (22) Black, P. C.; Mize, G. J.; Karlin, P.; Greenberg, D. L.; Hawley, S. J.; True, L. D.; Vessella, R. L.; Takayama, T. K. *Prostate* **2007**, *67*, 743–756.
- (23) Hyun, E.; Andrade-Gordon, P.; Steinhoff, M.; Vergnolle, N. *Gut* **2008**, *57* (9), 1222–1229.
- (24) Shi, X.; Gangadharan, B.; Brass, L. F.; Ruf, W.; Mueller, B. M. *Mol. Cancer Res.* **2004**, *2* (7), 395–402.
- (25) Uusitalo-Jarvinen, H.; Kurokawa, T.; Mueller, B. M.; Andrade-Gordon, P.; Friedlander, M.; Ruf, W. *Arterioscler. Thromb. Vasc. Biol.* **2007**, *27* (6), 1456–1462.
- (26) Kamath, L.; Meydani, A.; Foss, F. *Cancer Res.* **2001**, *61*, 5933–5940.
- (27) Jahan, I.; Fujimoto, J.; Alam, S. M.; Sato, E.; Sakaguchi, H.; Tamaya, T. *Ann. Oncol.* **2007**, *18* (9), 1506–1512.
- (28) Al-Ani, B.; Saifeddine, M.; Hollenberg, M. D. *Can. J. Physiol. Pharmacol.* **1995**, *73* (8), 1203–1207.
- (29) Kanke, T.; Ishiwata, H.; Kabeya, M.; Saka, M.; Doi, T.; Hattori, Y.; Kawabata, A.; Plevin, R. *Br. J. Pharmacol.* **2005**, *145* (2), 255–263.
- (30) Barry, G. D.; Suen, J. Y.; Low, H. B.; Pfeiffer, B.; Flanagan, B.; Halili, M.; Le, G. T.; Fairlie, D. P. *Bioorganic Med. Chem. Lett.* **2007**, *17* (20), 5552–5557.
- (31) Hollenberg, M. D.; Renaux, B.; Hyun, E.; Houle, S.; Vergnolle, N.; Saifeddine, M.; Ramachandran, R. *J. Pharmacol. Exp. Ther.* **2008**, *326* (2), 453–462.

- (32) Hoffman, J.; Flynn, A. N.; Tillu, D. V.; Zhang, Z.; Patek, R.; Price, T. J.; Vagner, J.; Boitano, S. *Bioconjug. Chem.* **2012**, *23* (10), 2098–2104.
- (33) Yau, M. K.; Suen, J. Y.; Xu, W.; Lim, J.; Liu, L.; Adams, M. N.; He, Y.; Hooper, J. D.; Reid, R. C.; Fairlie, D. P. *ACS Med. Chem. Lett.* **2016**, *7* (1), 105–110.
- (34) Jiang, Y.; Yau, M. K.; Kok, W. M.; Lim, J.; Wu, K. C.; Liu, L.; Hill, T. A.; Suen, J. Y.; Fairlie, D. P. *ACS Chem. Biol.* **2017**, *12* (5), 1217–1226.
- (35) McGuire, J.; Saifeddine, M.; Triggle, C. *J. Pharmacol. Exp. Ther.* **2004**, *309* (3), 1124–1131.
- (36) Al-Ani, B.; Saifeddine, M.; Kawabata, a; Renaux, B.; Mokashi, S.; Hollenberg, M. D. *J. Pharmacol. Exp. Ther.* **1999**, *290* (2), 753–760.
- (37) Lau, C.; Lytle, C.; Straus, D. S.; DeFea, K. A. *AJP Cell Physiol.* **2011**, *300* (1), C113–C123.
- (38) Jacobson, O.; Kiesewetter, D. O.; Chen, X. *Bioconjug. Chem.* **2014**, *26*, 1–18.
- (39) Schubiger, P. A.; Lehmann, L.; Friebe, M. *PET Chemistry book*; 2007.
- (40) Lasne, M.-C.; Perrio, C.; Rouden, J.; Barré, L.; Roeda, D.; Dolle, F.; Crouzel, C. *Top. Curr. Chem.* **2002**, *222*, 203–258.
- (41) Olberg, D. E.; Hjelstuen, O. K. *Curr. Top. Med. Chem.* **2010**, *10* (16), 1669–1679.
- (42) Hollenberg, M. D.; Saifeddine, M.; Al-Ani, B.; Kawabata, A. *Can. J. Physiol. Pharmacol.* **1997**, *75* (7), 832–841.
- (43) Maryanoff, B. E.; Santulli, R. J.; McComsey, D. F.; Hoekstra, W. J.; Hoey, K.; Smith, C. E.; Addo, M.; Darrow, A. L.; Andrade-Gordon, P. *Arch. Biochem. Biophys.* **2001**, *386* (2), 195–204.
- (44) Wüst, F.; Hultsch, C.; Bergmann, R.; Johannsen, B.; Henle, T. *Appl. Radiat. Isot.* **2003**, *59* (1), 43–48.
- (45) Mäding, P.; Füchtner, F.; Wüst, F. *Appl. Radiat. Isot.* **2005**, *63* (3), 329–332.
- (46) MedChem Designer ADMET Predictor, version 3.1.0.30, Simulations Plus, Inc., California, US.
- (47) Mihara, K.; Ramachandran, R.; Saifeddine, M.; Hansen, K. K.; Renaux, B.; Polley, D.; Gibson, S.; Vanderboor, C.; Hollenberg, M. D. *Mol. Pharmacol.* **2016**, *89* (5), 606–614.
- (48) Fowkes, M. M.; Leonard, S.; Luyt, G. Peptidomimetic GHS-R1a Agonists as PET Imaging Agents for Prostate Cancer, 2014.

Chapter 4

4 Conclusions and Future Work

4.1 Conclusions

Aberrant function and over-expression of PAR2 is known to be involved in many cancers, including cancer progression, as well as multiple inflammatory diseases.¹⁻¹⁷ PAR2 is therefore an important biological target for the development of targeted therapeutics and imaging agents. Ligands targeting this receptor have been widely studied, with the development of various agonists and antagonists showing therapeutic potential. Some examples include agonists such as 2f-LIGRLO-NH₂, Isox-Cha-Chg-AR-NH₂, and GB110 (Figure 4.1A) and antagonists such as GB88, C391, and K-14585 (Figure 4.1B).¹⁸⁻²² Yet, imaging probes for this receptor are scarce. There are only a few fluorescent and tritiated probes that have been developed (examples shown in Figure 4.1C), which all have a limited depth of penetration, lack of applicable *in vivo* imaging potential, and still show potential for significant PAR2 binding affinity improvement.²³⁻²⁵ This thesis addresses this paucity of research through the design, synthesis, and evaluation of novel PAR2-targeting fluorescent and ¹⁸F-PET imaging agents.

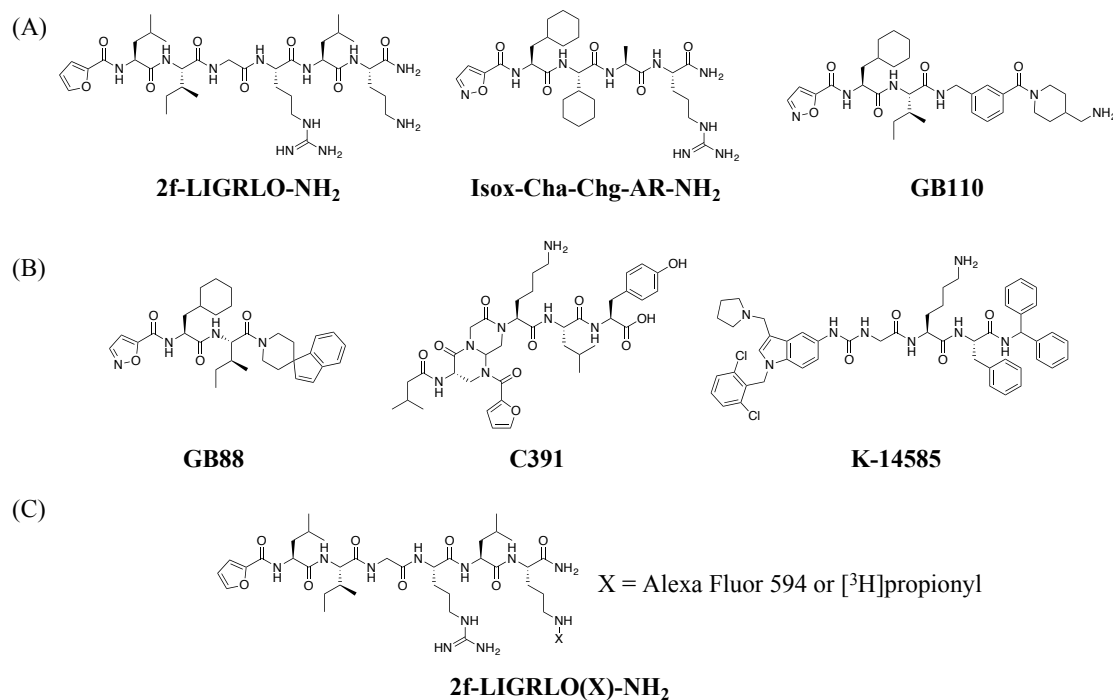


Figure 4.1: Several reported leading (A) agonists, (B) antagonists, and (C) imaging probes targeting PAR2.^{18–22,24}

This thesis has three main goals. The first goal was the development and evaluation of novel PAR2-targeting peptides with primary amines to allow for facile conjugation of imaging components. The second goal was to develop an improved PAR2-selective fluorescent probe for use in various *in vitro* experiments and potential clinical applications in PAR2-related diseases. The third goal was the development of the first ever *in vivo* imaging agent targeting PAR2 for use in PET imaging, providing insight into PAR2 expression *in vivo* and potential clinical applications in the treatment and diagnosis of PAR2-related diseases.

To achieve these goals, peptides were synthesized through standard Fmoc-SPPS, purified and characterized through RP-HPLC and HRMS, and evaluated for PAR2-binding through β -arrestin recruitment, calcium release, flow cytometry, and cell uptake assays.

The beginning portion of Chapter 2 addressed the first goal of the thesis. Modifications were made to known PAR2-targeting peptides to include a free primary amine allowing

for facile conjugation of the various imaging components. Several synthesized peptides (**8-11**) showed strong potencies ($EC_{50} = 10$ nM to 23 nM, Table 2.1, Chapter 2) and selectivity for PAR2 with varying structural and hydrophobic properties. This preliminary work demonstrated the suitability of Isox-Cha-Chg-Ala-Arg related peptides for conjugation to various imaging components.

The later portion of Chapter 2 addressed the second goal of the thesis. A Sulfo-Cy5 dye was conjugated to **11** to yield **15** (Isox-Cha-Chg-ARK(Sulfo-Cy5)-NH₂). Peptide **15** (Figure 4.2A) was found to be a PAR2-selective fluorescent probe with a greater than ten-fold increase in potency and binding affinity ($EC_{50} = 16$ nM and $K_D = 38$ nM, respectively) compared to an analogue of the best known PAR2-targeting fluorescent probe (2f-LIGRLO(Cy5)-NH₂, Table 2.3, Chapter 2). Peptide **15** was then further evaluated in an *in vitro* confocal microscopy experiment, showing PAR2-selective uptake in PC3 cells (Figure 2.4, Chapter 2).

Chapter 3 addressed the third goal of the thesis. To achieve PAR2-targeting ¹⁸F-PET imaging agents, [¹⁹F]4-fluorobenzoyl-standards were conjugated to peptides for *in vitro* evaluation before generating the ¹⁸F-labeled analogue. A PAR2-targeting peptide of Class I showed promise (**19**, Table 3.1, Chapter 3), but many Class II peptides showed greater promise. First generation Class II peptides showed poor potency and loss of PAR2-selectivity (**21**, Table 3.2, Chapter 3), but the second generation of Class II peptides showed substantial improvements in PAR2 potency comparable to **8-11** (**22-25**, Table 3.3, Chapter 3). Unfortunately, the most potent candidates **22-24**, were found to lose PAR2-selectivity (Table 3.3, Chapter 3). Thus, third generation Class II peptides were synthesized, many of which (**26**, **27**, and **29**) showed high potency and selectivity for PAR2 (Table 3.4, Chapter 3). The lead candidate, **29** (Isox-Cha-Chg-AR-Dpr(4-FB)-NH₂, $EC_{50} = 13$ nM) was synthesized successfully with fluorine-18 in place of fluorine-19 using [¹⁸F]SFB to yield [¹⁸F]**29** (Figure 4.2B) with a radiochemical yield of $37 \pm 3\%$, greater than 98% radiochemical purity, molar activity of 20 ± 2 GBq/ μ mol, and end-of-synthesis time of 125 ± 2 min ($n = 4$). Peptide [¹⁸F]**29** was then evaluated in *in vitro* cell uptake studies using PC3 and PAR2 KO PC3 cells where it showed significant uptake in

the PAR2-expressing cells compared to controls ($P < 0.001$, Figure 3.4, Chapter 3). Peptide [^{18}F]29 is the first PAR2-selective *in vivo* imaging agent ever developed.

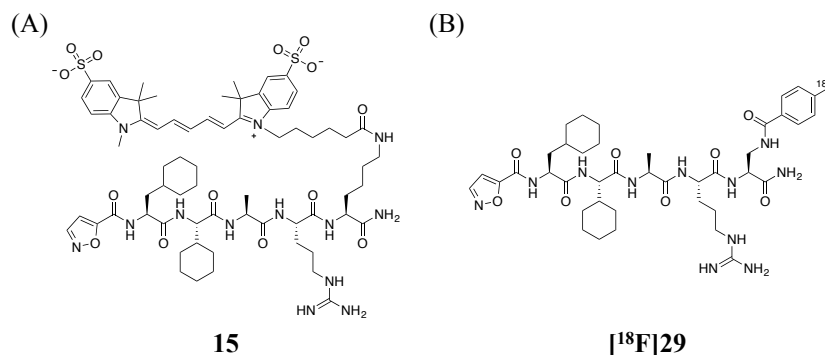


Figure 4.2: Structures of the lead PAR2-targeting (A) fluorescent probe, **15**, and (B) PET imaging agent, [^{18}F]29, developed in this thesis.

These novel probes, specifically **15** and [^{18}F]29, are chemical tools that could provide insight into areas of PAR2 expression *in vitro* and *in vivo* with potential clinical applications in the diagnosis and treatment of various cancers and inflammatory diseases.

4.2 Future Work and Outlook

Studies to evaluate [^{18}F]29 in normal mice are underway to determine *ex vivo* biodistribution of the tracer as well as to determine non-specific and specific uptake in various tissues through the use of a blocking peptide. In addition, a PC3 xenograft mouse model in immunodeficient mice will be used as a preclinical model of cancer for evaluation of [^{18}F]29 uptake in the tumour and other tissue through PET imaging.

In the long term, both probes (**15** and [^{18}F]29) will be evaluated in various *in vitro* and *in vivo* models of PAR2-related diseases, providing insights into PAR2 expression as well as advancing their potential for future clinical translation. More specifically in research purposes, **15** could be used in experiments such as PAR2-targeted competitive binding assays, determination of PAR2 expression levels for different cell types, and determination of PAR2 trafficking. Compound [^{18}F]29 could potentially be used in

experimental research such as providing insight into endogenous PAR2 expression *in vivo*, providing insight into PAR2 expression and relevance in models of disease *in vivo* (e.g. a colon cancer model), and determining the effectiveness of new PAR2-targeting therapies *in vivo*. The research-based applications of **15** and [¹⁸F]**29** will help the future development of PAR2-targeting imaging agents, ligands, and drug therapies, as well as improve the understanding of PAR2 expression and pathogenesis in relevant diseases.

Clinically, since PAR2 is implicated in various cancers and inflammatory diseases and since its expression levels are linked to cancer staging, **15** has potential applications in pathological histology staining and intraoperative imaging for image-guided surgeries.¹⁻¹⁷ Similarly, [¹⁸F]**29** has potential clinical applications as a non-invasive imaging approach for patient diagnosis, stratification, treatment monitoring, and early-stage detection of PAR2-related diseases. Both **15** and [¹⁸F]**29** especially have strong potential in the stratification and treatment monitoring of patients with PAR2-related diseases as medicine continues to advance towards personalized medicine approaches.

This thesis also provides a good platform for the development of targeted drug delivery conjugates for PAR2-related diseases. The targeted drug delivery approach generally involves a therapeutic component (e.g. a chemotherapy drug), a linker, and a targeting moiety, similar to the design of the imaging agents described in this thesis.^{26,27} The target is a biomarker which is inappropriately found in a disease in comparison to normal tissue, and so the targeted drug delivery approach helps maximize therapeutic effect while minimizing off-target side effects.^{26,27} The first component to this thesis that helps give a good platform for the development of targeted drug delivery conjugates is the extensive PAR2-ligand SAR. The second is the many lead candidates that could be used as the targeting moiety of the targeted drug delivery conjugate. The third is the amine handle on the various peptides, which would allow for facile conjugation of the PAR2-targeting moiety with the remaining component of the targeted drug delivery conjugate.

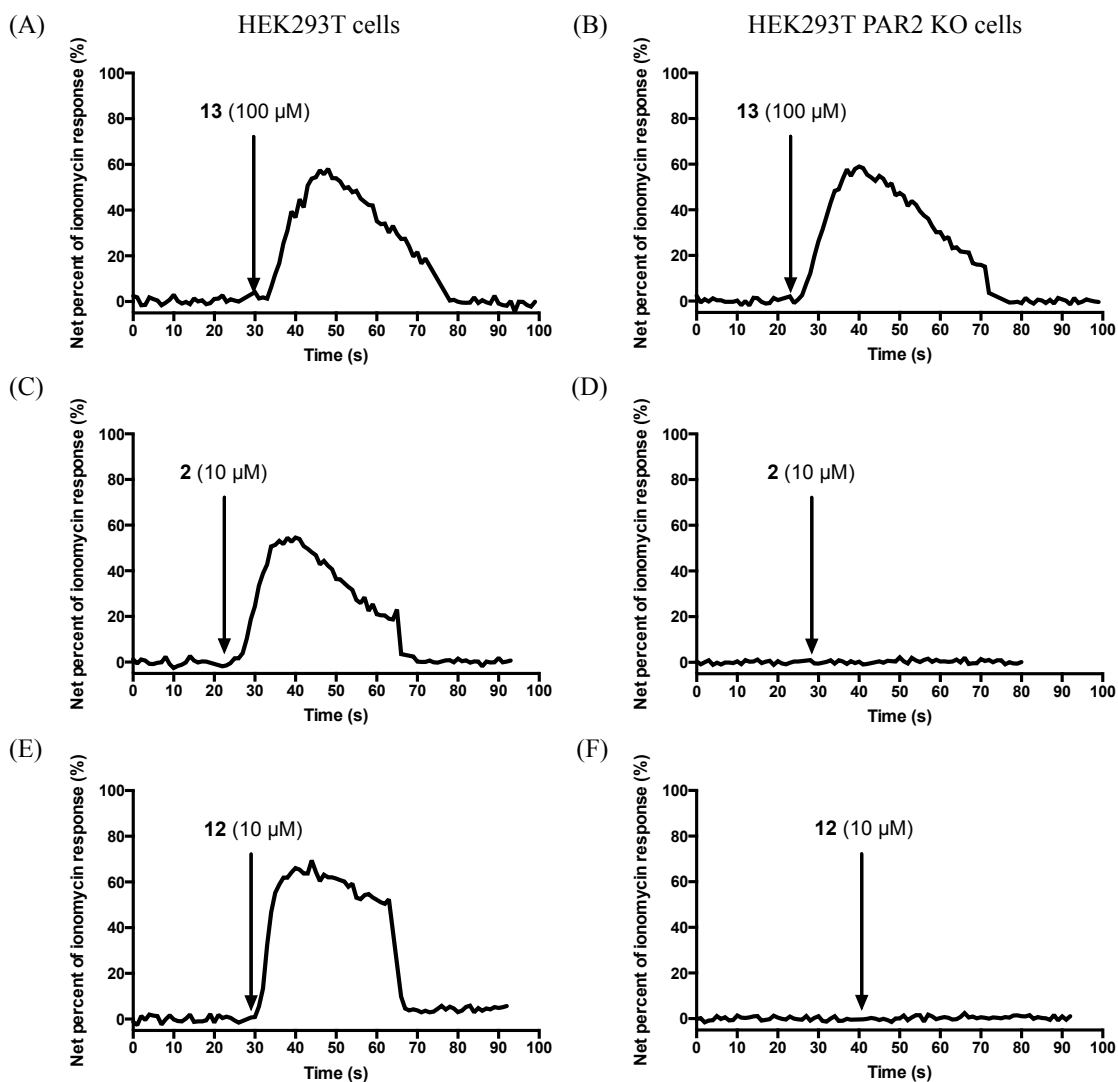
4.3 References

- (1) Cocks, T. M.; Fong, B.; Chow, J. M.; Anderson, G. P.; Frauman, A. G.; Goldie, R. G.; Henry, P. J.; Carr, M. J.; Hamilton, J. R.; Moffatt, J. D. *Nature* **1999**, *398* (6723), 156–160.
- (2) Damiano, B. P.; Cheung, W. M.; Santulli, R. J.; Fung-Leung, W. P.; Ngo, K.; Ye, R. D.; Darrow, a L.; Derian, C. K.; de Garavilla, L.; Andrade-Gordon, P. *J. Pharmacol. Exp. Ther.* **1999**, *288* (2), 671–678.
- (3) Massi, D.; Naldini, A.; Ardinghi, C.; Carraro, F.; Franchi, A.; Paglierani, M.; Tarantini, F.; Ketabchi, S.; Cirino, G.; Hollenberg, M. D.; Geppetti, P.; Santucci, M. *Hum. Pathol.* **2005**, *36* (6), 676–685.
- (4) Caruso, R.; Pallone, F.; Fina, D.; Gioia, V.; Peluso, I.; Caprioli, F.; Stolfi, C.; Perfetti, A.; Spagnoli, L. G.; Palmieri, G.; MacDonald, T. T.; Monteleone, G. *Am. J. Pathol.* **2006**, *169* (1), 268–278.
- (5) Fujimoto, D.; Hirono, Y.; Goi, T.; Katayama, K.; Hirose, K.; Yamaguchi, A. *J. Surg. Oncol.* **2006**, *93* (2), 139–144.
- (6) Black, P. C.; Mize, G. J.; Karlin, P.; Greenberg, D. L.; Hawley, S. J.; True, L. D.; Vessella, R. L.; Takayama, T. K. *Prostate* **2007**, *67*, 743–756.
- (7) Hyun, E.; Andrade-Gordon, P.; Steinhoff, M.; Vergnolle, N. *Gut* **2008**, *57* (9), 1222–1229.
- (8) Kamath, L.; Meydani, A.; Foss, F. *Cancer Res.* **2001**, *61*, 5933–5940.
- (9) Jahan, I.; Fujimoto, J.; Alam, S. M.; Sato, E.; Sakaguchi, H.; Tamaya, T. *Ann. Oncol.* **2007**, *18* (9), 1506–1512.
- (10) Su, S.; Li, Y.; Luo, Y.; Sheng, Y.; Su, Y.; Padia, R. N.; Pan, Z. K.; Dong, Z.; Huang, S. *Oncogene* **2009**, *28* (34), 3047–3057.
- (11) Antoniak, S.; Rojas, M.; Spring, D.; Bullard, T. A.; Verrier, E. D.; Blaxall, B. C.; MacKman, N.; Pawlinski, R. *Arterioscler. Thromb. Vasc. Biol.* **2010**, *30* (11), 2136–2142.
- (12) Kim, D. H.; Cho, Y. J.; Kim, J. H.; Kim, Y. B.; Lee, K. J. *J. Korean Med. Sci.* **2010**, *25* (9), 1330–1335.
- (13) Lohman, R.-J.; Cotterell, A. J.; Barry, G. D.; Liu, L.; Suen, J. Y.; Vesey, D. A.; Fairlie, D. P. *FASEB J.* **2012**, *26* (7), 2877–2887.
- (14) Aman, M.; Ohishi, Y.; Imamura, H.; Shinozaki, T.; Yasutake, N.; Kato, K.; Oda, Y. *Hum. Pathol.* **2017**, *64*, 156–163.
- (15) Cenac, N.; Coelho, A. M.; Nguyen, C.; Compton, S.; Andrade-Gordon, P.; MacNaughton, W. K.; Wallace, J. L.; Hollenberg, M. D.; Bunnett, N. W.; Garcia-Villar, R.; Bueno, L.; Vergnolle, N. *Am. J. Pathol.* **2002**, *161* (5), 1903–1915.
- (16) Ferrell, W. R.; Lockhart, J. C.; Kelso, E. B.; Dunning, L.; Plevin, R.; Meek, S. E.; Smith, A. J. H.; Hunter, G. D.; Mclean, J. S.; McGarry, F.; Ramage, R.; Jiang, L.;

- Kanke, T.; Kawagoe, J. *J. Clin. Invest.* **2003**, *111* (1), 35–41.
- (17) Jin, E.; Fujiwara, M.; Pan, X.; Ghazizadeh, M.; Arai, S.; Ohaki, Y.; Kajiwara, K.; Takemura, T.; Kawanami, O. *Cancer* **2003**, *97* (3), 703–713.
- (18) Barry, G. D.; Suen, J. Y.; Le, G. T.; Cotterell, A.; Reid, R. C.; Fairlie, D. P. *J. Med. Chem.* **2010**, *53* (20), 7428–7440.
- (19) Suen, J. Y.; Cotterell, A.; Lohman, R. J.; Lim, J.; Han, A.; Yau, M. K.; Liu, L.; Cooper, M. A.; Vesey, D. A.; Fairlie, D. P. *Br. J. Pharmacol.* **2014**, *171* (17), 4112–4124.
- (20) Boitano, S.; Hoffman, J.; Flynn, A. N.; Asiedu, M. N.; Tillu, D. V.; Zhang, Z.; Sherwood, C. L.; Rivas, C. M.; Defea, K. A.; Vagner, J.; Price, T. J. *Br. J. Pharmacol.* **2015**, *172* (18), 4535–4545.
- (21) Yau, M.-K.; Lim, J.; Liu, L.; Fairlie, D. P. *Expert Opin. Ther. Pat.* **2016**, *26* (4), 471–483.
- (22) Jiang, Y.; Yau, M. K.; Kok, W. M.; Lim, J.; Wu, K. C.; Liu, L.; Hill, T. A.; Suen, J. Y.; Fairlie, D. P. *ACS Chem. Biol.* **2017**, *12* (5), 1217–1226.
- (23) Kanke, T.; Ishiwata, H.; Kabeya, M.; Saka, M.; Doi, T.; Hattori, Y.; Kawabata, A.; Plevin, R. *Br. J. Pharmacol.* **2005**, *145* (2), 255–263.
- (24) Hollenberg, M. D.; Renaux, B.; Hyun, E.; Houle, S.; Vergnolle, N.; Saifeddine, M.; Ramachandran, R. *J. Pharmacol. Exp. Ther.* **2008**, *326* (2), 453–462.
- (25) Lau, C.; Lytle, C.; Straus, D. S.; DeFea, K. A. *AJP Cell Physiol.* **2011**, *300* (1), C113–C123.
- (26) Gilad, Y.; Firer, M.; Gellerman, G. Recent Innovations in Peptide Based Targeted Drug Delivery to Cancer Cells. *Biomedicines* **2016**, *4* (2), 11.
- (27) Srinivasarao, M.; Low, P. S. Ligand-Targeted Drug Delivery. *Chem. Rev.* **2017**, *117* (19), 12133–12164.

Appendices

Appendix 1: Representative Examples of PAR2-Selectivity Measurements as Determined Through Calcium Response Assay in HEK293T and PAR2 KO HEK293T Cells



(A) HEK293T cells + 100 μ M of **13**, (B) HEK293T PAR2 KO cells + 100 μ M of **13**, (C) HEK293T cells + 10 μ M of **2**, (D) HEK293T PAR2 KO cells + 10 μ M of **2**, (E) HEK293T cells + 10 μ M of **12**, (F) HEK293T PAR2 KO cells + 10 μ M of **12**.

Appendix 2: Validation of Specific Binding for Flow Cytometry Experiments

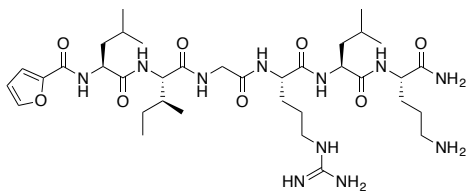
#	Concentration (nM)	Normalized fluorescence signal \pm SEM	Normalized fluorescence signal with block \pm SEM*
14	200	22.2 \pm 2.3	10.8 \pm 1.1
14	1000	64.5 \pm 2.1	38.2 \pm 0.2
15	200	24.8 \pm 4.2	7.3 \pm 2.3
15	1000	60.2 \pm 7.2	32.7 \pm 7.4

*Block done with 20 μ M of a known PAR2-selective peptide, Isox-Cha-Chg-AR-NH₂ (7).

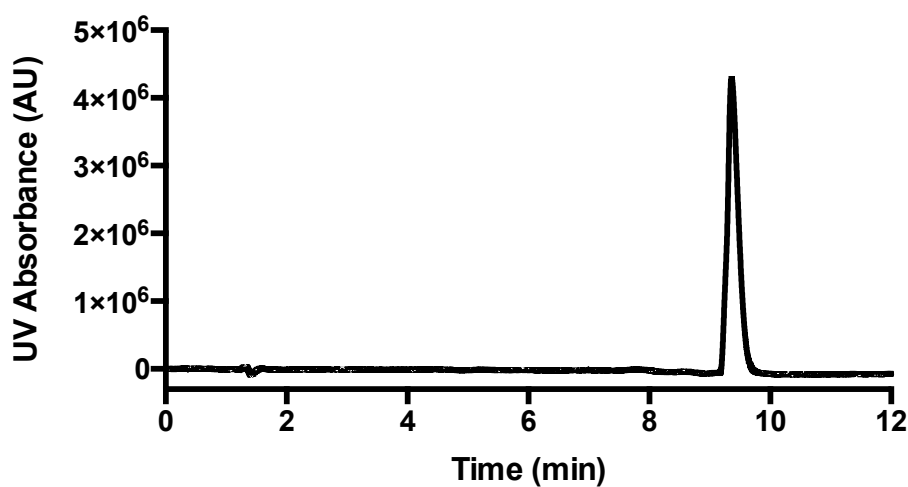
Appendix 3: Characterization of Synthesized Peptides (2, 6-12, and 14-15)

All peptides were >95% pure as determined by analytical RP-HPLC UV detection (see chromatograms below).

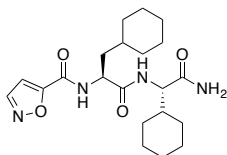
2f-LIGRLO-NH₂, **2** (C₃₆H₆₃N₁₁O₈):



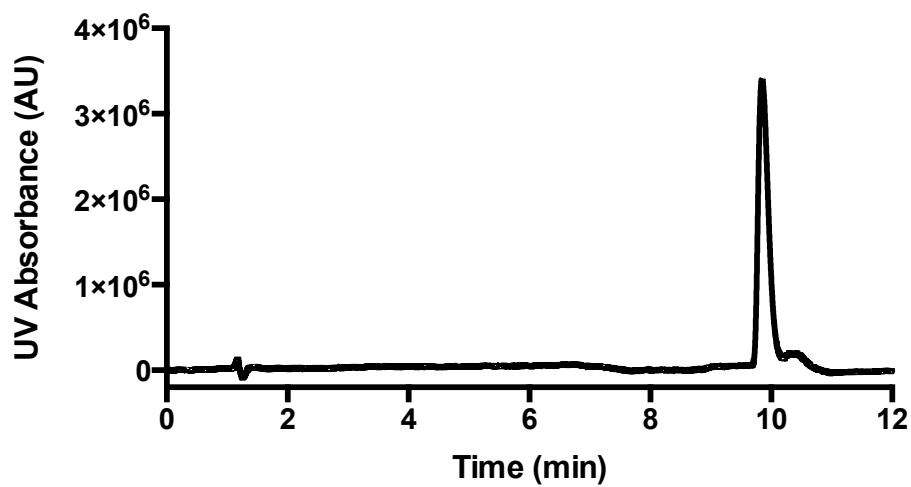
t_R = 9.36 min; HRMS (ESI-MS): [M+H]⁺ 778.4939 (calc.) 778.4945 (found).



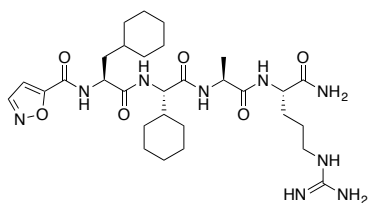
Isox-Cha-Chg-NH₂, **6** (C₂₁H₃₂N₄O₄):



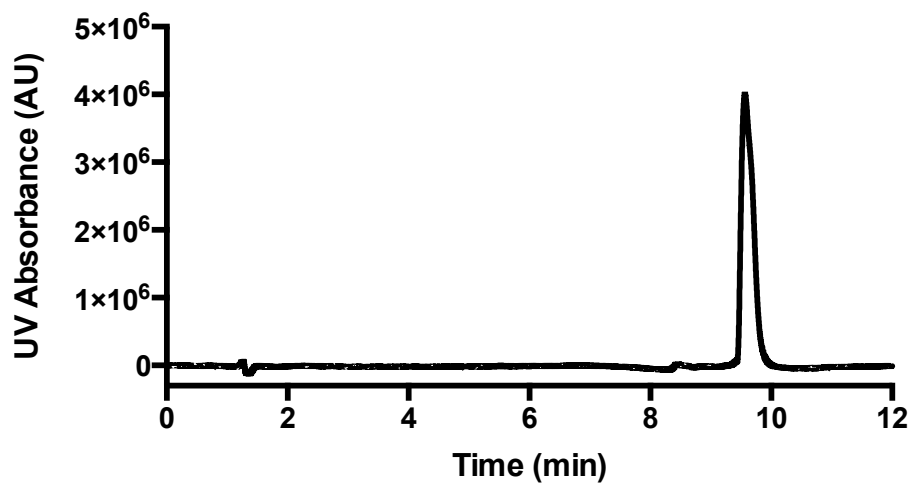
$t_R = 9.85$ min; HRMS (ESI-MS): $[M+Na]^+$ 427.2321 (calc.) 427.2309 (found).



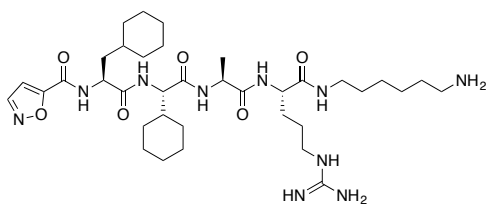
Isox-Cha-Chg-AR-NH₂, **7** (C₃₀H₄₉N₉O₆):



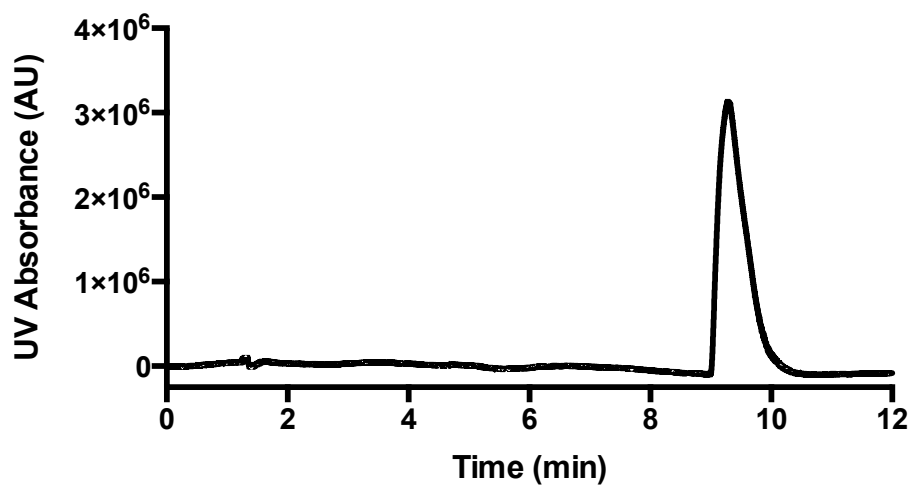
$t_R = 9.57$ min; HRMS (ESI-MS): $[M+H]^+$ 632.3884 (calc.) 632.3892 (found).



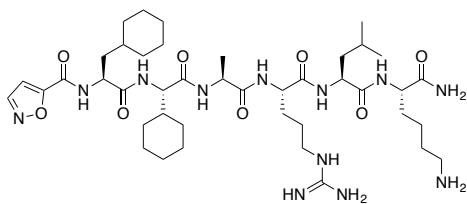
Isox-Cha-Chg-AR-NH(CH₂)₆NH₂, **8** (C₃₆H₆₂N₁₀O₆):



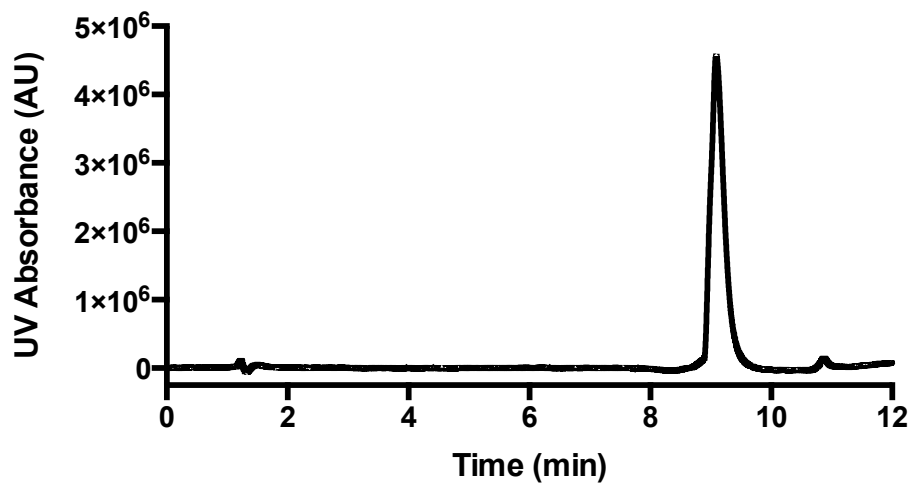
$t_R = 9.29$ min; HRMS (ESI-MS): $[M+H]^+$ 731.4932 (calc.) 731.4944 (found).



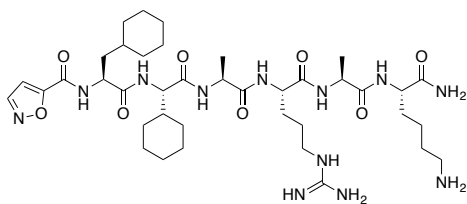
Isox-Cha-Chg-ARLK-NH₂, **9** (C₄₂H₇₂N₁₂O₈):



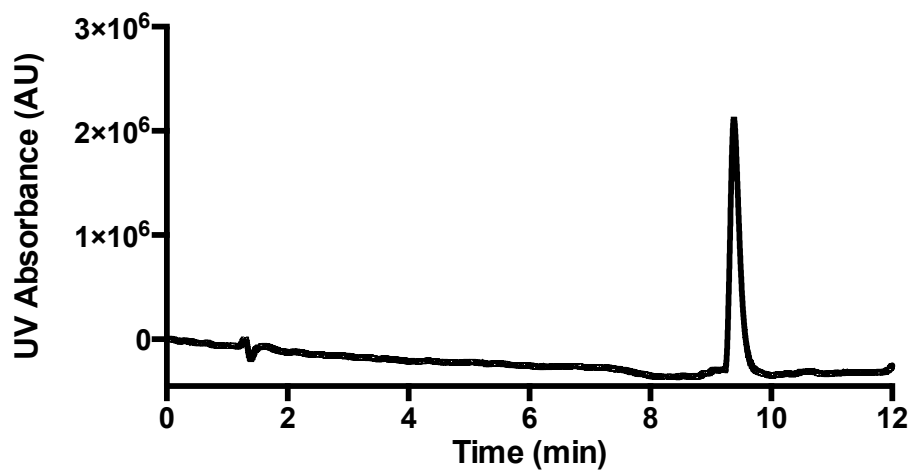
$t_R = 9.09$ min; HRMS (ESI-MS): $[M+H]^+$ 873.5674 (calc.) 873.5685 (found).



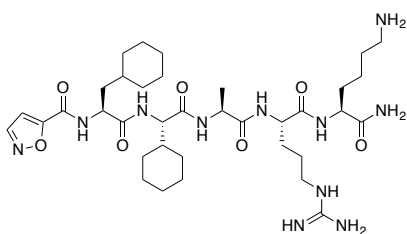
Isox-Cha-Chg-ARAK-NH₂, **10** (C₃₉H₆₆N₁₂O₈):



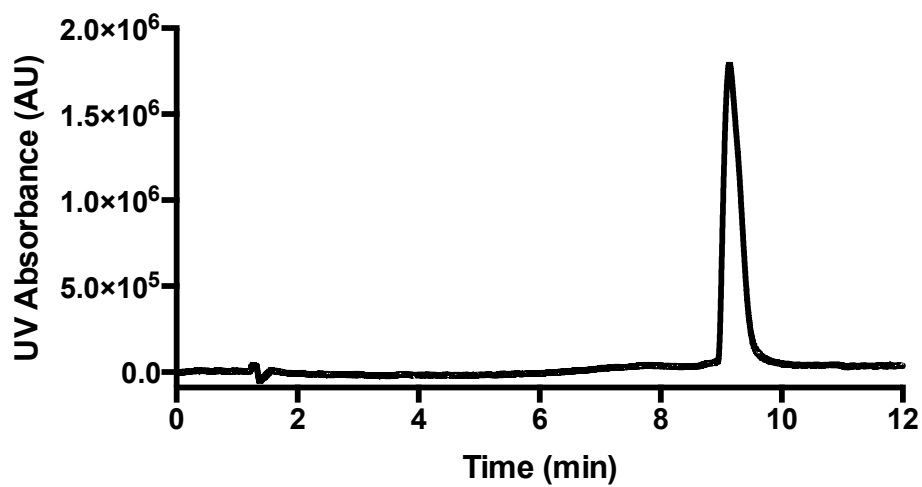
$t_R = 9.38$ min; HRMS (ESI-MS): $[M+H]^+$ 831.5205 (calc.) 831.5197 (found).



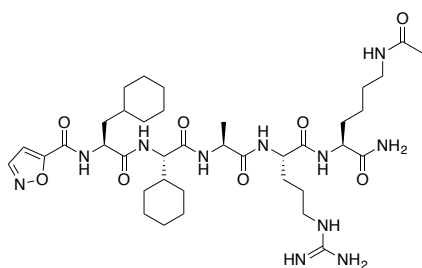
Isox-Cha-Chg-ARK-NH₂, **11** (C₃₆H₆₁N₁₁O₇):



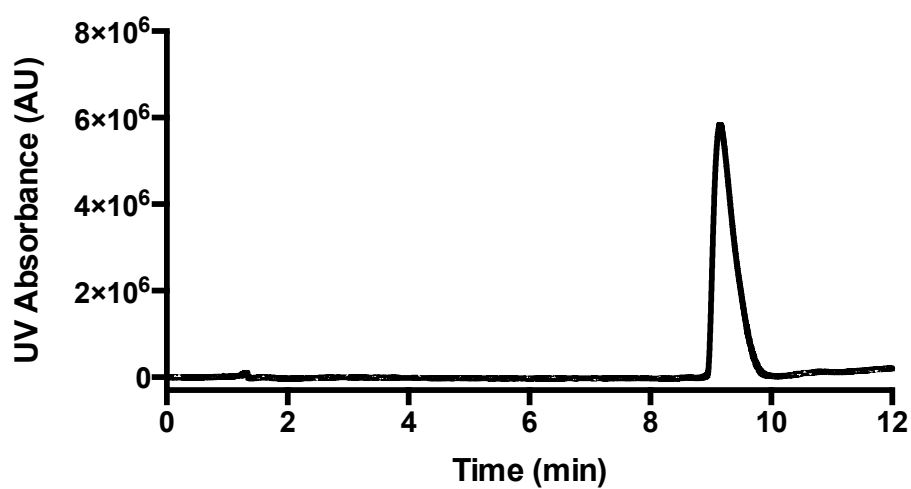
$t_R = 9.14$ min; HRMS (ESI-MS): $[M+H]^+$ 760.4834 (calc.) 760.4841 (found).



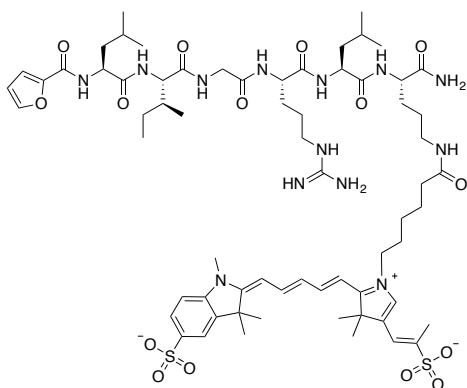
Isox-Cha-Chg-ARK(COCH₃)-NH₂, **12** (C₃₈H₆₃N₁₁O₈):



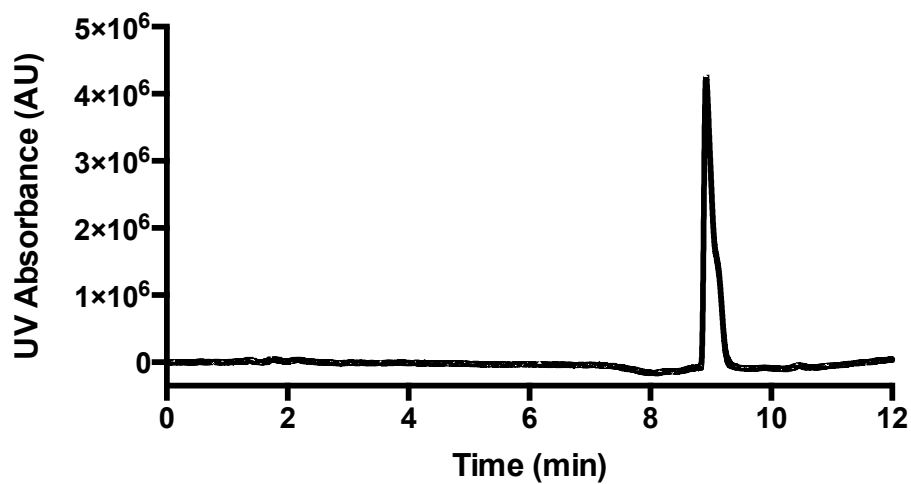
$t_R = 9.15$ min; HRMS (ESI-MS): $[M+H]^+$ 802.4939 (calc.) 802.4952 (found).



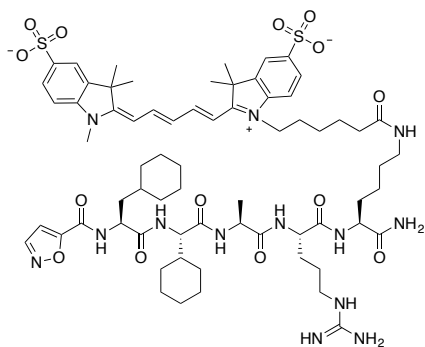
2f-LIGRLIO(Sulfo-Cy5)-NH₂, **14** (C₆₈H₉₈N₁₃O₁₅S₂⁻):



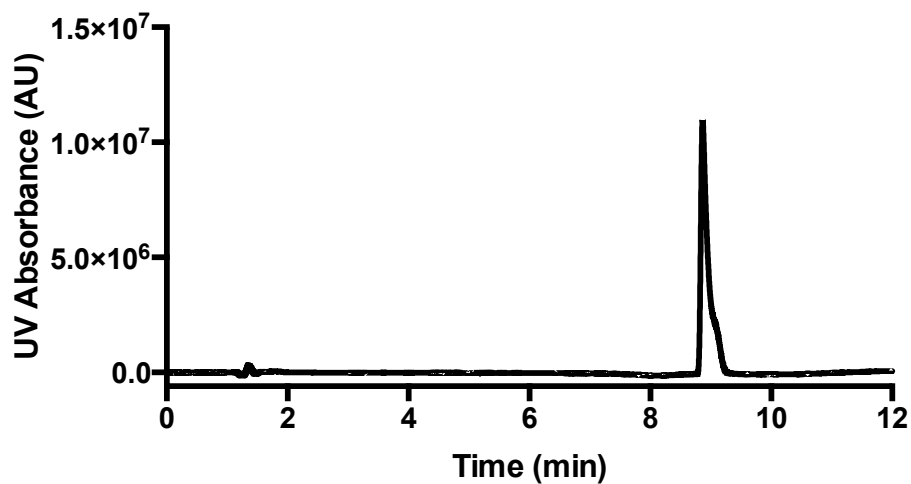
$t_R = 8.92$ min; HRMS (ESI-MS): $[M^-]$ 1400.6747 (calc.) 1400.6714 (found).



Isox-Cha-Chg-ARK(Sulfo-Cy5)-NH₂, **15** (C₆₈H₉₆N₁₃O₁₄S₂⁻):

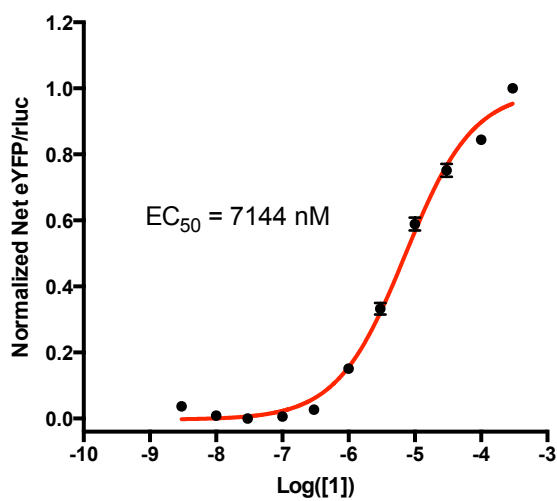


$t_R = 8.87$ min; HRMS (ESI-MS): [M⁻] 1382.6641 (calc.) 1382.6589 (found).

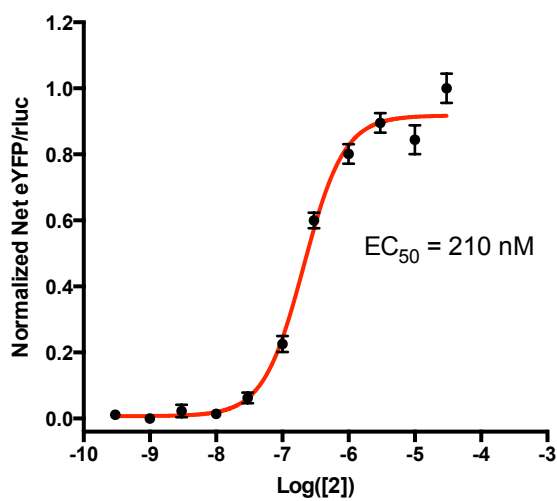


Appendix 4: PAR2 β -Arrestin 2 Recruitment Dose-Response Curves for Peptides 1, 2, 6-12, and 14-15 in HEK293T Cells

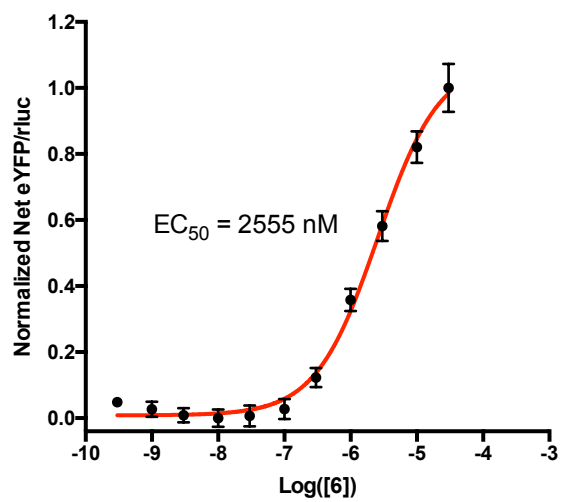
Compound 1



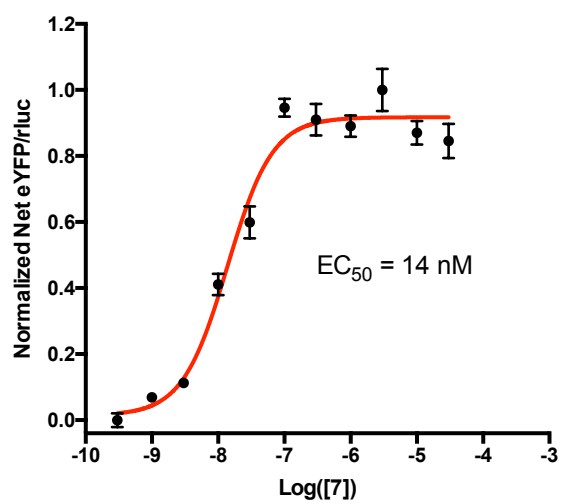
Compound 2



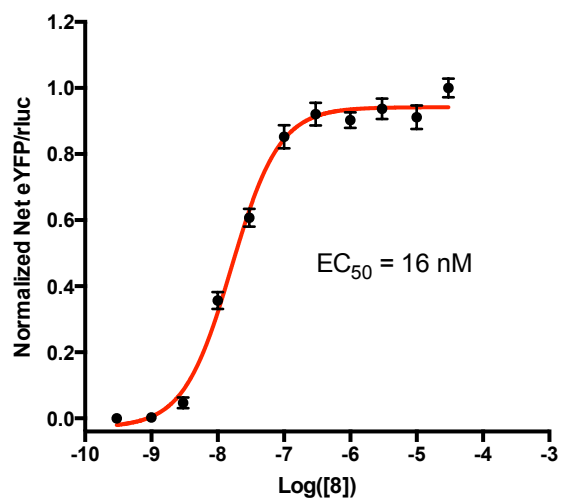
Compound 6



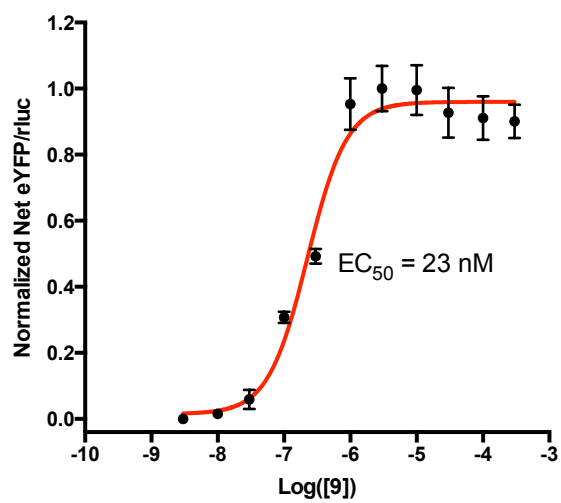
Compound 7



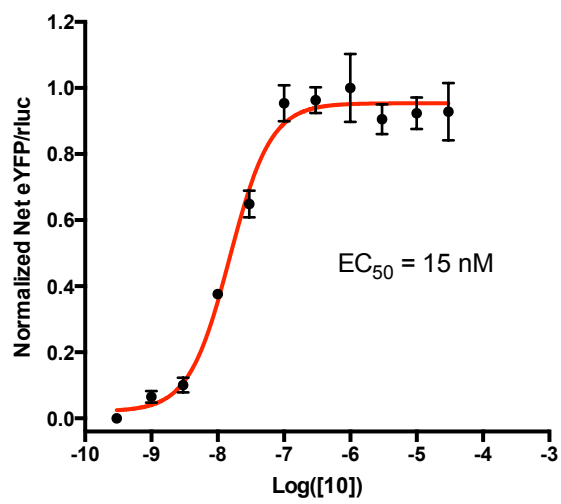
Compound 8



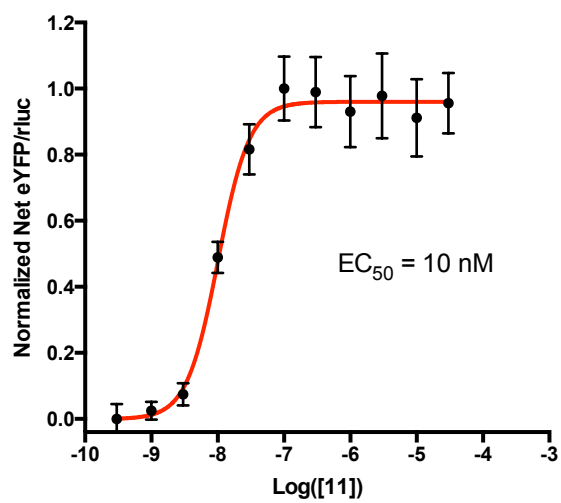
Compound 9



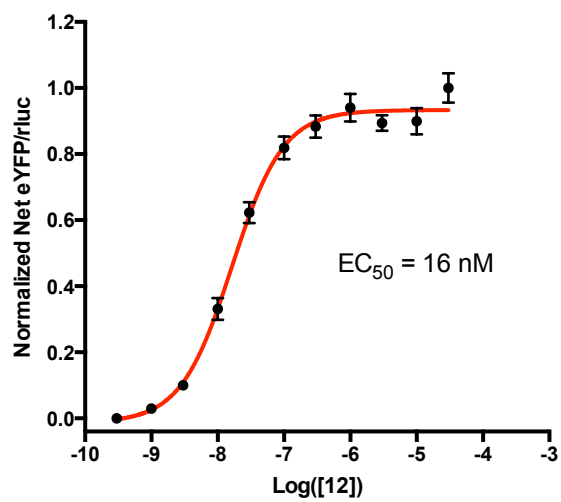
Compound 10



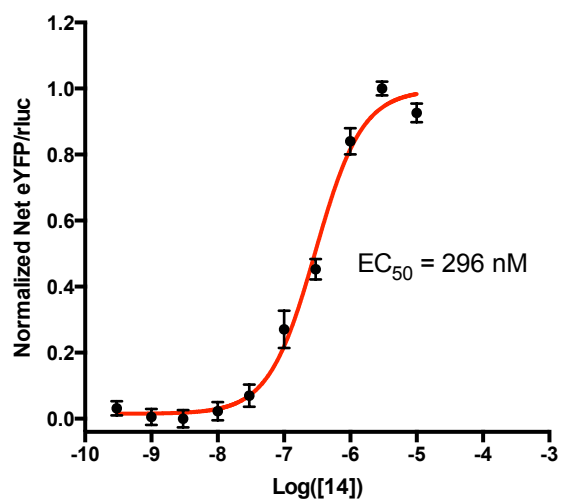
Compound 11



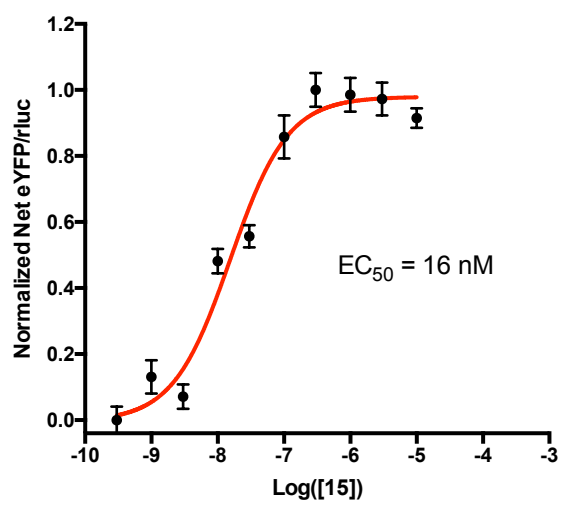
Compound 12



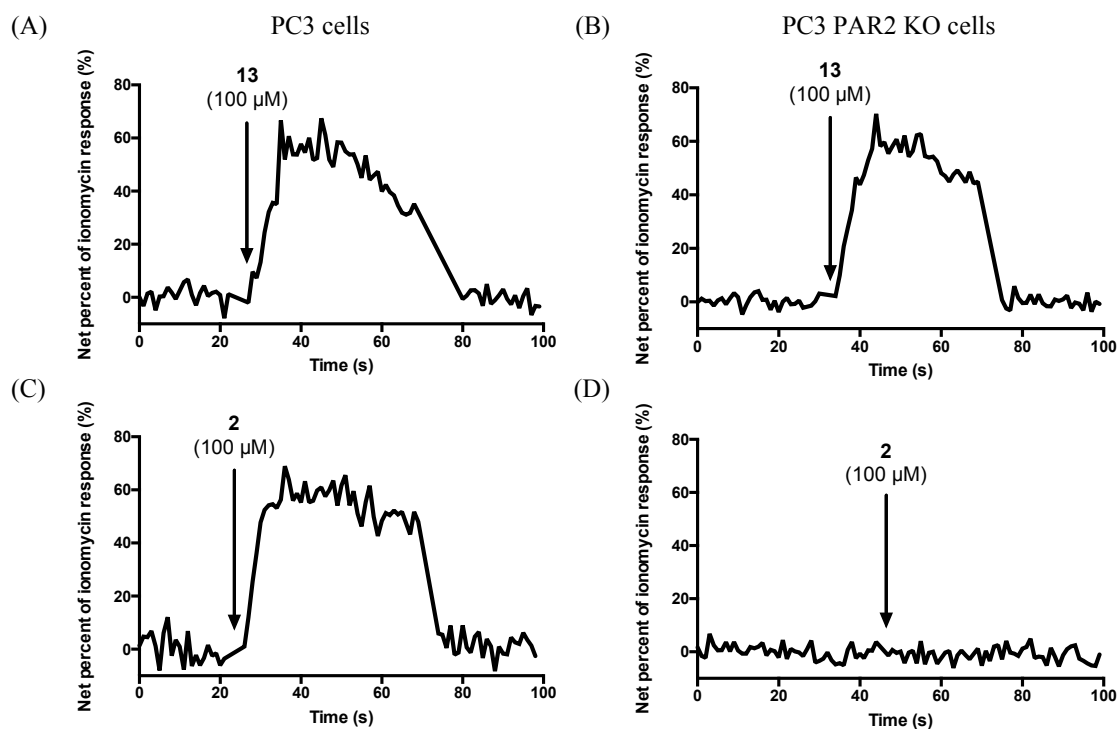
Compound 14



Compound 15

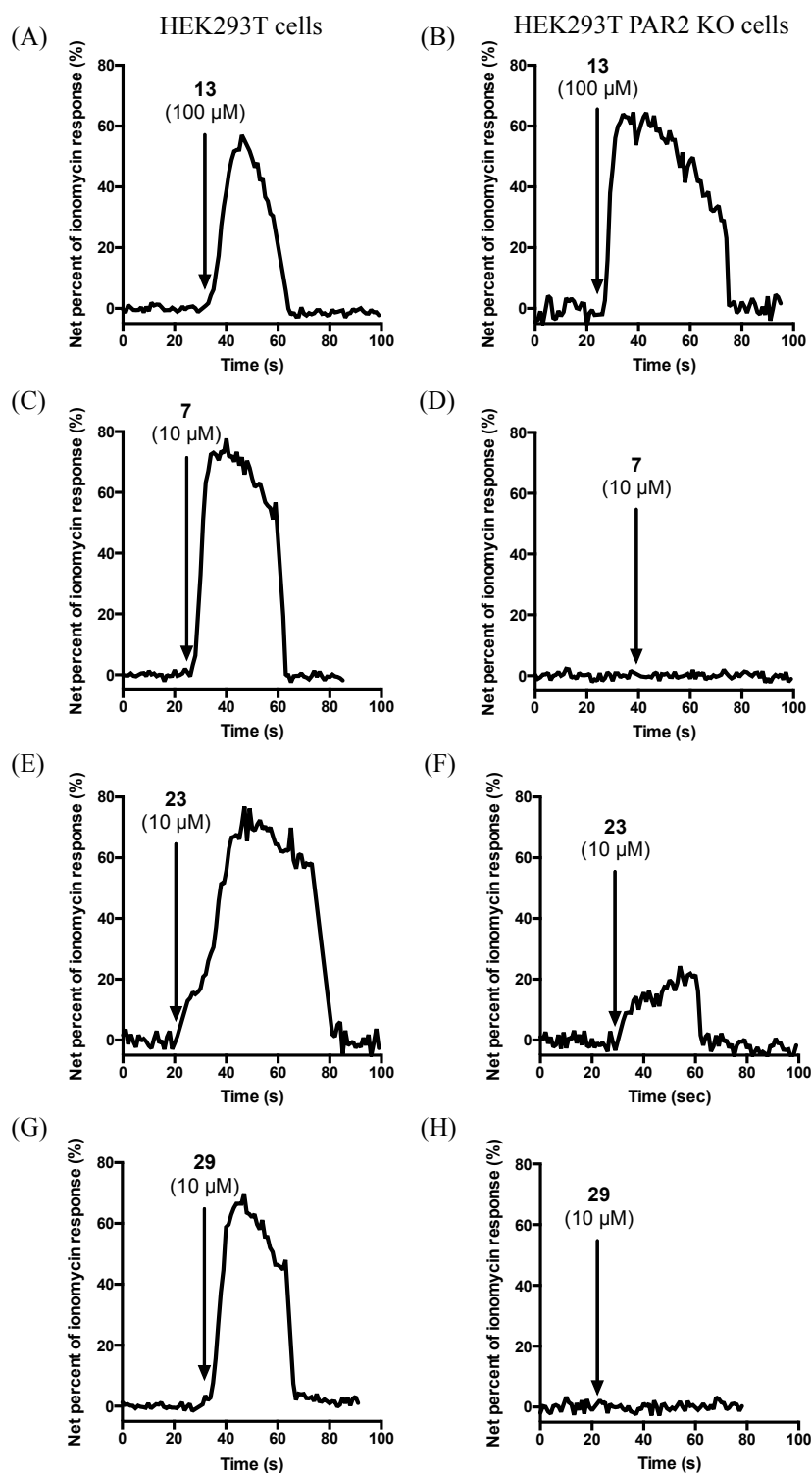


Appendix 5: Representative Examples of PAR2-Selectivity Measurements as Determined Through Calcium Response Assay in PC3 and PAR2 KO PC3 Cells



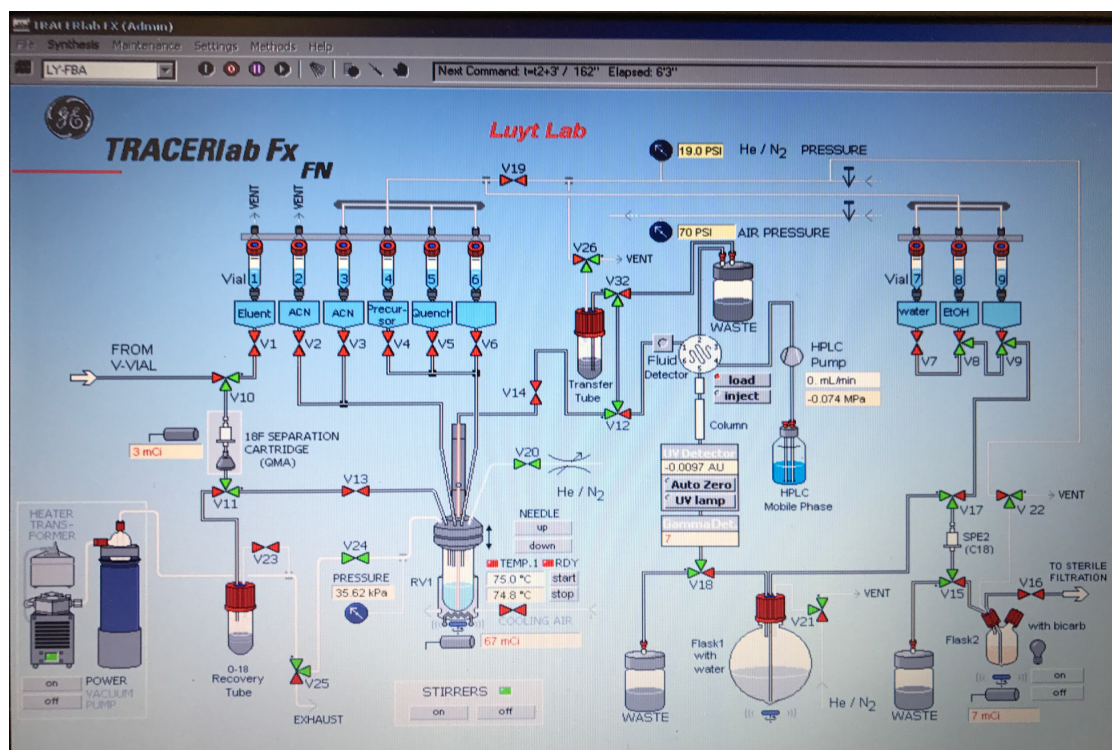
(A) PC3 cells + 100 μ M of **13**, (B) PC3 PAR2 KO cells + 100 μ M of **13**, (C) PC3 cells + 100 μ M of **2**, (D) PC3 PAR2 KO cells + 100 μ M of **2**.

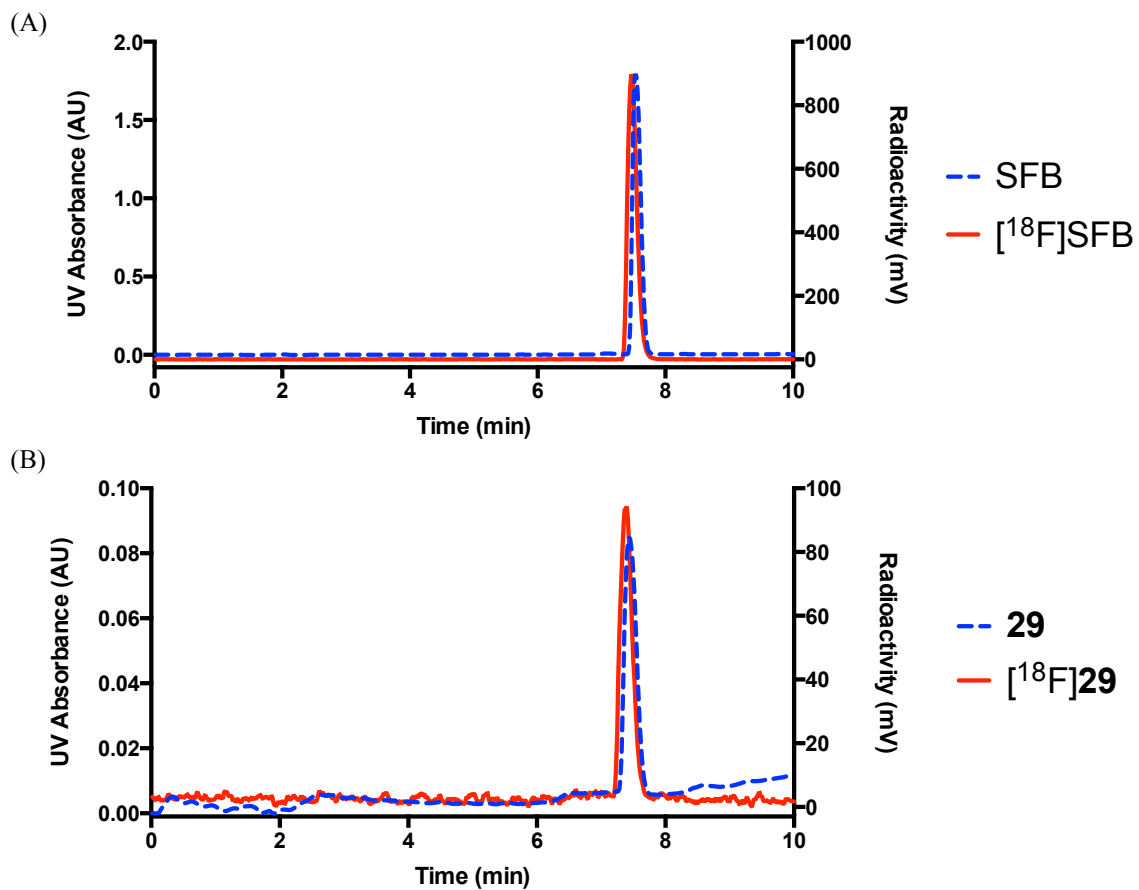
Appendix 6: Representative Examples of PAR2-Selectivity Measurements as Determined Through Calcium Response Assay in HEK293T and PAR2 KO HEK293T Cells



(A) HEK293T cells + 100 μ M of **13**, (B) HEK293T PAR2 KO cells + 100 μ M of **13**, (C) HEK293T cells + 10 μ M of **7**, (D) HEK293T PAR2 KO cells + 10 μ M of **7**, (E) HEK293T cells + 10 μ M of **23**, (F) HEK293T PAR2 KO cells + 10 μ M of **23**, (G) HEK293T cells + 10 μ M of **29**, (H) HEK293T PAR2 KO cells + 10 μ M of **29**.

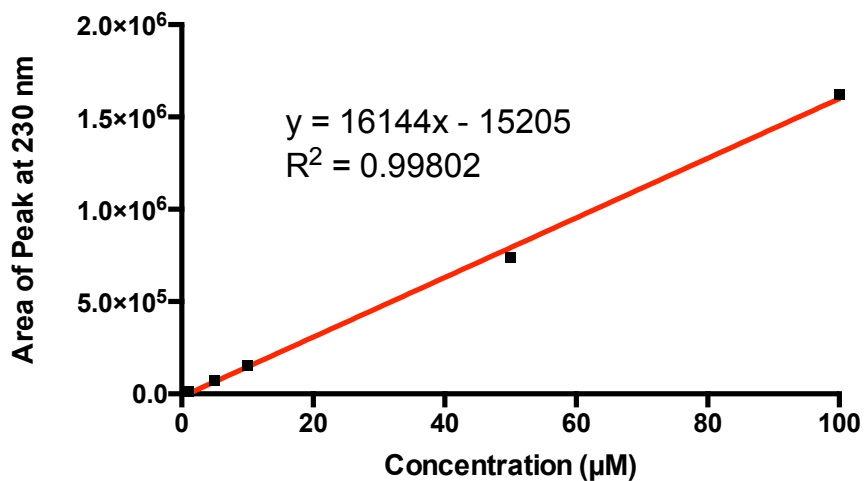
Appendix 7: GE Tracer Lab FXN Automated Synthesis Display.



Appendix 8: Fluorine-18 Co-Injection Radio-traces and Chromatograms.

(A) Overlay of RP-HPLC radio-trace and chromatogram of SFB and [¹⁸F]SFB co-injection and of (B) **29** and [¹⁸F]**29** co-injection.

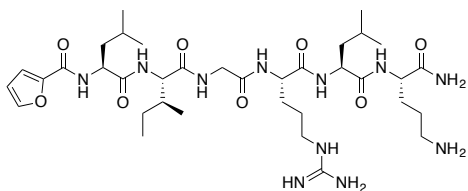
Appendix 9: Calibration Curve of 29 to Determine Molar Activity of [¹⁸F]29.



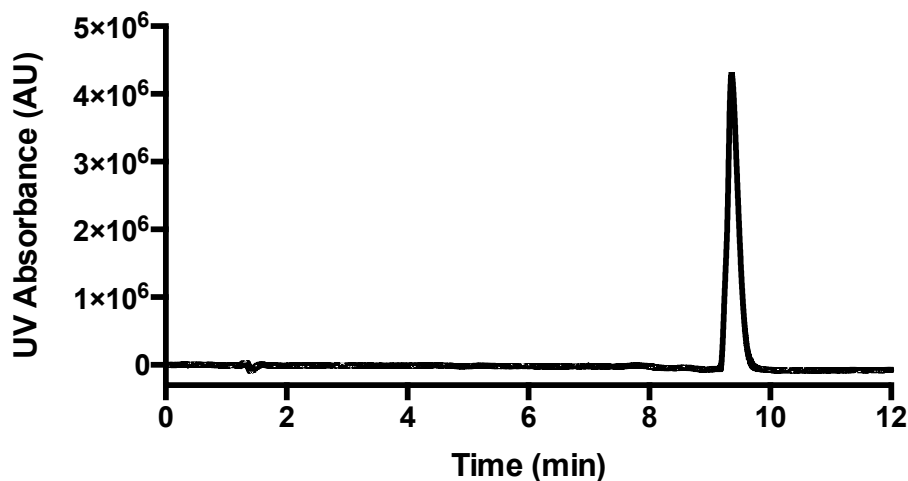
Appendix 10: Characterization of Synthesized Peptides (2, 6, 7, 16-29, and 35)

All peptides were >95% pure as determined by analytical RP-HPLC UV detection (see chromatograms below).

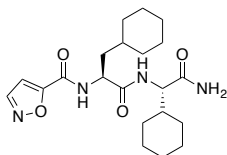
2f-LIGRLO-NH₂, **2** (C₃₆H₆₃N₁₁O₈):



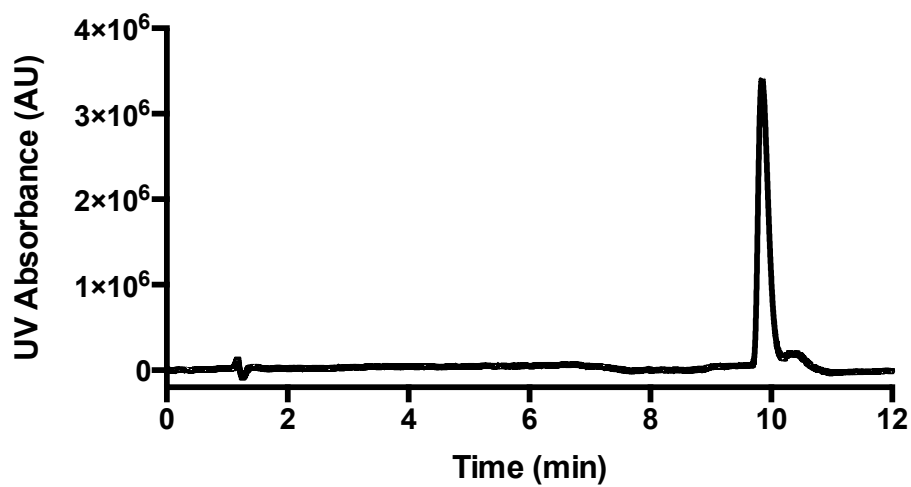
$t_R = 9.36$ min; HRMS (ESI-MS): $[M+H]^+$ 778.4939 (calc.) 778.4945 (found).



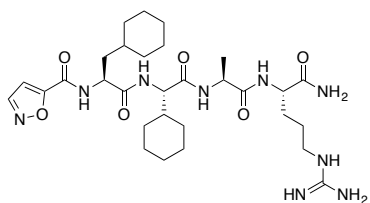
Isox-Cha-Chg-NH₂, **6** (C₂₁H₃₂N₄O₄):



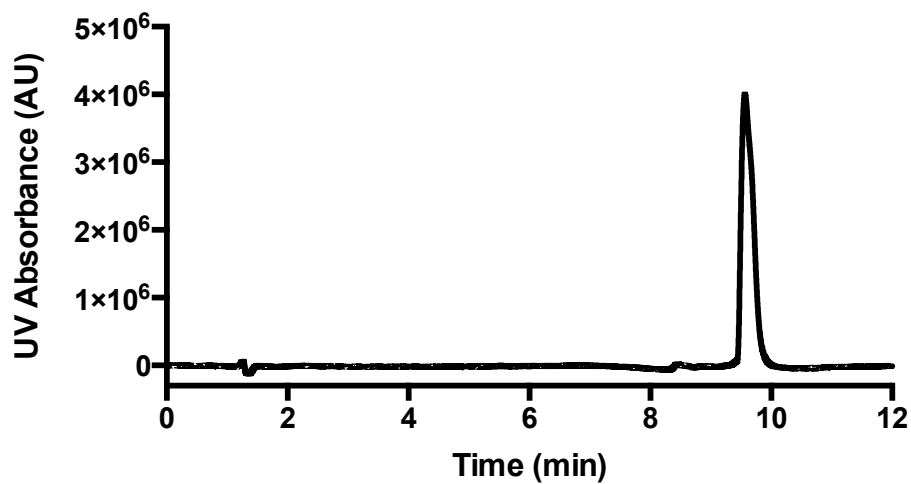
$t_R = 9.85$ min; HRMS (ESI-MS): $[M+Na]^+$ 427.2321 (calc.) 427.2309 (found).



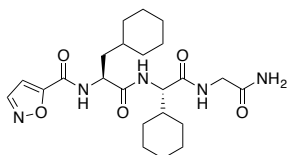
Isox-Cha-Chg-AR-NH₂, **7** (C₃₀H₄₉N₉O₆):



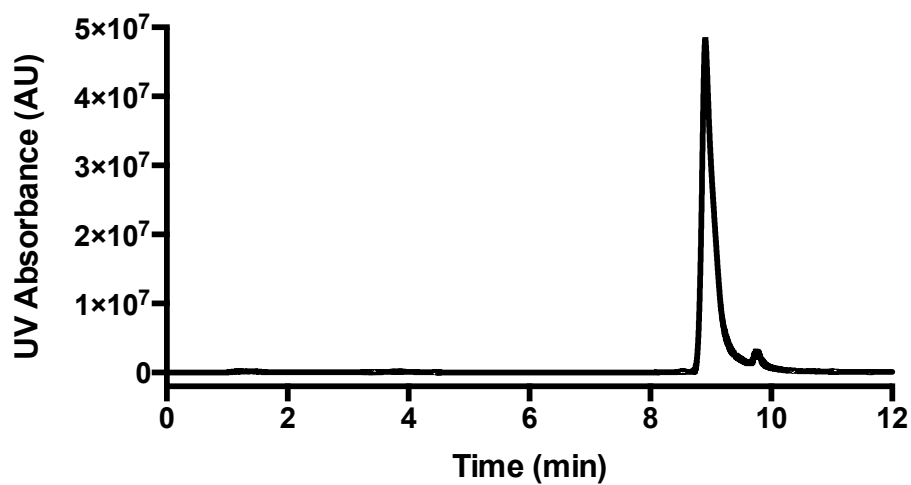
$t_R = 9.57$ min; HRMS (ESI-MS): $[M+H]^+$ 632.3884 (calc.) 632.3892 (found).



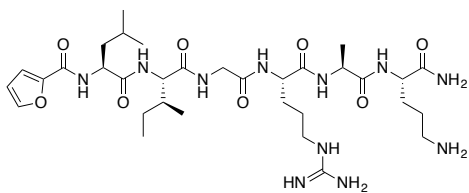
Isox-Cha-Chg-G-NH₂, **16** (C₂₃H₃₅N₅O₅):



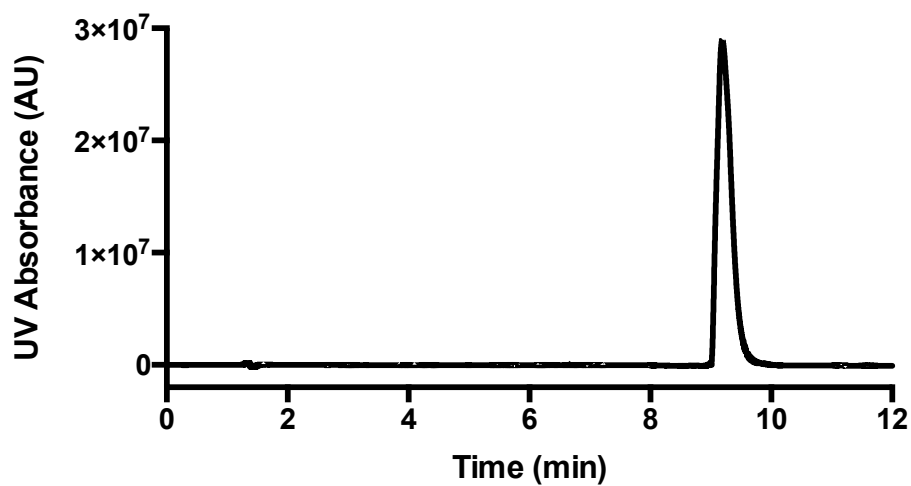
$t_R = 8.91$ min; HRMS (ESI-MS): $[M+Na]^+$ 484.2536 (calc.) 484.2526 (found).



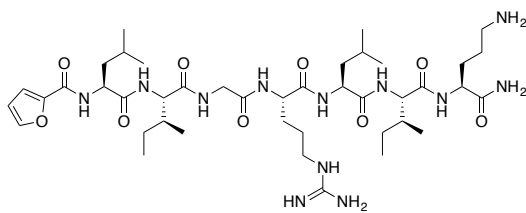
2f-LIGRAO-NH₂, **17** (C₃₃H₅₇N₁₁O₈):



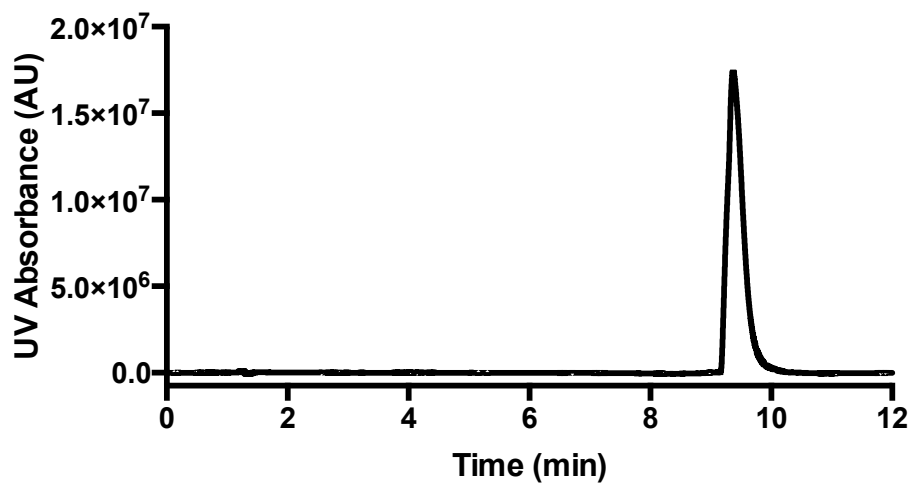
$t_R = 9.19$ min; HRMS (ESI-MS): $[M+H]^+$ 736.4470 (calc.) 736.4475 (found).



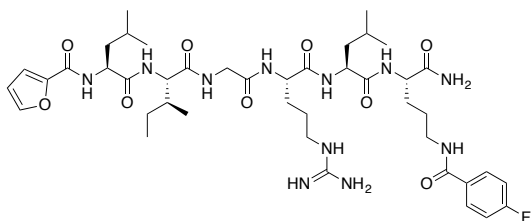
2f-LIGRLIO-NH₂, **18** (C₄₂H₇₄N₁₂O₉):



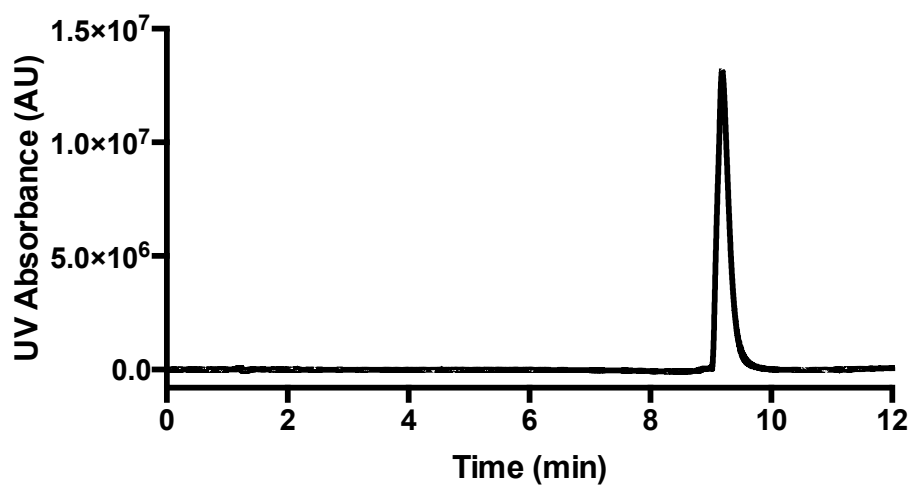
$t_R = 9.37$ min; HRMS (ESI-MS): $[M+H]^+$ 891.5780 (calc.) 891.5801 (found).



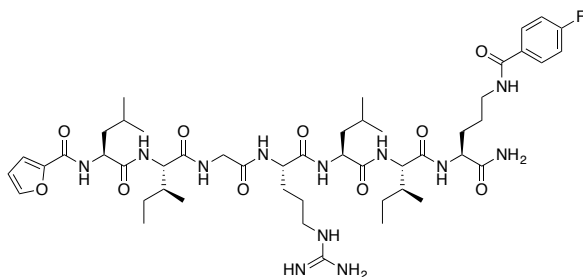
2f-LIGRLO(4-FB)-NH₂, **19** (C₄₃H₆₆FN₁₁O₉):



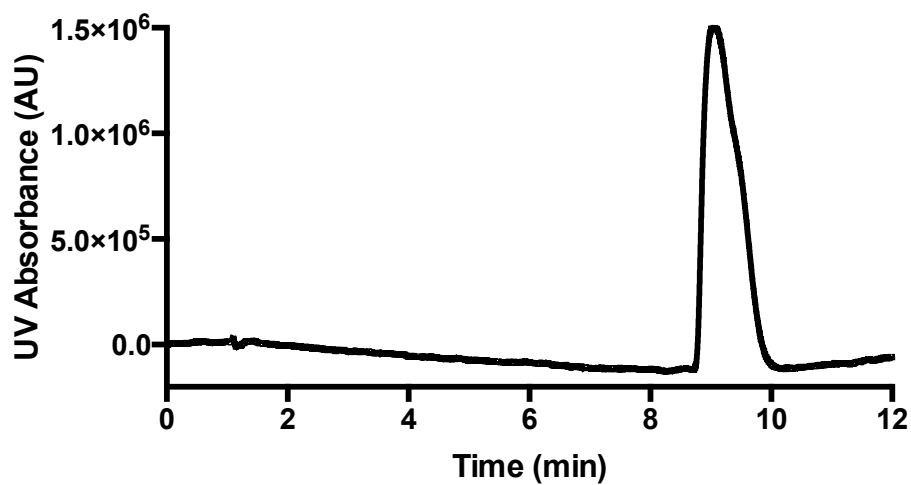
$t_R = 9.19$ min; HRMS (ESI-MS): $[M+H]^+$ 900.5107 (calc.) 900.5129 (found).



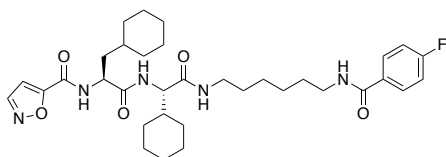
2f-LIGRLIO(4-FB)-NH₂, **20** (C₄₉H₇₇FN₁₂O₁₀):



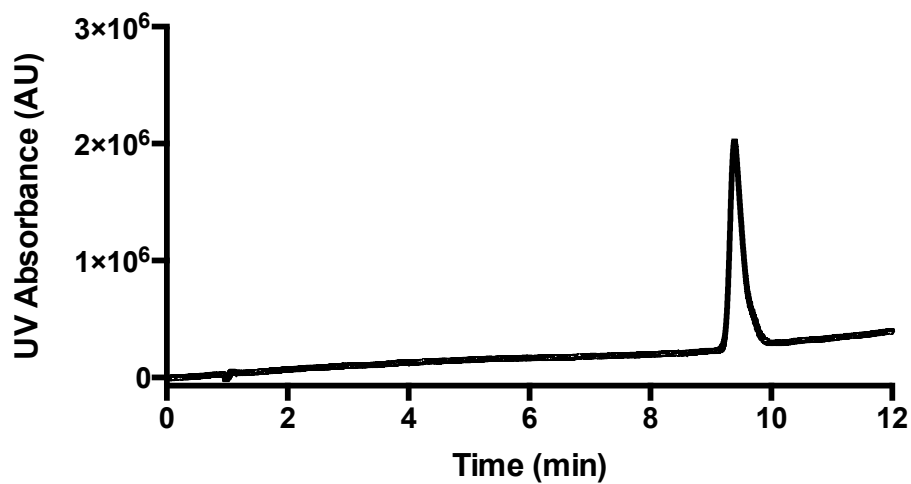
$t_R = 9.04$ min; HRMS (ESI-MS): $[M+H]^+$ 1013.5948 (calc.) 1013.5955 (found).



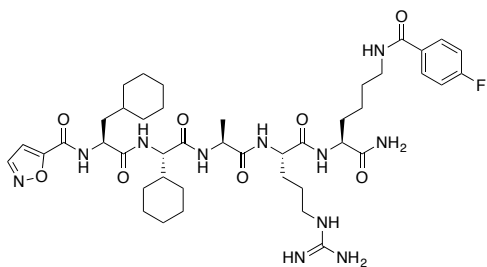
Isox-Cha-Chg-NH(CH₂)₆NH-4-FB, **21** (C₃₄H₄₈FN₅O₅):



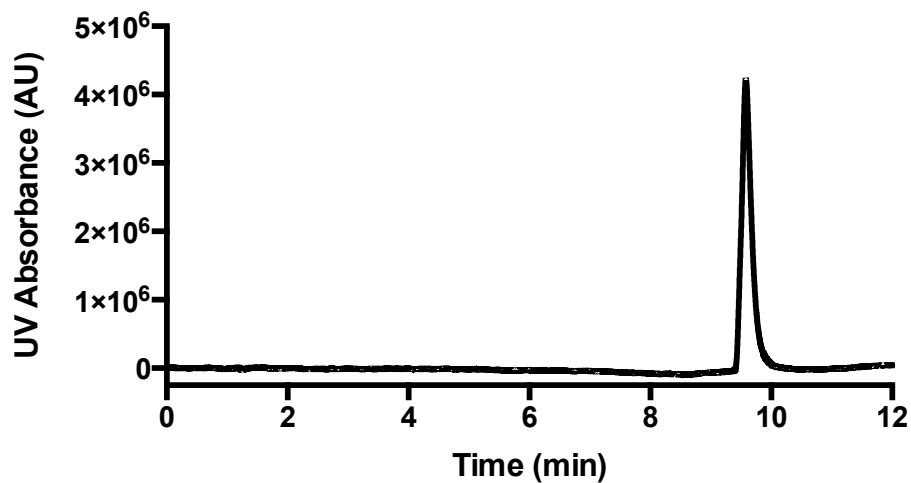
$t_R = 9.39$ min; HRMS (ESI-MS): $[M+Na]^+$ 648.3537 (calc.) 648.3550 (found).



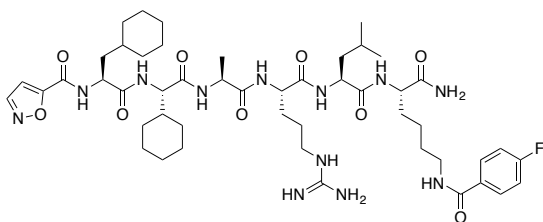
Isox-Cha-Chg-ARK(4-FB)-NH₂, **22** (C₄₃H₆₄FN₁₁O₈):



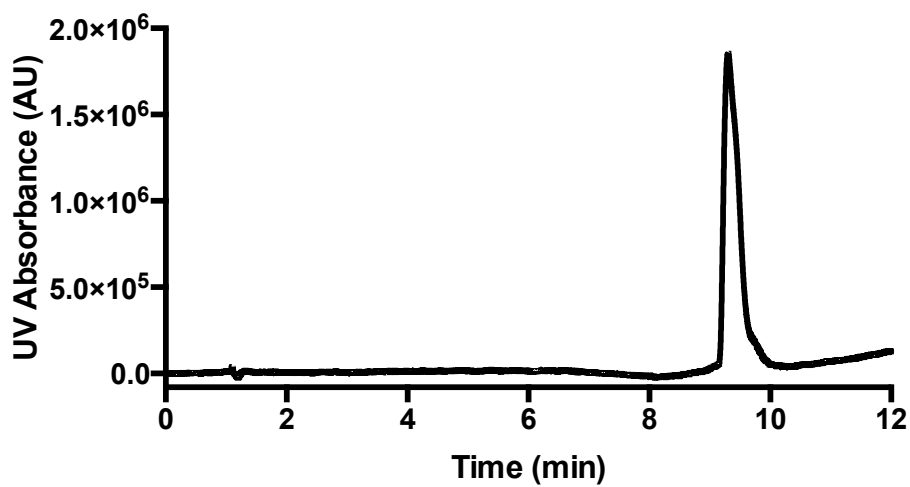
$t_R = 9.58$ min; HRMS (ESI-MS): $[M+H]^+$ 882.5002 (calc.) 882.5011 (found).



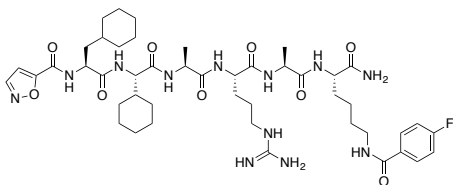
Isox-Cha-Chg-ARLK(4-FB)-NH₂, **23** (C₄₉H₇₅FN₁₂O₉):



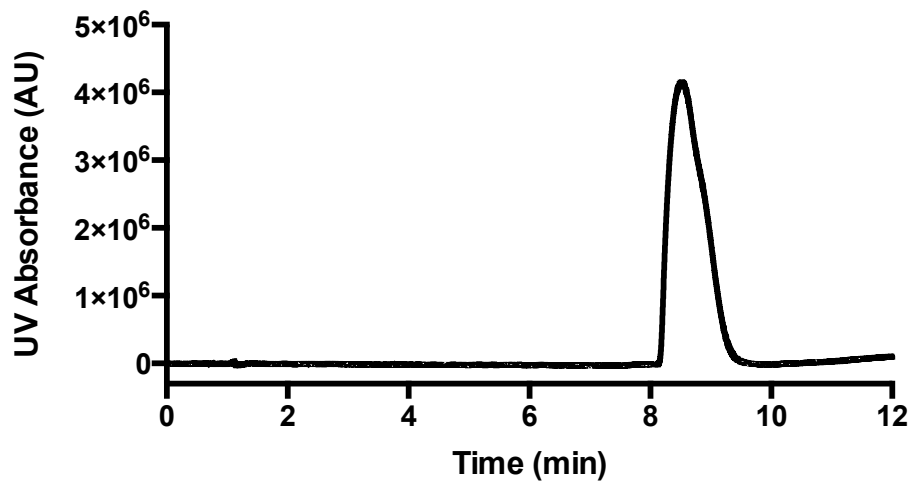
$t_R = 9.30$ min; HRMS (ESI-MS): $[M+H]^+$ 995.5842 (calc.) 995.5852 (found).



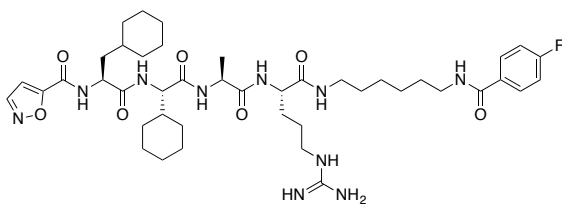
Isox-Cha-Chg-ARAK(4-FB)-NH₂, **24** (C₄₆H₆₉FN₁₂O₉):



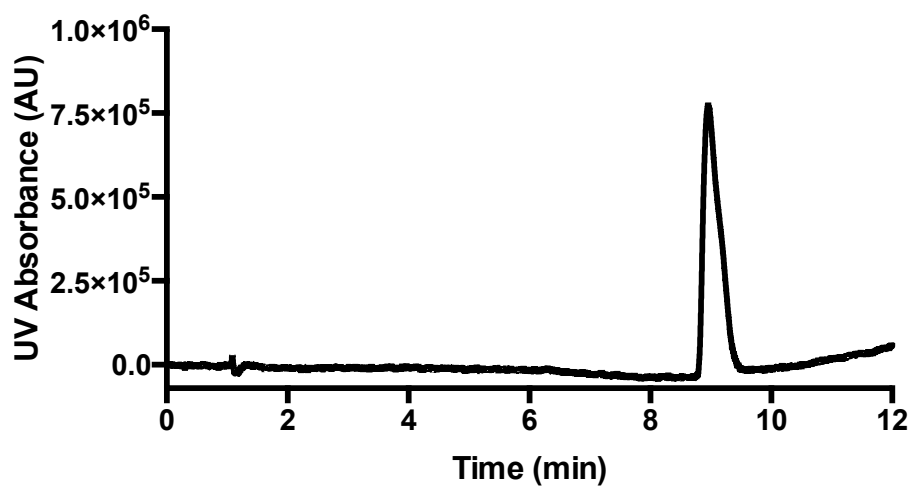
$t_R = 8.52$ min; HRMS (ESI-MS): $[M+H]^+$ 953.5373 (calc.) 953.5398 (found).



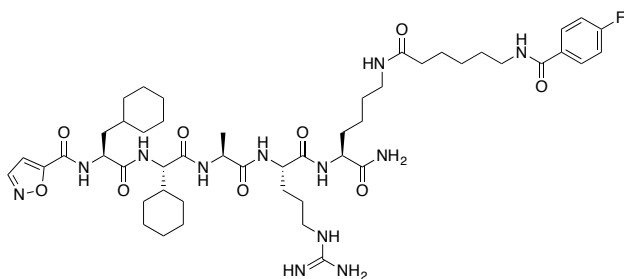
Isox-Cha-Chg-AR-NH(CH₂)₆NH-4-FB, **25** (C₄₃H₆₅FN₁₀O₇):



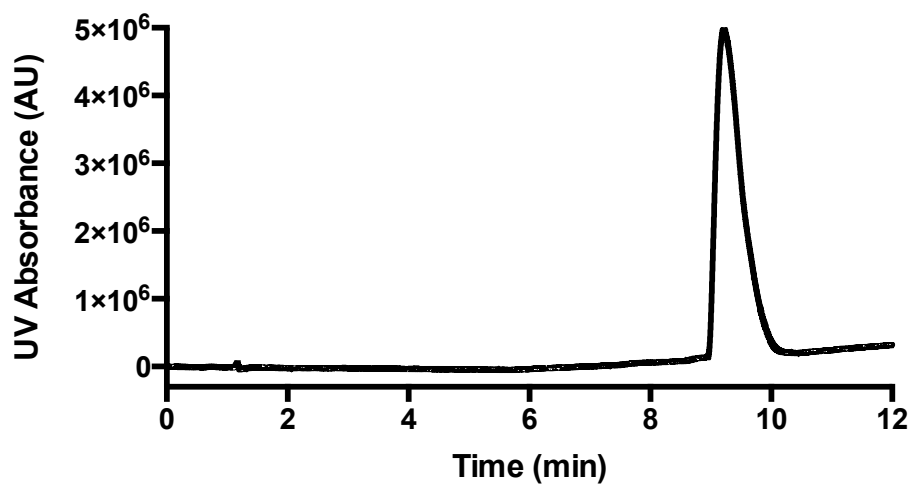
$t_R = 8.96$ min; HRMS (ESI-MS): $[M+H]^+$ 853.5100 (calc.) 853.5110 (found).



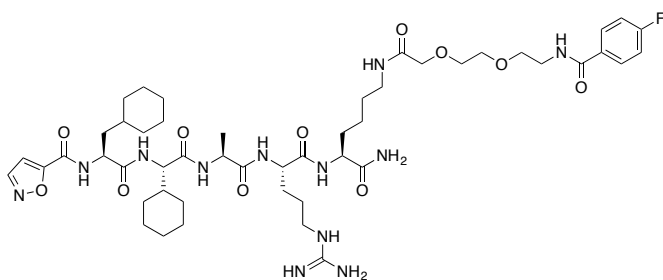
Isox-Cha-Chg-ARK(Ahx-4-FB)-NH₂, **26** (C₄₉H₇₅FN₁₂O₉):



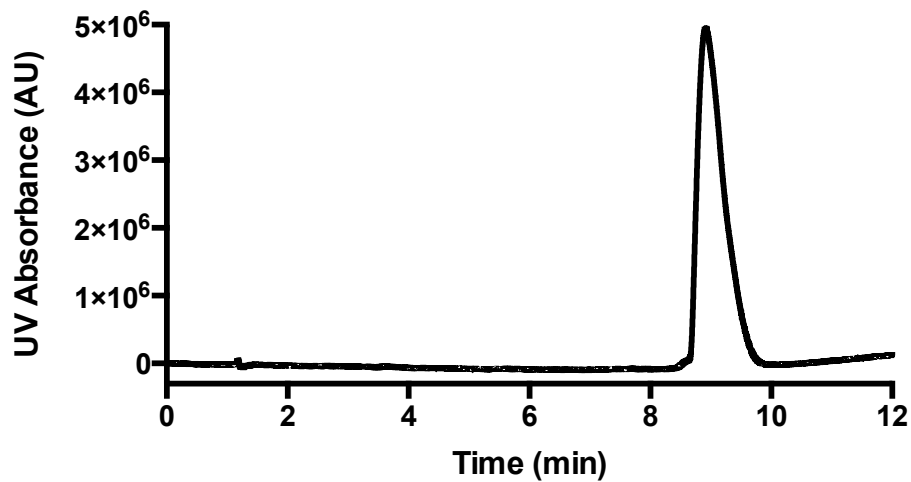
$t_R = 9.22$ min; HRMS (ESI-MS): $[M+H]^+$ 995.5842 (calc.) 995.5855 (found).



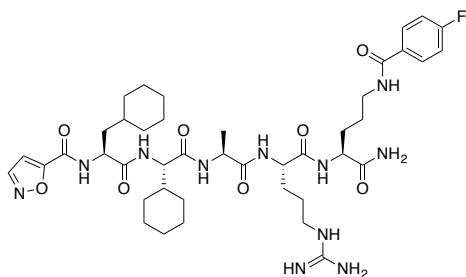
Isox-Cha-Chg-ARK(AEEA-4-FB)-NH₂, **27** (C₄₉H₇₅FN₁₂O₁₁):



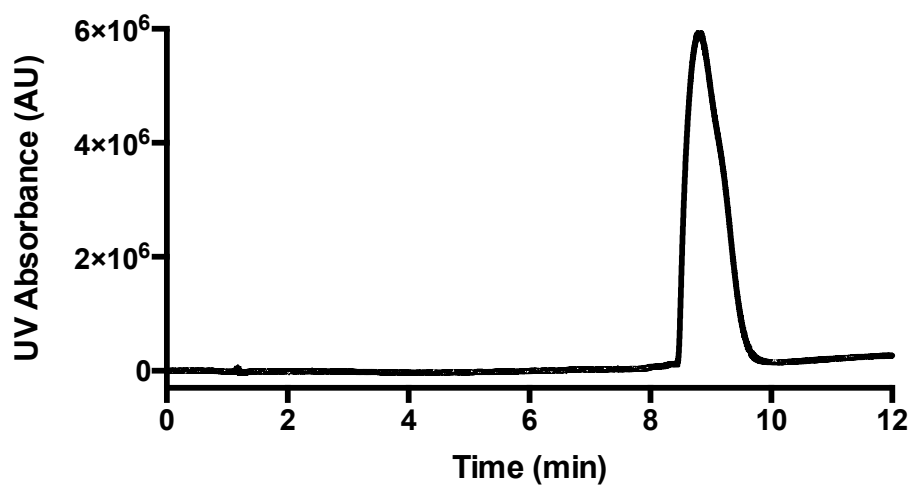
$t_R = 8.92$ min; HRMS (ESI-MS): $[M+H]^+$ 1027.5741 (calc.) 1027.5745 (found).



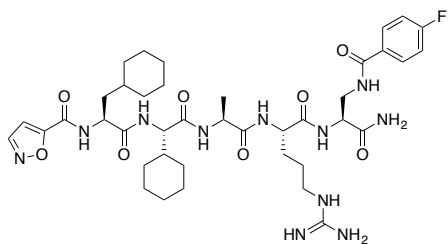
Isox-Cha-Chg-ARO(4-FB)-NH₂, **28** (C₄₂H₆₂FN₁₁O₈):



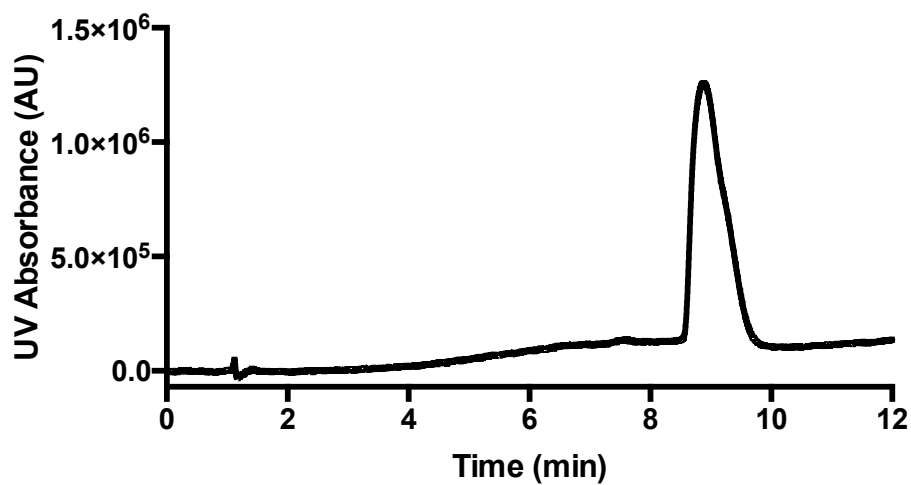
$t_R = 8.81$ min; HRMS (ESI-MS): $[M+H]^+$ 868.4845 (calc.) 868.4864 (found).



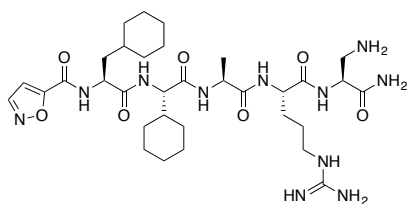
Isox-Cha-Chg-AR-Dpr(4-FB)-NH₂, **29** (C₄₀H₅₈FN₁₁O₈):



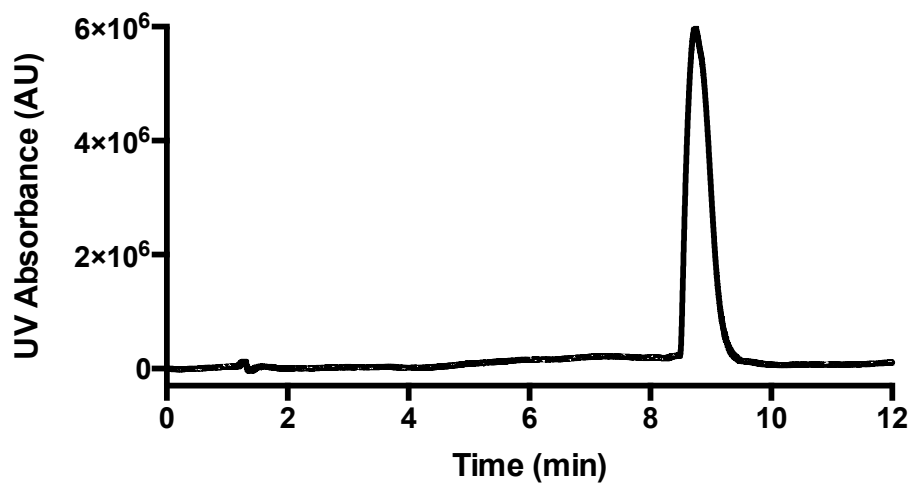
$t_R = 8.87$ min; HRMS (ESI-MS): $[M+H]^+$ 840.4532 (calc.) 840.4525 (found).



Isox-Cha-Chg-AR-Dpr-NH₂, **35** (C₃₃H₅₅N₁₁O₇):

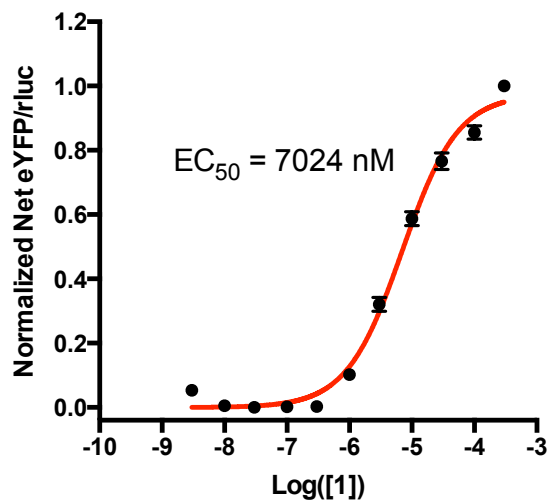


$t_R = 8.74$ min; HRMS (ESI-MS): $[M+H]^+$ 718.4364 (calc.) 718.4372 (found).

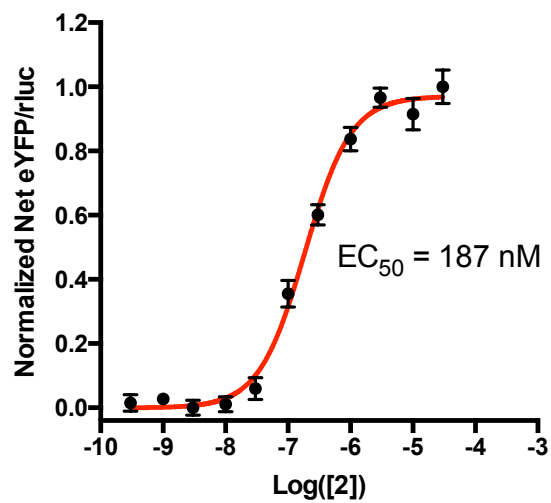


Appendix 11: PAR2 β -Arrestin 2 Recruitment Dose-Response Curves for Peptides 1, 2, 6-7, and 16-29 in HEK293T Cells

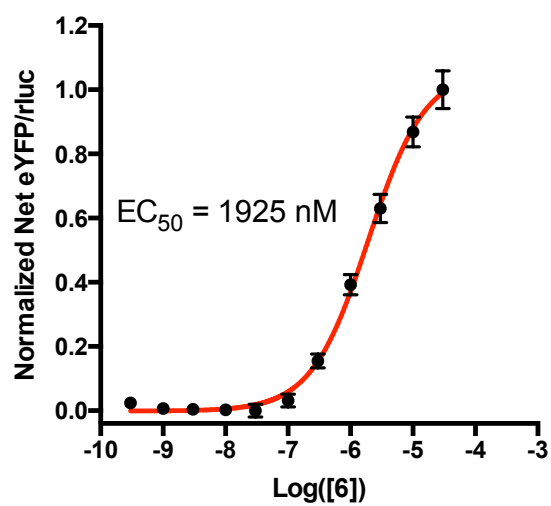
Compound 1



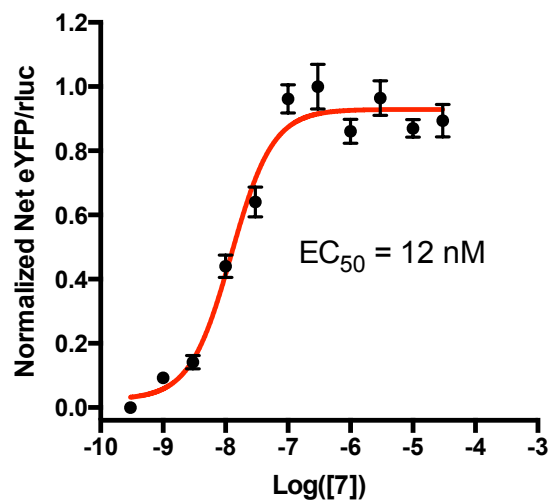
Compound 2



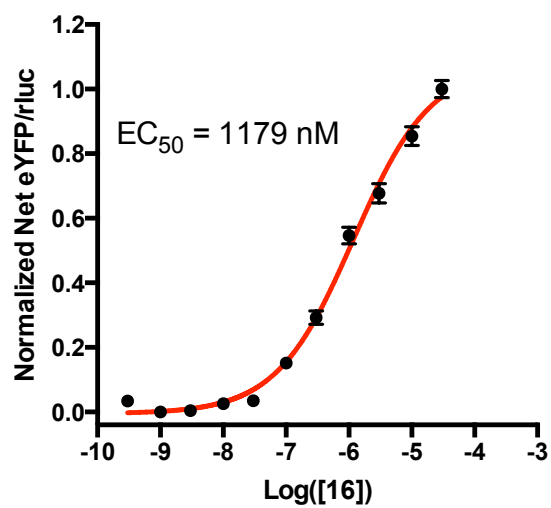
Compound 6



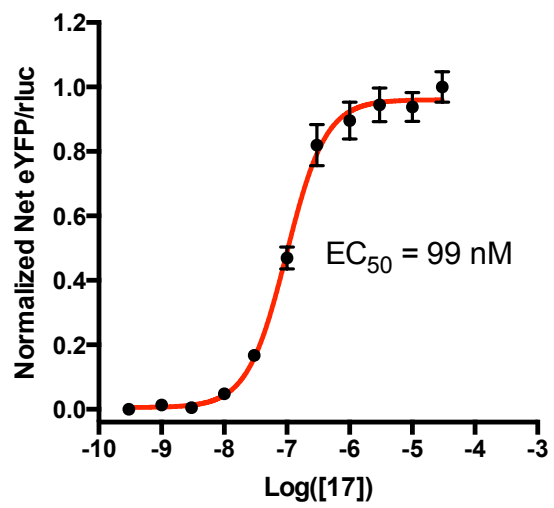
Compound 7



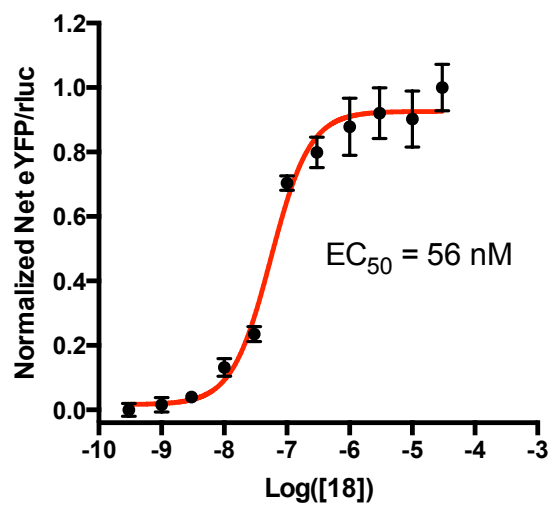
Compound 16



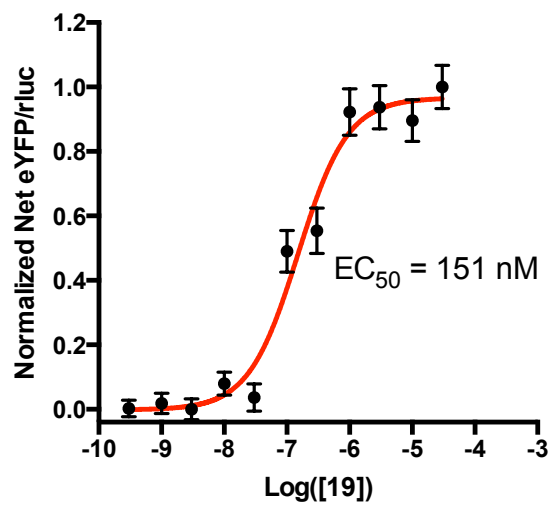
Compound 17



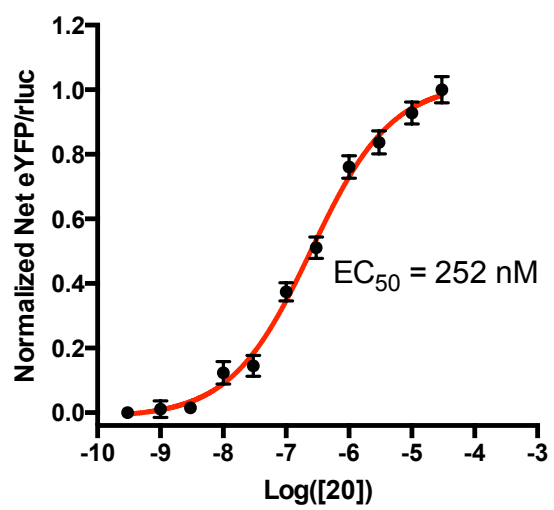
Compound 18



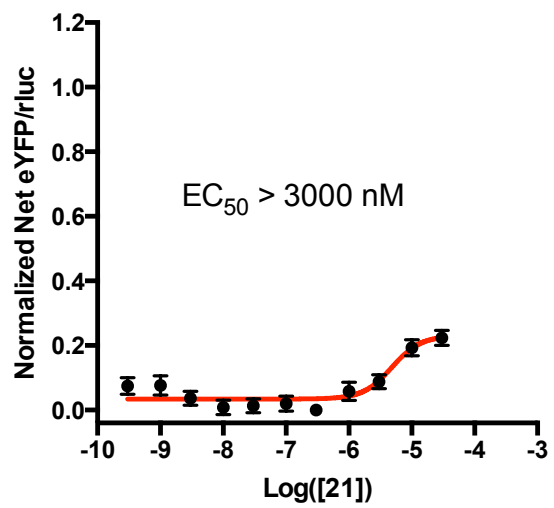
Compound 19



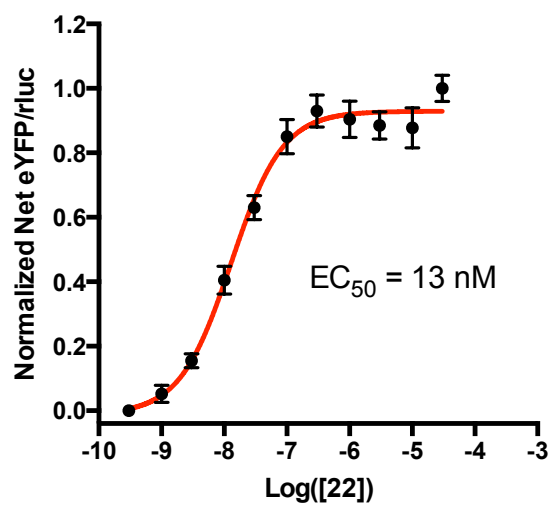
Compound 20



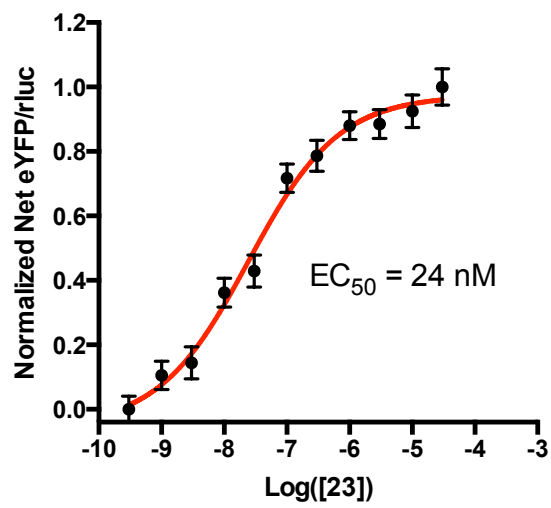
Compound 21



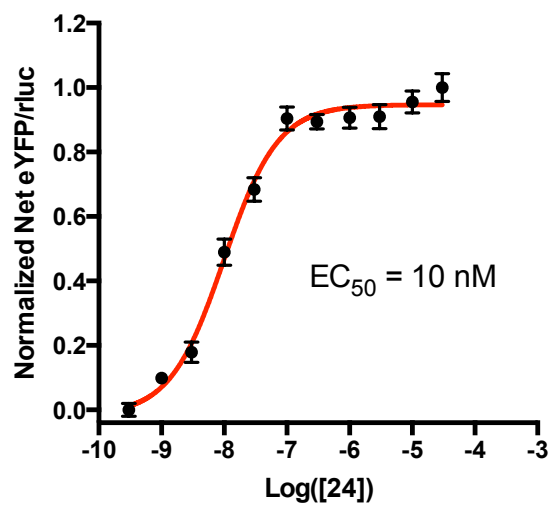
Compound 22



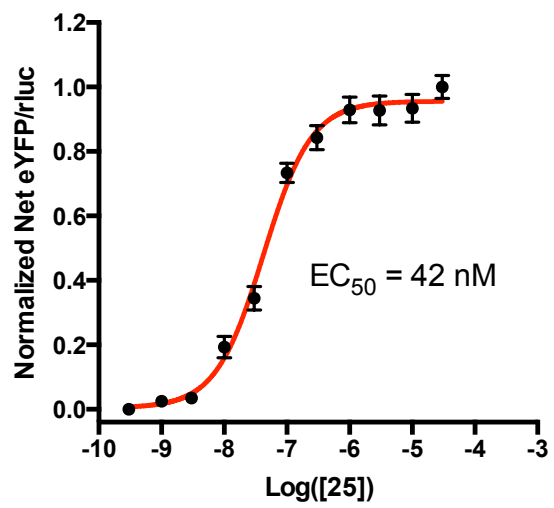
Compound 23



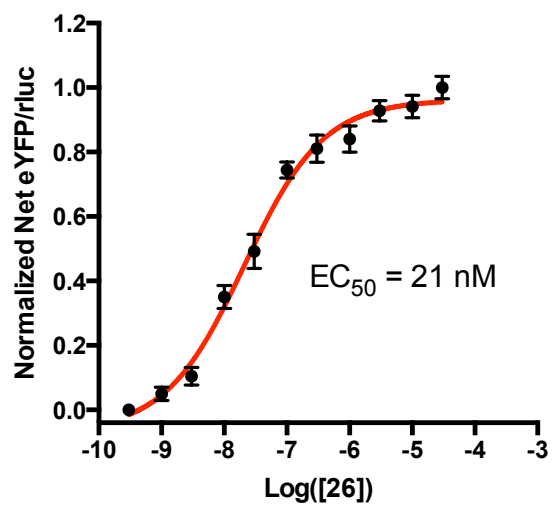
Compound 24



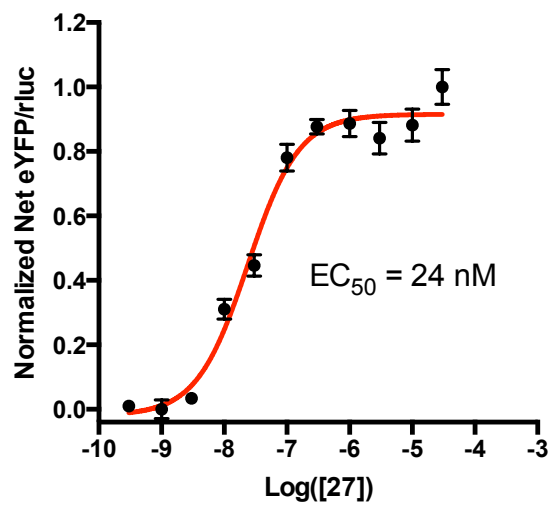
Compound 25



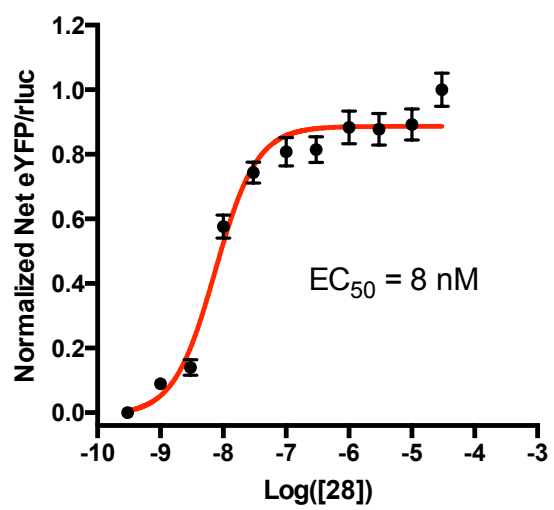
Compound 26



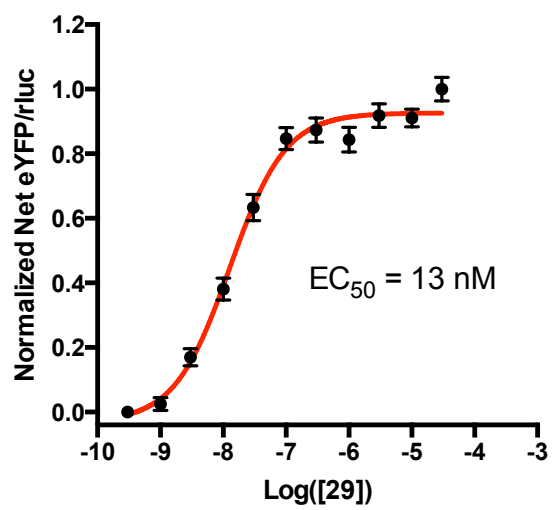
Compound 27

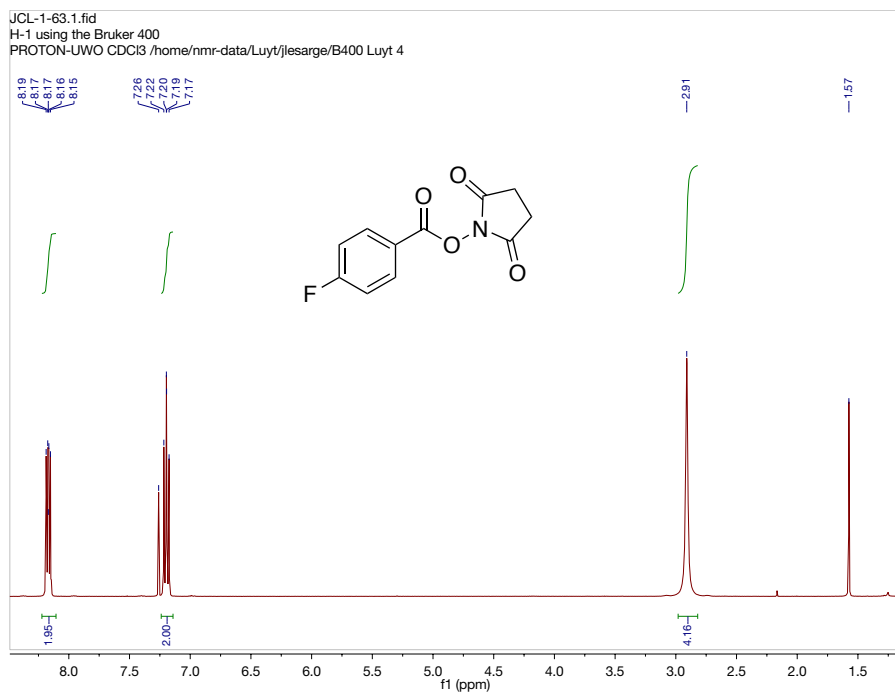
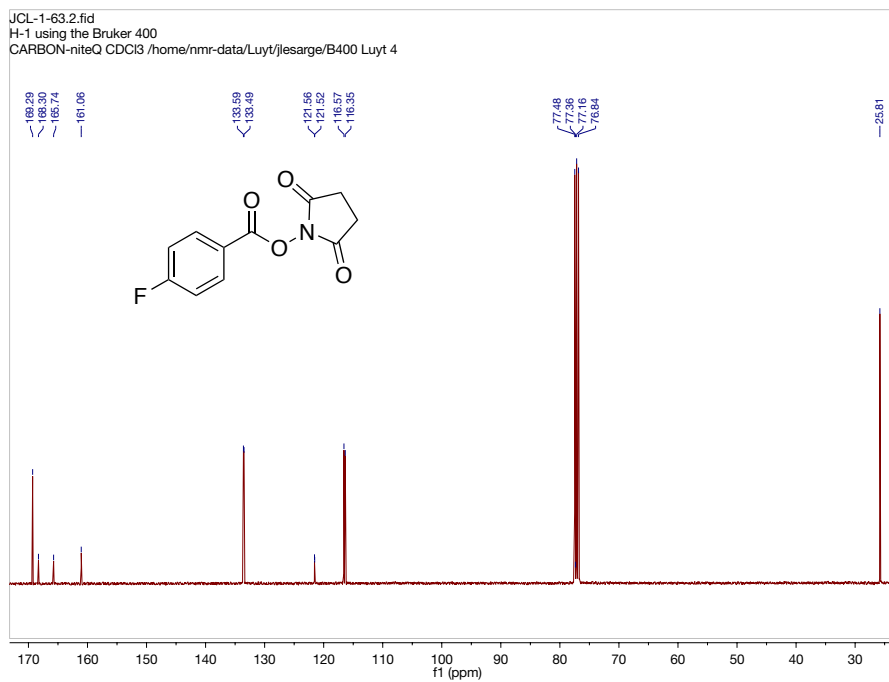


Compound 28



Compound 29



Appendix 12: NMR of *N*-succinimidyl 4-fluorobenzoate (34)¹H NMR:¹³C NMR:

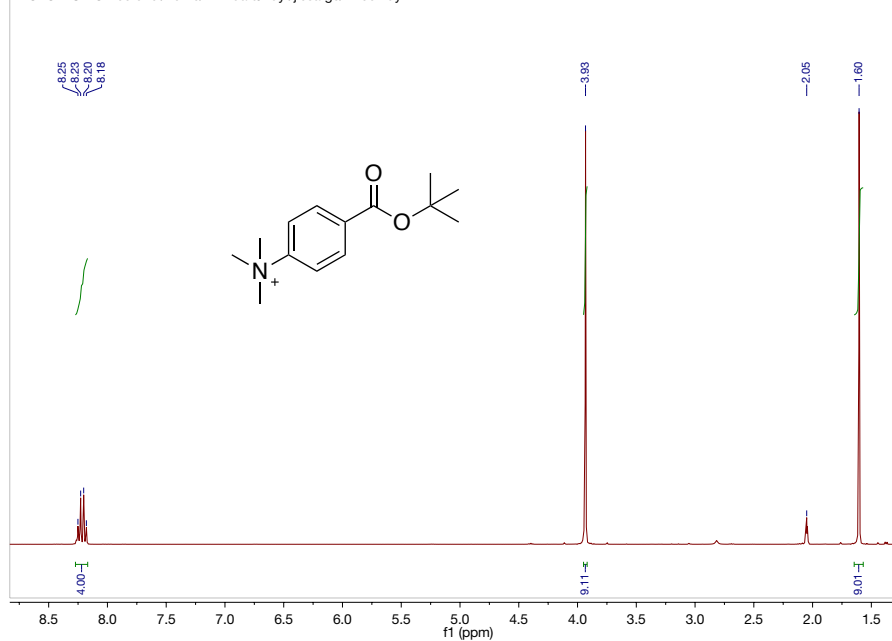
Appendix 13: NMR of 4-(*tert*-butoxycarbonyl)-N,N,N-trimethylbenzenammonium triflate (32)

^1H NMR:

JCL-1-64b.1.fid

H-1 using the Bruker 400

PROTON-UWO Acetone /home/nmr-data/Luyt/jlesarge/B400 Luyt 14

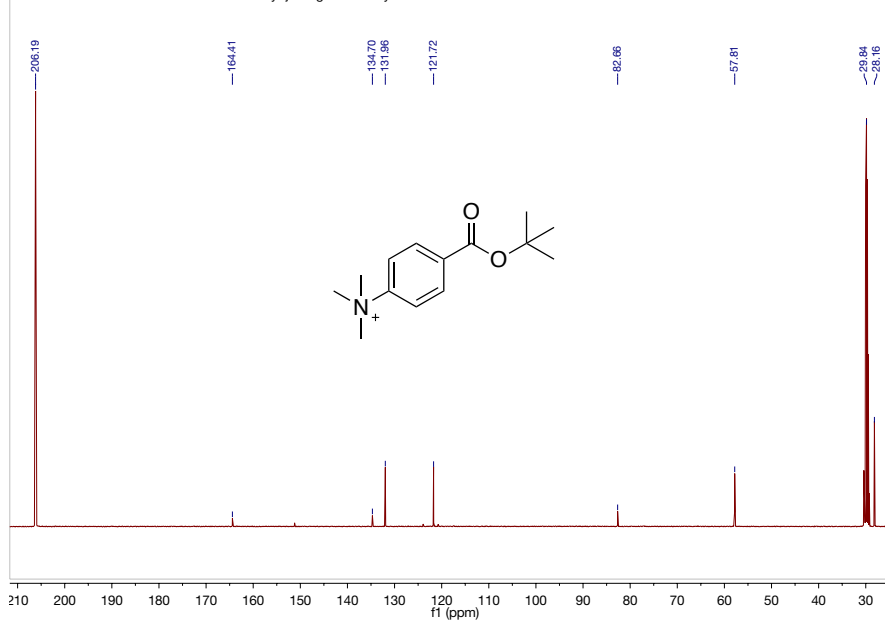


^{13}C NMR:

JCL-1-64b.2.fid

H-1 using the Bruker 400

CARBON-niteQ Acetone /home/nmr-data/Luyt/jlesarge/B400 Luyt 14



Curriculum Vitae

Name: Jordan LeSarge

Post-secondary Education and Degrees: B.Sc. University of Western Ontario, Canada, 2012-2016 (conferred)
M.Sc. University of Western Ontario, Canada, 2016-2018 (in progress)

Honours and Awards: Natural Sciences and Engineering Research Council (NSERC) Master's Fellowship, Canada, 2017-2018.

Province of Ontario Graduate Scholarship (OGS), Canada, 2016-2017, 2017-2018 (declined), and 2018-2019 (declined)

National Inorganic Chemistry Exchange Scholarship and NSERC Undergraduate Student Research Award (USRA), Canada, 2015

The University of Western Ontario Chemistry Alumni Scholarship, Canada, 2015

The University of Western Ontario Continuing Admission Scholarship, Canada, 2012-2016

Related Work Experience Teaching Assistant, 2016-2018
The University of Western Ontario

Undergraduate Research Student, 2014-2015
The University of Western Ontario and Université de Montréal

National and International Conference Presentations:

Thibeault, P.; LeSarge, J. C.; Fernandes, M.; Arends, D.; Luyt, L.; Ramachandran, R. Insights into PAR4 signalling and biased agonism. World Congress of Basic and Clinical Pharmacology Conference. Oral Presentation. June 2018. Kyoto, Japan. International.

LeSarge, J. C.; Thibeault, P.; Kovacs, M.; Ramachandran, R.; Luyt, L. Design, synthesis, and evaluation of novel protease activated receptor 2 (PAR2)-targeting peptides as PET imaging agents for cancer. Canadian Society of Chemistry Conference. Oral Presentation, May 2018. Edmonton, AB, Canada. National.